Institut für Nutzpflanzenwissenschaften und Ressourcenschutz (INRES)

High precision lysimeters improve our understanding of water cycle and solute transport dynamics

Inaugural-Dissertation

zur

Erlangung des Grades

Doktor der Agrarwissenschaften

(Dr. agr.)

der

Landwirtschaftlichen Fakultät

der

Rheinischen Friedrich-Wilhelms-Universität Bonn

von

Jannis Groh

aus

Reutlingen

Bonn 2018

Referent:	Prof. Dr. Harry Vereecken
Korreferent:	Prof. Dr. Bernd Diekkrüger
Tag der mündlichen Prüfung:	29.10.2018

Anfertigung mit Genehmigung der Landwirtschaftlichen Fakultät der Universität Bonn

Zusammenfassung

Wasser ist die kostbarste natürliche Ressource der Erde. Das Verständnis über die Bewegung von Wasser und gelösten Substanzen zwischen den verschiedenen Kompartimenten Boden, Vegetation und Atmosphäre ist von entscheidender Bedeutung, um zahlreiche Umweltprobleme zu lösen. Das Thema umfasst den Schutz der Grundwasserqualität und -quantität, die Optimierung der Pflanzenproduktion und dem effizienten Einsatz von Dünge- und Pflanzenschutzmitteln in der Landwirtschaft. Vorhersagemodelle für den Transport von Wasser und gelösten Stoffen können Entscheidungsträgern dabei helfen, diese verfügbaren natürlichen Ressourcen zu verwalten, zu schützen und zu erhalten. Modelle sind eine Vereinfachung komplexer Naturprozesse und verbinden bekannte Flüsse an den Modellgrenzen mit Zustandsvariablen aus der ungesättigten Zone (vadose Zone). Die Kalibrierung solcher Modelle erfordert präzise Kenntnis über die Randbedingungen und Zustandsvariablen, um die Eigenschaften der vadosen Zone zu identifizieren. Die Eigenschaften verknüpfen Flüsse mit Zustandsvariablen und benötigen dazu die Parameter der Bodenwasser-Retentionskurve, der ungesättigten hydraulischen Leitfähigkeitsfunktion und des Dispersionskoeffizienten.

Das Ziel dieser Studie war es, zu untersuchen, wie nützlich hoch präzise Lysimeter Daten sind, um die Komponenten des Wasserzyklus zu quantifizieren und wie wichtig solche Informationen sind, um ein Model der vadosen Zone zu kalibrieren und welches ermöglicht die Bewegung von Wasser im Boden zu verfolgen. Wir verwendeten synthetische und reale Lysimeter Daten, um die folgenden Ziele zu untersuchen: (1) den Einfluss von sich ändernden Umgebungsbedingungen unter der Oberfläche (Bodentextur und Grundwasserspiegel) auf die gemessenen Saugspannungen im Boden zu bestimmen, welche verwendet werden, um den Wasserfluss am unteren Rand von transportierten Lysimetern in einem Klimafolgenforschungsprojekt zu steuern, (2) tragen Wassermengen aus Nicht-Niederschlagsereignissen (Tau und Raureif) substantiell zur Wasserbilanz von Graslandschaften bei, (3) ist die nächtliche Evapotranspiration ein relevanter Prozess, der die gesamte Evapotranspiration beeinflusst, und (4) sind hochgenaue Wasserbilanz-, Bodenwassergehalt-, Saugspannungsdaten und natürlich stabile Isotopen des Wassers, gleichzeitig notwendig, um Wasserfluss- und Stofftransportparameter eines horizontierten Bodens zu bestimmen.

Zusammenfassung

Unsere Untersuchung zeigt, dass Wasserkreislaufkomponenten hochsensibel auf Änderungen der Untergrundbedingungen (Bodentextur und Grundwasserspiegel) reagieren und daher unbedingt in Klimafolgenforschungsstudien berücksichtigt werden müssen. Lysimeter Beobachtungen zeigten, dass Wasser aus Nicht-Niederschlagsereignissen und nächtlicher Wasserverlust durch Evapotranspiration für die Wasserbilanzen von Grasland-Ökosystems bisher nicht sichtbar waren, aber von großer Relevanz sind. Die gleichzeitige Verwendung von genauen Informationen des gesamten Wasserkreislaufs, des Bodenwassergehaltes, der Bodensaugspannungen und der Isotopendaten aus Lysimetern war während der inversen Modellkalibrierung erforderlich, um Parameter der Bodenwasserretentionscharakteristik, der ungesättigten hydraulischen Leitfähigkeitsfunktion, und der Dispersionskoeffizient von gelösten Stoffes für horizontierte Böden zu identifizieren.
Mit dieser Studie zeigen wir, dass hochpräzise Lysimeter Messungen, kombiniert mit internen Sensoren die erforderlichen Beobachtungen liefern, um komplexe Schlüsselprozesse im Boden zu quantifizieren, die den Energie - und Stoffaustausch zwischen Atmosphäre und Untergrund steuern und somit das Verständnis des gesamten Wasserzyklus und der Stofftransportdynamik in der vadosen Zone verbessern.

Abstract

Water is the most precious natural resource on earth. Understanding the movement of water and dissolved substances between the different compartments soil, vegetation, and atmosphere is of crucial importance to resolve various environmental issues. The issue comprises the protection of groundwater quantity and quality, the optimization of crop production and the efficient use of fertilizer and crop protection products in agriculture. Predictive modeling of water and solute transport can help to provide information for decision makers to manage, protect and sustain these available natural resources. Models are a simplification of complex natural processes and connect known fluxes at the model boundaries with state variables from the unsaturated zone (vadose zone). The calibration of such models requires precise knowledge about the boundary conditions and state variables to identify the properties of the vadose zone that link fluxes with state variables, such as soil water retention characteristic, unsaturated hydraulic conductivity, and solute dispersion coefficient.

The aim of this study was to investigate how beneficial are high precision lysimeter data to quantify water cycle components and how useful are such information's to calibrate a vadose zone model and obtain the parameters, to track the movement of water through the soil. We used synthetic and real lysimeter data to investigate the following objectives: (1) influence of changing surrounding subsurface conditions (soil texture and groundwater table) on the measured matric potentials that are used to control the water fluxes across the bottom boundary of transferred lysimeters in a climate change impact assessment, (2) do water from non-rainfall events (dew, hoar frost) contribute substantial to the water budgets of grasslands, (3) is nighttime evapotranspiration an relevant process that impacts the total evapotranspiration, and (4) are highly accurate water cycle terms, soil water content, matric potential, and water stables isotope data obtained from lysimeters simultaneously necessary to estimate water flow and solute transport parameters of a layered soil.

Our investigation indicates that water cycle components are highly sensitive onto changes in subsurface conditions (soil texture and groundwater table) and thus climate change impact studies need to account for it. Lysimeter observations uncovered that non-rainfall water and nighttime water losses from evapotranspiration were until now unseen but relevant processes for the water budgets of grassland ecosystem. The simultaneous use of an accurate information on the complete water cycle, soil water content, matric potential, and stables

isotope data obtained from lysimeter data were necessary during inverse model calibration to identify parameters of layered soils for the soil water retention characteristic, unsaturated hydraulic conductivity, and solute dispersion coefficient.

In this work, we propose that high precision lysimeter combined with internal sensors devices provide the required observations to quantify complex key processes that control the energy and mass exchanges between atmosphere and subsurface and thus improve our understanding of the complete water cycle and solute transport dynamics in the vadose zone.

List of publications

Bogena, H., Bol, R., Borchard, N., Brüggemann, N., Diekkrüger, B., Drüe, C., **Groh, J.**, Gottselig, N., Huisman, J. A., Lücke, A., Missong, A., Neuwirth, B., Pütz, T., Schmidt, M., Stockinger, M., Tappe, W., Weihermüller, L., Wiekenkamp, I., and Vereecken, H., 2015, A terrestrial observatory approach to the integrated investigation of the effects of deforestation on water, energy, and matter fluxes, *Science China Earth Sciences*, (58)1, 61-75, doi: 10.1007/s11430-014-4911-7

Groh, J., Vanderborght, J., Pütz, T., and Vereecken, H., 2016, How to control the lysimeter bottom boundary to investigate the effect of climate change on soil processes, *Vadose Zone Journal* (15)7, doi: 10.2136/vzj2015.08.0113

Pütz, T., Kiese, R., Wollschläger, U., **Groh, J.**, Rupp, H., Zacharias, S., Priesack, E., Gerke, H. H., Gasche, R., Bens, O., Borg, E., Baessler, C., Kaiser, K., Herbrich, M., Munch, J.-C., Sommer, M.,Vogel, H.-J., Vanderborght, J., and Vereecken, H., 2016, TERENO-SOILCan: a lysimeter-network in Germany observing soil processes and plant diversity influenced by climate change, *Environmental Earth Sciences* (75)18, 1-14, doi: 10.1007/s12665-016-6031-5

Peters, A., **Groh, J.**, Schrader, F., Durner, W., Vereecken, H., and Pütz, T., 2017, Towards an unbiased filter routine to determine precipitation and evapotranspiration from high precision lysimeter measurements, *Journal of Hydrology* (549), 731-740, doi: 10.1016/ j.jhydrol.2017.04.015

Trigo, I. F., de Bruin, H., Beyrich, F., Bosveld, F., Gavilán, P., **Groh, J.**, and López-Urrea, R., Validation of reference evapotranspiration from Meteosat Second Generation (MSG) Observations, *Agricultural and Forest Meteorology*, (submitted)

Groh, J., Slawitsch, V., Herndl, M., Graf, A., Vereecken, H., and Pütz, T., Determining dew and hoar frost formation for a low mountain range and alpine grassland site by weighable lysimeter, *Journal of Hydrology*, (submitted)

Groh, J., Pütz, T., Vanderborght, J., and Vereecken, H., Quantification of nighttime evapotranspiration for two distinct grassland ecosystems, *Water Resources Research*, (submitted)

Groh, J., Stumpp, C., Lücke, A., Pütz, T., Vanderborght, J., and Vereecken, H., 2018, Inverse estimation of soil hydraulic and transport parameters of layered soils from water stable isotope and lysimeter data, Vadose Zone Journal, (accepted)

Bogena, H., Montzka, C., Huisman, J.A., Graf, A., Schmidt, M., Stockinger, M., von Hebel, C., Hendricks-Franssen, H.J., van der Kruk, J, Tappe, W., Lücke, A., Baatz, R., Bol, R., **Groh, J.,** Pütz, T., Jakobi, J., Kunkel, R., Sorg, J, and Vereecken, H. The TERENO – Rur hydrological observatory: A multi-scale multi-compartment research platform for the advancement of hydrological science, Vadose Zone Journal, (submitted)

Contents

List of figures

List of figures

List of tables

List of abbreviations

AV-heat-wave	ET rates during the heat waves in July	
AV-July2016	ET rates in July 2016	
AV-July	ET rates in July 2013 – 2016	
AV-NSE	Average NSE for the entire vadose zone	
AWAT	Adaptive Window and Adaptive Threshold	
BL	Bad Lauchstädt	
BOS1	Bi-objective Optimization Strategy one	
BOS2	Bi-objective Optimization Strategy two	
Br^-	Bromide	
BTC	Breakthrough curve	
C	Tracer concentration	$M\ L^{-3}$
Cd	Coefficient for the FAO-PM equation	-
Cn	Coefficient for the FAO-PM equation	-
CV	Coefficient of variation	
D	Dispersion coefficient	$L^2\ T^{-1}$
Dd	Dedelow	
D_L	Longitudinal dispersivity	L
DWD	Deutscher Wetterdienst	
E_a	Actual evaporation	$L\ T^{-1}$
E_P	Potential evaporation	$L\ T^{-1}$
e_a	Actual vapour pressure	$M\ L^{-1}\ T^{-2}$
e_s	Saturation vapour pressure	$M\ L^{-1}\ T^{-2}$
ET	Evapotranspiration	$L\ T^{-1}$
ET_D	Daytime evapotranspiration	$L\ T^{-1}$
ET_{dawn}	Evapotranspiration between nautical dawn and sunrise	$L\ T^{-1}$
ET_{dusk}	Evapotranspiration between sunset and nautical dusk	$L\ T^{-1}$
ET_N	Nighttime evapotranspiration	$L\ T^{-1}$
ET_{noc}	Evapotranspiration between nautical dusk and nautical dawn	$L\ T^{-1}$

List of abbreviations

FAO	Food and Agriculture Organization of the United Nations	
G	Soil heat flux	$M\ T^{-3}$
GS	Growing-season (March - September)	
GWT	Water table	L
hCritA	Threshold for minimum pressure at the surface	L
h_{dr}	Height of the water table above the drain at the midpoint between the drains	L
$h_{dr,eff}$,	Effective average groundwater layer thickness	L
KBr	Potassium bromide	
K_H	Horizontal saturated hydraulic conductivity of the ground water layer above the drain system	$L\ T^{-1}$
K(h)	Unsaturated hydraulic conductivity function	
K_S	Saturated hydraulic conductivity	$L\ T^{-1}$
LAI	Leaf area index	$L^3\ L^{-3}$
L_{dr}	Drain spacing	L
MOS	Multi-objective Optimization Strategy	
MvG	Mualem-van Genuchten	
n	MvG empirical shape parameter	-
N-GS	Non-growing season (October – February)	
NSE	Nash-Sutcliffe efficiency	-
OF	Objective function	
P	Precipitation	$L\ T^{-1}$
P_a	Air pressure	L
PET	Potential evapotranspiration	$L\ T^{-1}$
PET_{dawn}	PET between nautical dawn and sunrise	$L\ T^{-1}$
PET_{dusk}	PET between sunset and nautical dusk	$L\ T^{-1}$
PET_{noc}	PET between nautical dusk and nautical dawn	$L\ T^{-1}$
PET_N	PET between sunset and sunrise	$L\ T^{-1}$
PM	Penman-Monteith	

P_{NR}	Water from non-rainfall events	
q	Number of complexes	
q_{drain}	Drain discharge	$L\ T^{-1}$
R	Retardation coefficient	
RH	Relative humidity	%
R_n	Net radiation	$M\ T^{-3}$
RO	Rollesbroich	
r_s	Canopy surface resistance	$T\ L^{-1}$
s	Population size	
S	Root water uptake	
Sb	Sauerbach	
SCEM	Shuffled Complex Evolution Metropolis	
Se	Selhausen	
SOILCan	Germany wide lysimeter network	
S0 - S3	Scenario 0 until Scenario 3	
TERENO	TERrestrial Environmental Observatories	
T_a	Actual transpiration	$L\ T^{-1}$
T_{air}	Air temperature	K
T_P	Potential transpiration	$L\ T^{-1}$
TT-DEWCE	Task Team on Definitions of Extreme Weather and Climate Events	
USDA	United States Department of Agriculture	
VPD	Vapor pressure deficit	$M\ L^{-1}\ T^{-2}$
WMO	World Meteorological Organization	
WUE	Water use efficiency	
W_s	Wind speed	$L\ T^{-1}$
α	MvG empirical shape parameter	L^{-1}
α_i	Radiation extinction	-
γ	Psychrometric constant	$M\ L^{-1}\ T^{-2}\ K^{-1}$

List of abbreviations

γ_{dr}	Total drainage resistance	T^{-1}
γ_{entr}	Entrance resistance into the drains	T^{-1}
Δ	Increase of saturation vapour pressure with temperature	$M\ L^{-1}\ T^{-2}\ K^{-1}$
δ^2H	Stable isotope ratio of $^2H/^1H$	‰
$\delta^{18}O$	Stable isotope ratio of $^{18}O/^{16}O$	‰
θ	Volumetric water content	
$\theta(h)$	Water retention characteristic	
θ_r	Residual water content	$L^3\ L^{-3}$
θ_s	Saturated water content	$L^3\ L^{-3}$
σ_{hdr}	Temporal variance of the groundwater layer thickness	L
τ	Pore connectivity parameter	-
τ_w	Tortuosity factor in liquid phase	-
Ψ	Matric potential	L

I General Introduction

I.1 Water and solute cycle

Knowledge about the water cycle and its components are essential in environmental science, because all ecosystems and living organisms are connected and maintained by water. A better understanding of water movement in terrestrial ecosystem is also of crucial importance for humanity, especially in the context of climate variability and climate change. Groundwater accounts for over 97 % of all unfrozen freshwater sources available on earth (Oliva et al. 2016) and supply drinking water for nearly half of the world´s population (Shah et al. 2007). There is an increasing interest and necessity to better understand land-surface, storage and recharge dynamics of water resources in the unsaturated (vadose) and saturated zone. The transfer of water within the soil-plant-atmosphere continuum is an important term of the global hydrological cycle and contains complex key processes like evaporation, precipitation, and transpiration, that control the energy and mass exchanges between atmosphere and subsurface. The knowledge of soil water balance components (precipitation, evaporation, transpiration, groundwater recharge and capillary rise) allows to determine the amount of stored water in the vadose zone, which are subjected to seasonal changes. Hence water is added to the vadose zone by precipitation in form of rain and snow, by non-rainfall events such as dew, fog, hoar frost or by upward directed water from deeper layers or shallow groundwater tables. A loss of water from the vadose zone occurs during evaporation, transpiration and recharge processes. All mentioned water fluxes are part of the terrestrial water balance, but components like dew, hoar frost or nighttime evapotranspiration are ignored in the vast majority of studies on the water budget. Recent investigation from different climate zone and land covers showed that the formation of dew typically ranged between 2 - 48 % of the total precipitation (Malek et al. 1999; Xiao et al. 2009; Hanisch et al. 2015) and that evapotranspiration during night can be up to 55 % of the daytime evapotranspiration (Caird et al. 2007a; Schoppach et al. 2014). These results suggest that both, dew formation and nighttime evapotranspiration, contributes substantially to the water balance of arid to humid climates (Vuollekoski et al. 2015; Lombardozzi et al. 2017). Standard measurement devices for precipitation (P) and evapotranspiration (ET; e.g. rain gauges, eddy covariance) tend to underestimate such land surface fluxes during night (Fank and Unold 2007; Meissner et al. 2007; Hirschi et al. 2017). Consequently underestimation of

land surface fluxes will propagate into estimates of down- and upward directed water fluxes and thus alter the water storage in the vadose zone.

The assessment of water fluxes are of crucial importance for plant growth and food production, as it determines the available stored water and nutrients in the soil. Water is also the main driver of the nutrient and contaminant transport in soils, including agrochemicals (fertilizer, pesticides), heavy metals, trace elements, pharmaceuticals, and pathogenic microbes which threatens groundwater quality (Singh et al. 2017). Thus the knowledge about terrestrial water cycle, nutrient budgets and fate of contaminants are prerequisite to manage, protect and sustain available resources in the vadose zone.

One possible way to make vadose zone fluxes and properties access- and usable for decision makers and practitioners is to set up models that compute the movement of water and solutes through soils by solving different equations e.g. Richards equations for water and the convection-dispersion equation for the solute transport. But those equations contain unknown parameter values that are commonly estimated during the model calibration process by a systematic adjustment of parameter values to match *in situ* observations such as soil water content, matric potential and solute concentration. *In situ* observations of state variables and water fluxes measured in outdoor experiments under natural conditions are frequently not simply available or associated with large uncertainties and errors (Vrugt et al. 2008b; Li et al. 2009; Mannschatz and Dietrich 2017) and stem often from different scales. Therefore, the determination of such water fluxes and state variables with high precision is of crucial importance for hydrological model calibrations. Such models can be used to test scientific hypotheses, to produce forecasts and to provide a decision support tool for scientists and water management practitioners to develop adaptation strategies in a changing world, to protect and sustain natural systems for present and future generations.

I.2 The need to account for realistic state and boundary conditions

In the last years many well-established experimental field, hillslope and catchment sites provided valuable observations on soil moisture, P, subsurface and stream flow for a wide range of simulation studies and helped to improve our hydrological understanding on e.g. the spatial organization of soil moisture (Western et al. 1999), preferential flow (Mosley 1979) and the mechanics of runoff generation (Horton 1933) of soil-plant-atmosphere systems (Paniconi and Putti 2015). Frequently investigations were designed to focus on the hydrological response of one specific variable (ET; Pronger et al. 2016) or used observations,

which were obtained at different spatial scales (e.g. Graf et al. 2014; Wiekenkamp et al. 2016a). In the past often weighable lysimeter were used as tools to measure all relevant water balance components in an entire soil profile and provided observations from an intermediate scale (Abdou and Flury 2004; Singh et al. 2017). The popularity of using lysimeter experiments to monitor and model water and solute transport processes across the soil-plant-atmosphere continuum has increased substantially since the beginning of the nineties (Figure I. 1), especially because lysimeters are the only device allowing directly to determine the quantity and quality of percolating water through the vadose zone (Meissner et al. 2010). However, we have to note for Figure I. 1 that the number of publications in the research domain of environmental science has also be growing over the last years (Wang and Ho 2011).

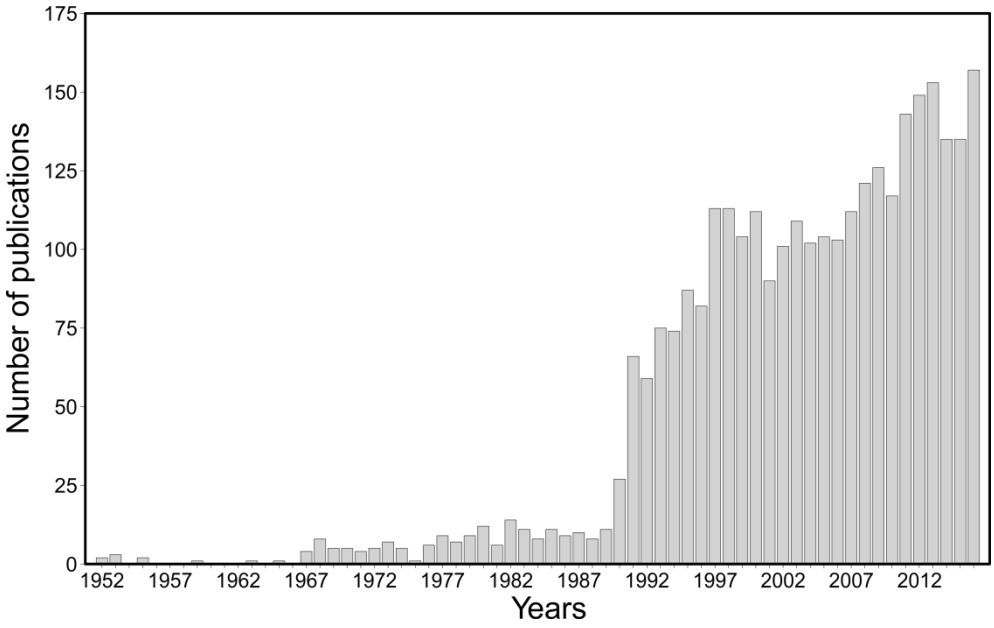

Figure I. 1: Number of publications per year related to the lysimeter topic (search criterion "lysimeter", source: Web of knowledge, November 2017).

Lysimeters are vessels filled with disturbed or undisturbed (monolithical) soil profiles and weighable lysimeters permit measuring the temporal changes of stored water in the respective soil. In the past measured weight loss from the lysimeter, the P and seepage water were used to estimate ET under natural conditions by solving the water balance equation (Meissner et al. 2000; Hirschi et al. 2017). When using P and percolation datasets as variable in the equation their device specific measurement uncertainties and errors (e.g. tipping bucket rain gauge)

propagate into the estimation of ET rates derived from lysimeter data. Brauer et al. (2016) showed for several rainfall measurement techniques, how their specific input uncertainties and errors propagate through the system and influenced the hydrological response of a catchment.

Additionally water from non-rainfall events like dew, fog, or hoar frost may add an unknown amount of water to the hydrological system (Buytaert et al. 2006). Recent investigation for mainly arid to semi-arid regions suggests that dew formation contributes substantially to the water budgets of various ecosystem around the world (Ninari and Berliner 2002; Graf et al. 2004; Jacobs et al. 2006; Ben-Asher et al. 2010; Guo et al. 2016). Various studies have shown the ecological, biological and economical benefit of dew for natural ecosystems, animals, collection of water for human consumption and the management of agricultural and forest land in arid- to semi-arid regions (Clus et al. 2013; Guadarrama-Cetina et al. 2014; Malik et al. 2015; Tomaszkiewicz et al. 2015; Tomaszkiewicz et al. 2017). Moreover in humid regions the amounts of dew might be important, because it supplies plants with additional water during heat waves / warm spells, and investigations showed that nocturnal dew formation (0.28 mm) reduced the water stress of lemon balm plants (Wang et al. 2017), led to a recovery of the relative water content of leaves within few days (Munné-Bosch and Alegre 1999), suppressed plant transpiration by 30 % (Colocasia esculenta leaves; Gerlein-Safdi et al. 2017), and allowed meanwhile leaves to maintain or even improve their CO_2 assimilation rates (Munné-Bosch and Alegre 1999). The formation of hoar frost might protect plant leaves from freezing during colder periods of the year. Tipping-bucket rain gauges, which are classically used by climatologist and hydrologist, are not able to monitor dew or hoar frost formation as the substrate of the measurement device largely differs in terms of wetting properties from natural surfaces (soil and plant).

The exchange of water between soil and atmosphere by evaporation and transpiration is after P the second largest component in the global terrestrial hydrological water cycle. Models often assume that water fluxes by ET occur mainly during daytime and are negligible at night, as the widespread stomatal optimization theory suggests that plants try to minimize the water loss during the CO_2 uptake (Cowan and Farquhar 1977). Thus scientists assume that plants close their stomata during non-photosynthetic periods to avoid a possible water loss through transpiration. Several investigations at the leaf level observed an incomplete stomatal closure during night for a range of different plant species (Caird et al. 2007a; Caird et al. 2007b; Forster 2014; Doronila and Forster 2015; Claverie et al. 2017). The loss of water during

nighttime in arid- to semi-humid regions accounts for 10 - 55 % of the daytime transpiration (Caird et al. 2007a; Skaggs and Irmak 2011; Wang and Dickinson 2012) and hence suggests to contribute substantial to water budget of terrestrial ecosystems. Considering an update in minimal stomatal conductance for different vegetation types in a recent simulation study with a global land surface model showed that such a consideration enlarged the transpiration up to 5 % globally and reduced soil moisture (Lombardozzi et al. 2017). Without an increase of biomass, the additional water loss at night will reduce the water use efficiency of ecosystems (e.g. grapevines; Medrano et al. 2015).

Apart from the impact on the land surface water fluxes, former lysimeters used classically a gravitational drainage system (seepage face boundary condition), through which water can leave the soil only during saturated conditions. Such an artificial boundary disconnects the capillary connection with deeper soil layers, prevents capillary rise and thus affect the water fluxes substantially. Also ET fluxes might be affected by the bottom boundary control of lysimeters, as several investigations have shown that groundwater from shallow water aquifers or water from deeper soil layer can supply in many regions of the world an substantial amount of water for ET processes (Schwaerzel and Bohl 2003; Yin et al. 2015; Liu et al. 2016; Balugani et al. 2017; Satchithanantham et al. 2017). In addition several studies showed that the use of a seepage face boundary condition may lead to a bias not only in percolation, but also in the transport of dissolved substances (Abdou and Flury 2004; Boesten 2007; Stenitzer and Fank 2007).

Recent developments in lysimeter sciences produced a new generation of lysimeter systems with a high measurement precision (0.01 mm) and a tension controlled bottom boundary of the lysimeter (Fank and Unold 2007; Unold and Fank 2008; Hertel and von Unold 2014). Lysimeter weight was in the past often recorded at relative large sampling intervals (e.g. hourly or daily) and thus required, in order to determine ET from the lysimeter weight change separate observations of P and seepage water. Unold and Fank (2008) proposed to record lysimeter data at a higher sample frequency than one minute to determine P directly from lysimeter weight observations. P can derived from a positive and ET from a negative change in lysimeter weight. This approach allows solving the water balance equation without the need of P time series from external rain gauges. The lysimeter water balance is given by:

$$\Delta S = P + P_{NR} - D + CR - ET \qquad [I.1]$$

where ΔS is the water stored in the soil, P_{NR} the non-rainfall events (dew, fog, hoar frost), D the drained/ leached water (second balance), and CR the upward directed water from deeper soil layer (capillary rise). In a first step lysimeter weight observations have to be corrected by the measured amount of seepage. Subsequently any in- and decreasing weight change during the one minute time interval can be counted as P, P_{NR} or ET. This data evaluation assumes that either P, P_{NR} or ET occurs during a specific time interval (e.g. one minute).

The inherent capabilities of soils contain apart from cultural aspects, the provisioning, regulating and supporting services of resources (e.g. flood regulation, nutrient cycle, and climate regulation). Those soil functions are key components to understand the redistribution of water and dissolved substances in soils, vadose zone and groundwater. But the question remains how to determine the parameters of those soil functions? In the past, the use of *in situ* observations of state variables and inverse modeling strategies have shown promising results to reliable estimate soil hydraulic and transport parameters, which regulates the transport of water and solute in the vadose zone. However, very little attention has been given in the past to investigate systematically which observation types are necessary, to calibrate water flow and transport models of the vadose zone.

Modern lysimeters systems provides all relevant state variables like water content, matric potential, solute concentration to determine soil hydraulic and solute transport parameters with soil models. In addition state of the art lysimeter systems provide all relevant surface and bottom boundary water fluxes under realistic field conditions at an intermediate scale.

I.3 Motivation and objectives

The overall objective of the present investigation was to use high precision lysimeter to improve our understanding of water cycle and solute transport dynamics. The main topics of this thesis include the precise quantification of fluxes at the land surface and at the bottom of the ‘critical zone’ and to use these fluxes to constrain vadose zone simulations of a soil-plant-atmosphere system. The objectives are addressed in four different chapters. The first study (Chapter II) used a synthetic dataset, to quantify to what extent surrounding subsurface conditions influence the water budget components of the critical zone and their measurements using lysimeters with a tension-controlled bottom boundary. The aim of the second (Chapter III) and third study (Chapter IV) was to quantify the contribution of non-rainfall events and nighttime ET on the soil water budget of grasslands. In the fourth study (Chapter V), we developed an inverse model calibration strategy under realistic boundary conditions to

optimize the identification of water and solute transport parameters for grassland lysimeter at Wüstebach. The used model simulation boundaries were obtained from the second and third investigation.

The following hypotheses are addressed in the respective study:

i) **Changes in surrounding soil texture properties and water table depths have a significant impact on the water fluxes across the boundaries of transferred lysimeters with a tension controlled bottom boundary.**

Daily meteorological observations combined with soil texture data were used as model input to investigate with a numerical study the potential impact of different bottom boundary conditions on the water budgets components of lysimeters that were transferred in a climate feedback experiment (TERENO-SOILCan; Pütz et al. 2016). Simulated matric potential from a hypothetical field soil profile with different soil texture and water table depths were used to control the bottom boundary of a second simulation, which represents the transferred lysimeters. Varying soil texture and water table depths in field soil profile simulations allowed quantifying the impact of surrounding subsurface conditions on the water budgets and state variables of transferred lysimeters with a tension-controlled bottom boundary.

ii) **Dew and hoar frost formation contributes substantially to the water budgets of a low mountain range and alpine grassland and can be predicted from standard meteorological variables.**

P data obtained from lysimeters and tipping bucket rain gauges were used to estimate the formation of dew and hoar frost. Knowing the permanent wilting point and the air temperature allowed quantifying possible indicator for the ecological relevance of dew and hoar frost. The Penman-Monteith model was used to evaluate the ability to estimate the seasonal amount of non-rainfall water from dew and hoar frost formation based on standard meteorological variables for a low mountain range and alpine grassland site.

iii) **Nighttime evapotranspiration contributes substantially to the total evapotranspiration, are driven by environmental variables and change under heat wave conditions.**

Lysimeter weight data from two distinct low mountain range grasslands ecosystem were used to determine seasonal contribution of nighttime ET to the total ET. Lysimeter data and functions based on astronomical algorithms were used to obtain

ET fluxes during different nighttime periods (dusk, nocturnal, and dawn). Environmental variables were used to investigate which atmospheric and soil related drivers controlled the ET during night- and daytime. Furthermore it was tested how useful are meteorological variables to predict nighttime ET of grassland and how heat waves can impact the rate of nighttime ET.

iv) **Simultaneous multiple observation types are required in the objective function during the inverse model calibration to optimize the identification of soil hydraulic properties and dispersivity of a layered soil under realistic boundary conditions.**

Water samples from four grassland lysimeters in various soil depths were collected and analyzed for stable isotopes and bromide. They were used in combination with soil water content and matric potential measurements to investigate which observation types are necessary in the objective function of the parameter optimization procedure to reproduce simultaneously water flow and solute transport of layered soils. Model simulation boundary water fluxes were obtained from lysimeter data and obtained parameter-sets were used to validate the identified solute transport parameters independently.

II How to control the lysimeter bottom boundary to investigate the effect of climate change on soil processes?

Modified on the basis of the published journal article:

Groh, J.*, Vanderborght, J., Pütz, T., and Vereecken, H. (2016), How to control the lysimeter bottom boundary to investigate the effect of climate change on soil processes?, Vadose Zone Journal 15(7), 1-15.

II How to control the lysimeter bottom boundary to investigate the effect of climate change on soil processes?

II.1 Introduction

Increasing variability of temperature and P by climate change will affect the water availability, nutrient supply and growth conditions for crop production (Thornton et al. 2014). Accurate and precise observations of the impact of climate variability and change on the water and matter fluxes in the unsaturated and saturated zone are therefore key information sources for the development of adaptation and management strategies of agricultural and environmental systems. Weighable lysimeters are frequently used tools to measure these fluxes in an entire soil profile (up to several meters deep) and provide us with observations that can be representative up to the field scale (Abdou and Flury 2004; Kasteel et al. 2007). Weighable lysimeters are vessels filled with disturbed or undisturbed soil volumes which are isolated from the surrounding field conditions. Lysimeters can be used to quantify the impacts of climate change on processes in the soil–vegetation–atmosphere continuum, for example, the influence of increasing soil temperature on dissolved organic carbon (Briones et al. 1998), of higher soil temperatures and CO_2- concentrations on the water and matter (carbon, nitrogen and phosphorus) budget of grassland (Herndl 2011), of change in rainfall patterns on plant productivity for different soil types (Tataw et al. 2014), of decreasing rainfall and temperature on nitrate dynamics (Ineson et al. 1998), and the ecological controls on water-cycle response to climate variability in deserts (Scanlon et al. 2005).

In the context of growing interest in changes in the hydrological cycle due to climate change, an experimental lysimeter network (SOILCan; Zacharias et al. 2011) was built up in Germany to study long-term effects of climate change on water and matter fluxes in soils and exchange of greenhouse gases. This network is embedded into the long-term observatories of TERrestiral ENvironmental Observatories (TERENO). The focus of the SOILCan project is to observe the impact of climate change on water and matter budgets in different grass and arable land lysimeters (Bogena et al. 2012; Pütz et al. 2016). A monitoring network of lysimeter stations was established across a rainfall and temperature transect, and lysimeters were transferred between the stations to subject them to different rainfall and temperature regimes (Pütz et al. 2013). The SOILCan setup and the transfer of lysimeters enable a comparison of water and matter fluxes in the same soil under different climatic conditions. The lateral separation of the lysimeter from its location in the landscape disturbs lateral inflows and outflows such as surface runoff and run-on and lateral flow on sloping subsurface soil horizons. Lysimeters are therefore not suited to investigate soil water balances at

locations where these nonlocal controls on the soil water balance are important. The separation of the lysimeter from its surroundings also introduces an artificial boundary at the bottom that may affect the soil water balance of the lysimeter. The classically used bottom boundary of a lysimeter is a seepage-face boundary through which water can only leave when the soil is saturated and through which no upward inflow is possible. Disconnecting the capillary connection with deeper soil affects the drainage and prevents capillary rise. Several studies have shown that upward directed water fluxes from shallow groundwater tables and deeper soil layers serve as an additional water supply for ET processes (Schwaerzel and Bohl 2003; Yang et al. 2007; Luo and Sophocleous 2010; Karimov et al. 2014). A seepage-face boundary condition may lead to a bias in the drainage (Stenitzer and Fank 2007) and in the solute transport processes (Abdou and Flury 2004; Boesten 2007) so that lysimeter observations are not directly transferable to field-scale conditions (Vereecken and Dust 1998; Flury et al. 1999). However, methods have been developed to control the bottom boundary of a lysimeter so that the water balance and moisture profiles in the lysimeter correspond closely with those that would prevail in the undisturbed soil profile (Fank and Unold 2007). The lysimeters in SOILCan have a controlled bottom boundary condition using a rake of suction candles that enables upward and downward flow of water from and to a weighted leachate tank. To ensure the lysimeter water dynamics are according to the field dynamics, the matric potential at the bottom is controlled and adjusted to measured matric potentials in an undisturbed soil profile next to the location where the lysimeter is installed and at the same depth as the bottom of the lysimeter. An adjustable control algorithm takes into account different soils and conductivities, allowing the bidirectional pumping system to control the water flow direction across the lysimeter bottom to minimize matric potential differences between the field and the lysimeter.

Often, lysimeters are transferred from the place where they were sampled (also for practical reasons) to another location. For transferred lysimeters this approach leads to artifacts since the properties and the hydrogeological setting of the soil profile where the control matric potential is measured may differ from the soil in the lysimeter and the conditions at the site where the lysimeter was taken. Furthermore, changing boundary conditions at the soil surface due to, for instance, climate change will have an effect on the hydrogeological conditions, the water and matter balance in the soil profile, and consequently the matric potential that should be used to control the bottom boundary. Therefore studies of climate change impacts on water fluxes in soils using transferred lysimeters have to take into account that a shift of the climatic

conditions will alter the top as well as the bottom boundary of soil monoliths. We hypothesize that the feedback between changing climate conditions, groundwater table depths, and boundary conditions that have to be applied at the bottom of lysimeters have important consequences for the water balance in the lysimeters. Not considering these feedbacks may lead to incorrect conclusions about the effect of climate change on changes of water and matter fluxes in soils.

To assess the potential impact of different bottom boundary conditions on the soil water balance of transferred lysimeters, a numerical study in soils was conducted. The use of synthetic data from numerical studies has the advantage that the assumed truth is known (Schelle et al. 2013b) and that the impact of certain changes on the system can be related to a single or several known factors. Using numerical simulation with the software HYDRUS-1D (Šimůnek et al. 2013), we will define (i) the potential impact of different approaches to control the bottom boundary on the water fluxes across the lysimeter, (ii) the sensitivity of water fluxes towards a changing water table depth, and (iii) the feedback between water table change, climate change, and drainage within a fixed hydrogeological setting. On the basis of this study, a proposal for the control of the bottom boundary condition of transferred lysimeters will be made to enable a measurement setup (SOILCan-network) that allows quantifying the influence of climate change on soil functions and relevant ecosystem variables.

II.2 Material and Methods

II.2.1 Site descriptions

For the simulation experiment, we considered all transfers of arable land lysimeters from four test sites of the SOILCan climate change lysimeter network. Lysimeters were transferred from Bad Lauchstädt (BL), Dedelow (Dd), Sauerbach (Sb), and Selhausen (Se) to the central tests sites for arable land lysimeters in BL and Se (see Table II. 1). Further information about the lysimeter sites, lysimeter transfer, soil texture, weather station, groundwater table depths, and mean annual climatic conditions during the simulation period (1981 – 2010) is given in Table II. 1. The transfer of arable land lysimeters to the central test site in BL represents a climate change scenario (1981 – 2010) with a decrease in mean annual P (range: 17 mm to 215 mm) and an increase in mean annual air temperature (range: 0.1°C to 0.7°C, exception, Se -0.9°C). The transfer of arable land lysimeters to the central test site Se corresponds to a scenario

(1981 – 2010) with increases in air temperature and P. Changes in mean annual air temperature are up to 1.6°C and annual amount of rain up to 215 mm (1981 – 2010). The higher annual rainfall amount in Se can be mainly related to wetter conditions during winter and autumn months.

II.2.2 Definition of simulated scenarios

The temporal evolution of the matric potential (values -/+ = unsaturated/saturated soil conditions) at 1.4-m soil depth depends on the local climate conditions, soil properties (water retention and hydraulic conductivity), and the depth of groundwater table. Simulations in soil profiles down to a groundwater table are used to obtain and/or mimic time series of matric potentials at 1.4-m depth. These matric potentials are then used to control the bottom boundary of the transferred lysimeters, which represent truncated soil profiles. Figure II. 1 shows the simulation proceeding for a transfer of soil from Sb to the central test site in BL. In a first step, we simulated matric potentials and fluxes in the soil profile where the lysimeter was taken (origin) to have the basis for comparison and identify the change in soil water balance components due to the transfer and due to the use of different scenarios to control the bottom boundary of transferred lysimeters. A second simulation represents the current control of transferred lysimeters at the central test sites of the SOILCan network and will be called the Scenario 0 (S0). In this scenario, matric potentials that are observed in the soil profile at the site where the lysimeters are transferred to are used to control the bottom boundary of the transferred lysimeters. These control matric potentials are influenced by the soil properties and groundwater table depths at the site where the lysimeters are transferred to and therefore differ from the soil properties of the lysimeters and the groundwater table depths in the profiles where the lysimeters were taken from. To evaluate the artifacts caused by this control of the lysimeter bottom boundary and to derive an alternative suited approach, water balance simulations were run for three additional scenarios. In Scenario 1 (S1), we used matric potentials at 1.4-m depth that were measured and/or simulated in the soil profile at the site where the lysimeters were taken from to control the lysimeter bottom conditions, that is, the bottom boundary condition in the truncated soil profile simulations was identical to the one in Scenario origin. However, these matric potentials are influenced by the climate at the site where the lysimeters were taken from and may therefore lead to artifacts when used to control the bottom boundary of lysimeters that are transferred to other sites with a different climate. Therefore we defined a Scenario 2 (S2) which used matric potentials that are simulated by

using the soil properties and the groundwater table depths from the site where the lysimeter were taken and the climate from the site where the lysimeters were transferred to. Although this approach takes account of the hydraulic properties and hydrological setting of the soil profile at the site from where the lysimeters were taken and the climatic boundary conditions at the site where they are transferred to, feedbacks between the climate and the groundwater table depth are not considered. When groundwater recharge decreases over a long time period, groundwater tables will sink. To consider these feedbacks, lateral water flow in the phreatic aquifer below the vadose zone, which depends on the hydrogeological setting of the region where the lysimeters are taken from, should be considered. Since there is a lot of uncertainty about this setting, we decided to evaluate the potential feedback between climate change and groundwater depth changes with Scenario 3 (S3) by assuming that the static groundwater level from S2 declines by 2 m when lysimeters are transferred from a wetter to a drier site or increases by 1 m when they are transferred from a drier to a wetter site. The decline or increase of water table was chosen arbitrarily. Information about the simulation setup of the different scenarios that were used to derive the control matric potentials at the bottom of the transferred lysimeters is summarized in

Table II. 2.

Several studies have shown the interdependence of land surface fluxes and groundwater dynamics (Kollet and Maxwell 2008; Maxwell and Kollet 2008; Ferguson and Maxwell 2010; Soylu et al. 2011). To explain the differences between the scenarios because of different groundwater table depths and to evaluate the effect of the groundwater table depth on soil water fluxes systematically, additional simulations in which the water table depth varied from 1.4 m to 20 m were performed. In the scenarios used so far, only the effect of a static groundwater table on the water balance of lysimeters was considered. Therefore additional simulations were conducted that consider the interactions between groundwater table depth and drainage – capillary rise within a fixed and hypothetical hydrogeological setting. We defined hydrogeological properties that control lateral groundwater flow such as the depth of an impermeable layer, the hydraulic conductivity of the groundwater layer, and the distance between surface water bodies that drain groundwater.

II How to control the lysimeter bottom boundary to investigate the effect of climate change on soil processes?

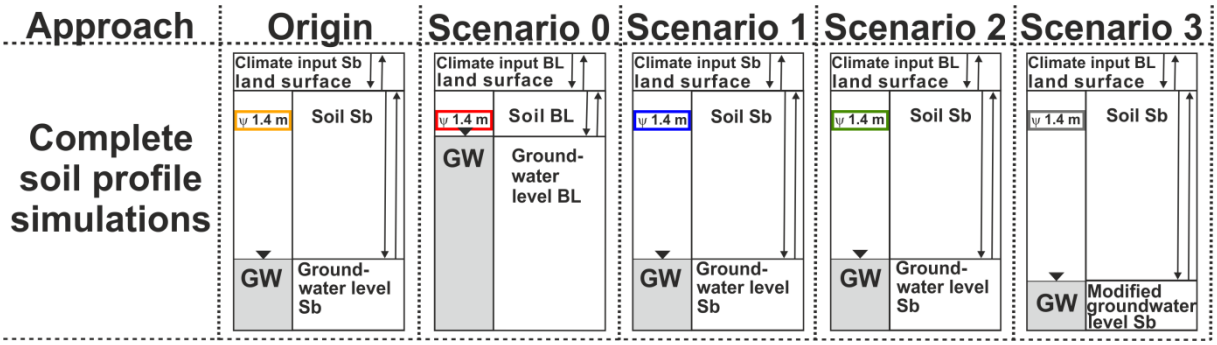

Figure II. 1: Experimental setup to derive synthetic data for the control of lysimeter bottom boundary derived by five approaches exemplarily for the lysimeter transfer from Sauerbach (Sb) to the central test site Bad Lauchstädt (BL). The approaches to derive matric potentials in 1.4-m soil depth from a complete soil profile to control the truncated soil of a lysimeter are the following: the origin approach represents conditions to calculate the soil water balance at the site where the lysimeter was taken from. The scenario Scenario 0 (S0) uses the climate conditions, soil characteristics, and groundwater (GW) level from BL (current control approach). The S1 uses the climate input, soil characteristics, and groundwater levels from Sb. The S2 uses climate conditions from BL and the soil characteristics and groundwater levels from Sb. The S3 uses climate from BL and the soil characteristics and 2-m declined groundwater level from Sb.

II.2.3 Model setup and parameterization

To model the impact of different bottom boundaries on the water balance of lysimeters, we used the one dimensional water flow model HYDRUS-1D (Šimůnek et al. 2013). The program solves numerically the Richards equation for unsaturated water flow. The upper boundary was a time dependent atmospheric boundary condition (daily resolution). Since the objective of this study was to investigate the effect of the bottom boundary control on the soil water balance and not to describe the water balance in the real lysimeters as accurately as possible, we made a few simplifying assumptions. We assumed a homogenous mean soil texture from the top to the bottom of the soil profile. The hydraulic soil parameters for the water retention curve and unsaturated hydraulic conductivity in the Mualem-van Genuchten model (van Genuchten 1980) were estimated from the averaged sand, silt, and clay content in the soil profile (see Table II. 3) by using the ROSETTA database. Saturated hydraulic conductivity (K_S) parameters estimated for the silt texture were replaced by the corresponding values from Carsel and Parrish (1988) to obtain a more realistic unsaturated conductivity for structured silt soils (Schlüter et al. 2013). The bottom boundary of the complete soil profile simulations was defined assuming a constant groundwater table depth at the bottom of the simulated soil profile (see Table II. 1).

II How to control the lysimeter bottom boundary to investigate the effect of climate change on soil processes?

Table II. 1: Basic information about test sites characteristics.

Test site		Coordinates		Weather station†	Altitude	Groundwater level‡	Texture class#	Profile mean			Mean annual		
								Sand	Silt	Clay	Temp.	Rainfall	PET¶
Origin	Transfer				m‡	m		%	%	%	°C	mm	mm
Bad Lauchstädt (BL)	Se	51°23´37”N	11°52´45”E	Halle-Kröllwitz	113	2	SiLo	66.3	20.8	9.6	9.6	503	633
Dedelow (Dd)	BL, Se	53°22´2”N	13°48´11”E	Angermünde	41	3	SaLo	27.0	18.0	8.9	8.9	522	659
Sauerbach (Sb)	BL, Se	52°04´47”N	11°16´58”E	Magdeburg	143	9	SiLo	71.9	19.2	9.5	9.5	520	646
Selhausen (Se)	BL	50°52´9”N	6°27´1”E	Jülich Forsch.-Anlage	104	4	SiLo	65.4	18.2	10.5	10.5	718	643

† Stations from the German Weather Service.

‡ Assumption of a constant groundwater table depth.

§ According to USDA textural classification chart.

¶ Potential evapotranspiration, FAO Penman-Monteith.

Table II. 2: Overview of the climate conditions, soil profiles, and groundwater (GW) table depths that were used to simulate the control matric potentials at the bottom of the lysimeters for the different scenarios.

Test site	Transfer	Origin			Scenario S0			Scenario S1			Scenario S2			Scenario S3		
		Climate	Soil	GW	Climate	Soil	GW	Climate	Soil	GW	Climate	Soil	GW	Climate	Soil	GW
				m			M						m			m
BL	Se	BL	BL	2	Se	Se	4	BL	BL	2	Se	BL	2	Se	BL	1
Dd		Dd	Dd	3	Se	Se	4	Dd	Dd	3	Se	Dd	3	Se	Dd	2
Sb		Sb	Sb	9	Se	Se	4	Sb	Sb	9	Se	Sb	9	Se	Sb	8
Dd	BL	Dd	Dd	3	BL	BL	2	Dd	Dd	3	BL	Dd	3	BL	Dd	5
Sb		Sb	Sb	9	BL	BL	2	Sb	Sb	9	BL	Sb	9	BL	Sb	11
Se		Se	Se	4	BL	BL	2	Se	Se	4	BL	Se	4	BL	Se	6

Table II. 3: Hydraulic parameters for the Mualem-van Genuchten model (van Genuchten 1980) of each test site were obtained from the HYDRUS-1D implemented ROSETTA database (Schaap et al. 2001), and saturated hydraulic conductivity for silt loam at Bad Lauchstädt, Sauerbach, and Selhausen were replaced by a value derived by soil texture class from Carsel and Parrish (1988).

Test site	θ_r	θ_s	α	N	K_s	τ
	$cm^3\ cm^{-3}$		cm^{-1}	-	$cm\ d^{-1}$	-
Bad Lauchstädt	0.0737	0.4461	0.0053	1.6298	10.80	0.5
Dedelow	0.0566	0.3912	0.0210	1.3924	18.43	0.5
Sauerbach	0.0737	0.4539	0.0056	1.6305	10.80	0.5
Selhausen	0.0685	0.4389	0.0048	1.6576	10.80	0.5

For the simulations in the lysimeters, we considered a soil profile of 1.4-m depth. To mimic the real control system of the lysimeter bottom boundary, time dependent matric potentials were defined at the bottom of the lysimeter. Time series of matric potentials at the bottom boundary of the lysimeters were obtained from simulated matric potentials at 1.4-m depth in the complete soil profiles that are considered for the origin and the S0 to S3 scenarios. Potential evapotranspiration (PET) was calculated using the FAO-Penman-Monteith equation (FAO 1990), assuming an albedo of 0.25 (-) for a wheat crop (Piggin and Schwerdtfeger 1973) and by using daily data of relative humidity, wind speed, sunshine hours, and minimum and maximum air temperature. The meteorological data for a 30 year time period from 1981 until 2010 were obtained from weather stations of the German Weather Service (DWD): Se (Jülich Forsch.- Anlage), BL (Halle-Kröllwitz), Sb (Magdeburg), and Dd (Angermünde). Missing values were completed by a linear interpolation between nearby stations of the German Weather Service.

Beer´s law was used to split the PET into potential evaporation (E_P) and transpiration (T_P) fluxes as follows:

$$E_P = PET\ exp(-\alpha_i\ LAI) \qquad [II.1]$$

$$T_P = PET\ (1 - exp(-\alpha_i\ LAI)\ ) \qquad [II.2]$$

where α_i is 0.463 (-) (Šimůnek et al. 2013) and LAI ($cm^2\ cm^{-2}$) is the leaf area index. The seasonal development of the LAI of wheat was approximated by a linear relation from sowing (1 March) until midseason (1 May) when it reached a maximum of 3.6 ($cm^2\ cm^{-2}$) (Breuer et al. 2003) and after which it remained constant until ripening started (1 June). The evolution of LAI during ripening until harvest (1 July) was approximated by a linear decrease from LAI

3.6 (cm^2 cm^{-2}, 01 June) until LAI 2 (cm^2 cm^{-2}; July). After harvest, soil stayed bare (LAI = 0 cm^2 cm^{-2}) until the next growing season on 1 March. The potential evaporation, E_p, was used as flux boundary condition at the soil surface until a critical threshold matric potential, hcrit = -100,000 cm at the soil surface, was reached. When this matric potential was reached, the evaporation flux from the soil surface was calculated by the prescribed critical matric potential. The potential transpiration, T_p, was linked to the depth-integrated potential water sink term. The potential water sink term is proportional to the normalized root length density which is described by the Hoffman and Van Genuchten (1983) function. The evolution of rooting depth for wheat was simulated by the Verhulst-Pearl logistic growth function (Šimůnek and Suarez 1993), and the root growth factor was defined so that 50 % of the rooting depth is reached at the first half of the growing season (16 May). The initial root growth time was set on 1 March with an initial rooting depth of 1 cm and harvest time on 1 July, with a maximum rooting depth of 120 cm for spring wheat (Allen et al. 1998). The potential water uptake is reduced when the soil is nearly saturated and when the soil water potential decreases below a critical value. The relation between actual water uptake and soil water potential was described by the Feddes et al. (1978) stress response function. The used Feddes parameters for the root water uptake were set according to values for wheat from Wesseling et al. (1991). The water uptake by roots is assumed to be zero at matric potentials higher than 0 cm (anaerobic stress) and lower than -16,000 cm (water stress), which corresponds to the permanent wilting point. The optimal range for water uptake is between -1 and -500 cm for a potential transpiration rate of 0.5 cm d^{-1} and between -1 and -900 cm for a potential transpiration rate of 0.1 cm d^{-1}. A linear decrease of water uptake is assumed between the limiting matric potentials and wilting point.

For the vegetation parameters, LAI, rooting depth, and their change over time were kept the same for all simulations. Therefore, feedbacks between weather- and climate-dependent vegetation dynamics and the hydrological system, which are important for climate change impact studies (van Walsum and Supit 2012; Pangle et al. 2014), were not considered. Ecohydrological vegetation feedbacks influence the upper boundary conditions and root water uptake in the soil profile. Since we did not consider these feedbacks, it must be noted that our simulations do not represent how the upper boundary conditions of transferred lysimeters will change. However, the objective of this study is to investigate how to control the bottom boundary conditions of transferred lysimeters so that the effect of changing upper boundary conditions due to climate change, including feedbacks with vegetation dynamics, can be

monitored in these systems without introducing a systematic bias resulting from improper bottom boundary conditions.

As initial conditions, we assumed a hydrostatic equilibrium from the groundwater table up to 1 m above the groundwater table. Above this depth, matric potential was assumed to be constant with depth and equal to -100 cm. For the lysimeter, the same initial matric potentials as in the complete soil profile between the bottom of the lysimeter and the soil surface were taken. A two year spin-up phase was used to minimize the effect of the chosen initial conditions. Long-term mean matric potential, actual evaporation (E_a), actual transpiration (T_a), and drainage (negative value) or upward flux (by capillary rise, positive value), that were simulated in the truncated profiles or lysimeters for the different approaches were compared.

To examine the impact of a changing groundwater depth on ET and drainage or upward flux, we varied the static groundwater table depth (bottom boundary) from 1.4 m up to 20 m for all four soils in Bad Lauchstädt and Selhausen. To account for feedback mechanisms between changing climate, groundwater table depth, and drainage, we conducted a sensitivity analysis in which we varied hydrogeological settings that determine lateral groundwater flow, such as the depth of an impermeable layer on which a groundwater table develops that discharges into drains that are located on this impermeable layer. This was done exemplarily for the Selhausen soil. To account in HYDRUS-1D for a dynamic positioning of the water table during the season and a lateral flow or drain discharge on top of an impermeable layer, we used a system dependent bottom boundary condition derived from the Hooghoudt equation (Šimůnek et al. 2013). The drain discharge (drainage) q_{drain} (cm d^{-1}) of a homogeneous soil profile in which the drains are located on top of an impermeable layer can be calculated by:

$$q_{drain} = \frac{h_{dr}}{\gamma_{dr}} \qquad \text{[II.3]}$$

where h_{dr} stands for the height of the water table (cm) above the drain at the midpoint between the drains and γ_{dr} for the total drainage resistance (d). The γ_{dr} is the sum of the radial flow and the entrance resistance, and can be calculated by Eq. [II.4]:

$$\gamma_{dr} = \frac{L_{dr}^2}{4\,K_H\,h_{dr}} + \gamma_{entr} \qquad \text{[II.4]}$$

where L_{dr} is the drain spacing (cm), K_H is the horizontal saturated hydraulic conductivity (cm d^{-1}) of the groundwater layer above the drain system(which was set to 15 cm d^{-1}), and γ_{entr} is the entrance resistance into the drains (d). The parameter γ_{entr} was set to zero, as we assumed

that the convergence of stream lines to the infinite perforations in the drainage tube does not lead to an additional flow resistance and head loss. The depth of the impermeable layer was varied from 4 m until 20 m with a fixed L_{dr} of 200 m. The relation between the groundwater table depth and drainage in Eq. [II.3] allows solving the soil water flow equation without having to prescribe matric potential or drainage at the bottom boundary. Therefore, both groundwater table depth and drainage and how they change when the upper boundary conditions change are simulated.

To compare the simulated dynamic groundwater table depths with fixed groundwater table depths, we defined a time-averaged groundwater layer thickness, $h_{dr,eff}$, that would lead to the same average drainage, $<q_{drain}>$:

$$h_{dr,eff} = \sqrt{\frac{\langle q_{drain} \rangle L_{dr}^2}{4 K_H}} \quad \text{[II.5]}$$

The effective average groundwater layer thickness $h_{dr,eff}$ can be related to the time-averaged groundwater layer thickness $<h_{dr}>$ and its temporal variance σ^2_{hdr} as:

$$h_{dr,eff} = \sqrt{\langle h_{dr} \rangle^2 + \sigma_{hdr}^2} \quad \text{[II.6]}$$

II.3 Results and Discussion

II.3.1 Impact of different bottom boundary conditions on the water balance of lysimeters

The distribution of matric potentials at 1.4-m soil depth during the 30 year simulation period that were used in the different approaches to control the bottom boundary of the lysimeters are shown as box plots in Figure II. 2. Also shown in Figure II. 2 are the matric potential distributions in the soil profiles at the sites where the lysimeters were taken (origin). For S0, the matric potentials are equal to those in the soil profiles at the site where the lysimeters are installed. For S1, they are equal to the distribution of matric potentials at the site where the lysimeters were taken (origin). Average yearly transpiration, evaporation and drainage or upward flux for the different control approaches are given as stacked bar plots in Figure II. 3.

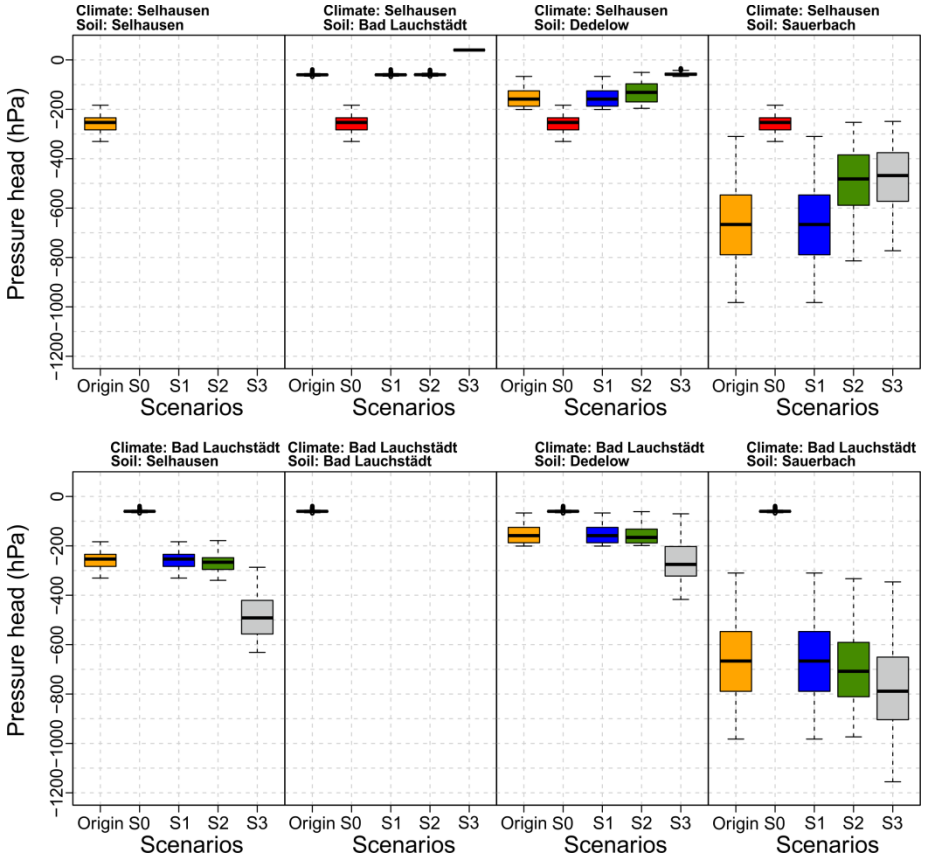

Figure II. 2: Matric potentials at 1.4-m depth from complete soil profile simulations at the site where the lysimeter was taken from (origin) and matric potentials that were used to control the bottom boundary of the lysimeters transferred to the central test site Se (top subplots) and BL (bottom subplots) for the different scenarios: S0-S3.

II.3.1.1 Transfer to the central test site Selhausen

The larger P due to the transfer of soils to Se (74 to 236 mm) led to a larger drainage in all transferred lysimeters for all considered controls of the bottom boundary. For the BL lysimeter, the upward directed water flux by capillary rise at the original location changed to a net drainage. The transpiration was larger in the lysimeters transferred to Se (max. 17 mm), except for the lysimeters from BL in which the transpiration rate was smaller than at the original location (6 mm). Also, the evaporation rates were higher in comparison with the original location (max. 109 mm), with exception for the S0 of the lysimeter from BL in Se, where evaporation rates declines by more than 18 mm. Using a bottom boundary from scenario simulations that was determined by a profile with a deeper groundwater table led to lower matric potentials at the bottom of the lysimeter (Figure II. 2) and therefore to a larger drainage (Figure II. 3). The influence of capillary rise from the water table on the soil water fluxes across the boundaries of the lysimeter declined with increasing depth to groundwater

table (see Sb to Se in Figure II. 3). However, the sensitivity of drainage or upward flux to the depth of groundwater table depends not only on the depth to groundwater table, but also on the soil properties. The coarser textured soil from Dd showed a smaller sensitivity of drainage on the depth to groundwater table. The larger pore size in the coarser textured Dd soil led to a smaller capillarity and capillary rise than in the other soils that have a finer texture and smaller pores (Li et al. 2013). Comparing the differences between S1 and S2 represents the effect of the change in climate on the simulated matric potentials at the bottom of the lysimeter in the soil profiles with same groundwater table depth (see Figure II. 2) and the effect of using these simulated matric potentials to control the bottom boundary (see Figure II. 3). Since the climate was wetter in Se than in the other locations, the simulated matric potentials at the bottom of the lysimeter were higher for S2 than for S1. But only in the Sb profile, which has a deep groundwater table, there was a considerable increase in matric potentials. But, when compared with the difference between simulated drainage between S0 and S1, the difference between S1 and S2 was small. For the other profiles, the matric potentials at the bottom of the lysimeter were stronger, as they were controlled by the presumed groundwater table depth in the soil profile than by the climate conditions at the soil surface. A low impact from climate conditions on the simulated fluxes in the transferred lysimeters might be related to the use of a constant water table (disconnected from land surface fluxes) in the complete soil profile simulations. Seasonal weather, drainage (Taylor et al. 2013b) and vegetation conditions lead to fluctuations of the water table, which play an important role for the diurnal or seasonal cycle of water uptake by plants (Gribovszki et al. 2010).

The raised groundwater level by 1 m from S2 to S3 led to higher simulated matric potentials at the bottom of the lysimeter. This led the Dd and Sb soils to a decrease in simulated drainage (max. 12 mm). For the BL soil, the simulated transpiration and evaporation from S1 and S2 were equal to the PET. A further increase in groundwater level would therefore not further enhance the ET. Conversely, a too shallow water table can lead to anaerobic conditions in the effective root zone and negatively affect the plant transpiration (Soylu et al. 2014). The order of magnitude of simulated fluxes at the lysimeter bottom boundary is, in consideration of the assumptions in the simulation setup (homogenous mean soil texture and constant water table), in good agreement with observations for two exemplary test sites. Measured drainage for the station Se was -53 mm a^{-1} (average value of three lysimeters, 2014 - 2015) and for Dd was -23 mm a^{-1} (average of six lysimeters, 2012 - 2013).

II How to control the lysimeter bottom boundary to investigate the effect of climate change on soil processes?

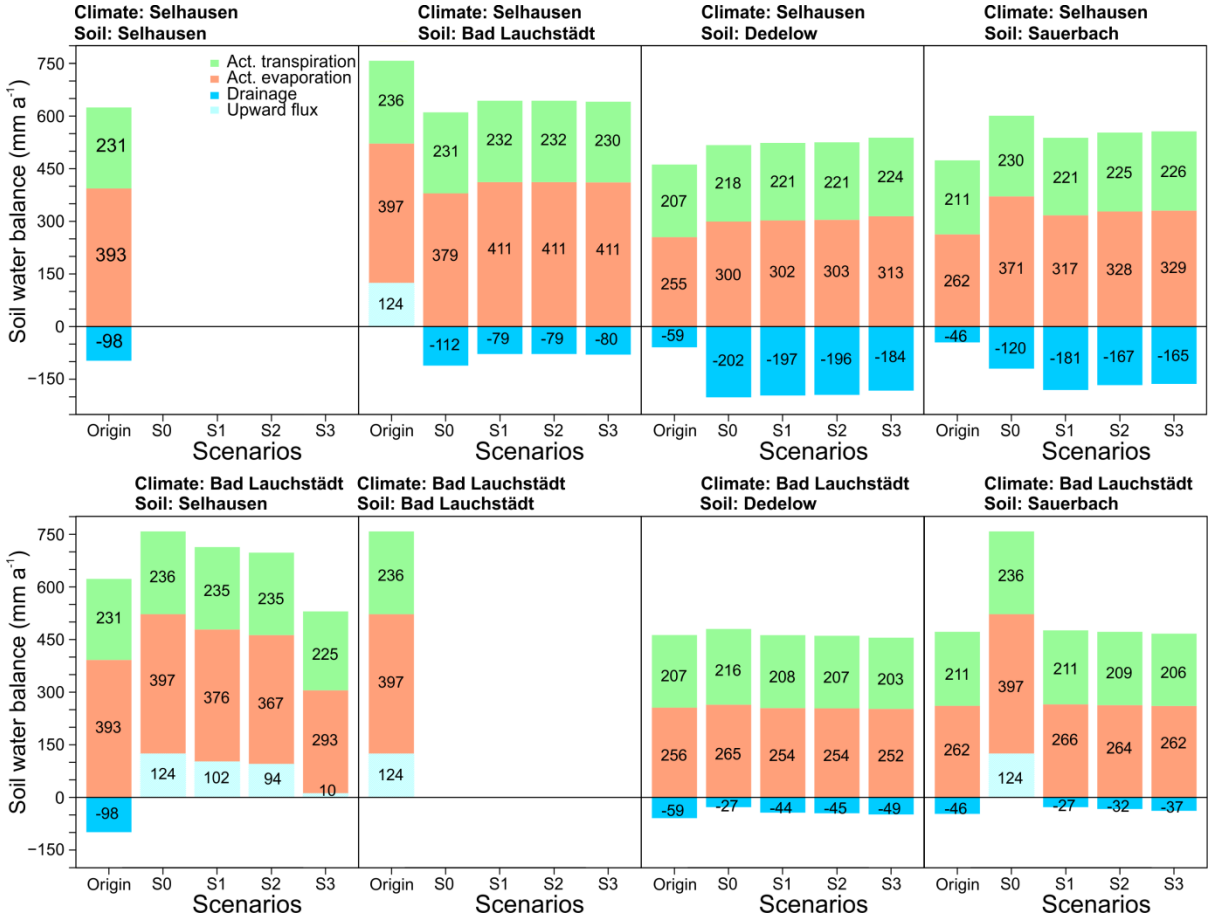

Figure II. 3: Averaged yearly transpiration, evaporation, and drainage (negative) or upward flux (positive) from lysimeter profile simulations (1981–2010). The water balance of the lysimeters were simulate at the site where the lysimeter were taken from (origin) and at the site where the lysimeter were transferred to. We used four different scenarios (S0 to S3) to control the bottom boundary of transferred lysimeters at the central test sites. Information about climate conditions and soil origin is given in the subplot headings.

II.3.1.2 Transfer to the central test site Bad Lauchstädt

The central test site BL is with 502 mm drier than the Se (718 mm), Dd (522 mm) and Sb (520 mm) test site. The rainfall but also the PET is higher at the latter two sites (Dd = 659 mm, Sb = 646 mm) than in BL (633 mm). The groundwater table in BL (2 m) is shallower than at the other sites. In general, the simulated drainage of the transferred lysimeters to BL was smaller than at the original locations. For the soils with a finer texture (silt loam: BL, Se and Sb), the shallow groundwater table in BL and the simulated matric potentials that were used in S0 led to an upward flux of water into the lysimeter and higher ET. Upward directed water flux from a shallow water table increased the water storage in the effective root zone and enhanced the ET (Leterme et al. 2012). This upward water flux

compensated the difference between the potential evaporation rate and P in BL so that the simulated ET in these lysimeters was equal to the potential ET. In the sandy loam soil from Dd, the simulated matric potentials at 1.4-m depth for S0 were not large enough to sustain a sufficient capillary rise to the root zone or soil surface so that for this soil, transpiration and evaporation were lower than the potential rates and there was still drainage. When soil profiles with groundwater table depths of the original locations (S1, S2) or even lower (S3) were considered to control the bottom boundary of the lysimeter the effect of capillary rise and groundwater uptake was smaller, drainage increased and ET was reduced. For the Se profile, a decrease of the groundwater table by 2 m led to a significant decrease in upward fluxes (difference between the S2 and S3). This was neither observed for the Sb profile, which had a similar texture as the Se profile but a deep groundwater table, nor for the Dd profile, which had a coarser texture but a similar groundwater table.

In general average annual water fluxes were strongly influenced by the surrounding field conditions (depth to water table and soil properties). The use of a shallow water table and finer textured soil in the scenario was essential for the water availability in the soil, influenced the plant water use (Soylu et al. 2014) and enhanced the evaporation from bare soil (Jin et al. 2014).

II.3.2 Impact of boundary conditions on dynamics of water fluxes at the bottom of lysimeters

Figure II. 4 gives an overview of the average monthly drainage or upward flux and their annual variability (period 1981 to 2010) across the lysimeter bottom for the different bottom boundary controls. Drainage occurred mainly during the autumn and winter months and was relatively small during spring. However, in summer the flux was directed upward. The intra-annual variation of the average monthly drainage or upward flux declined for bottom boundary control scenarios with deeper groundwater tables. In general, we found that using a bottom boundary control based on a scenario with a higher water table led to a higher upward flux during summer and higher drainage during winter. This indicates that a control by S0 will lead to an overestimation of upward flux during summer and of drainage during winter when the water table at the site where the lysimeters are transferred to is higher than at the original site (e.g. lysimeters transferred to BL).

II How to control the lysimeter bottom boundary to investigate the effect of climate change on soil processes?

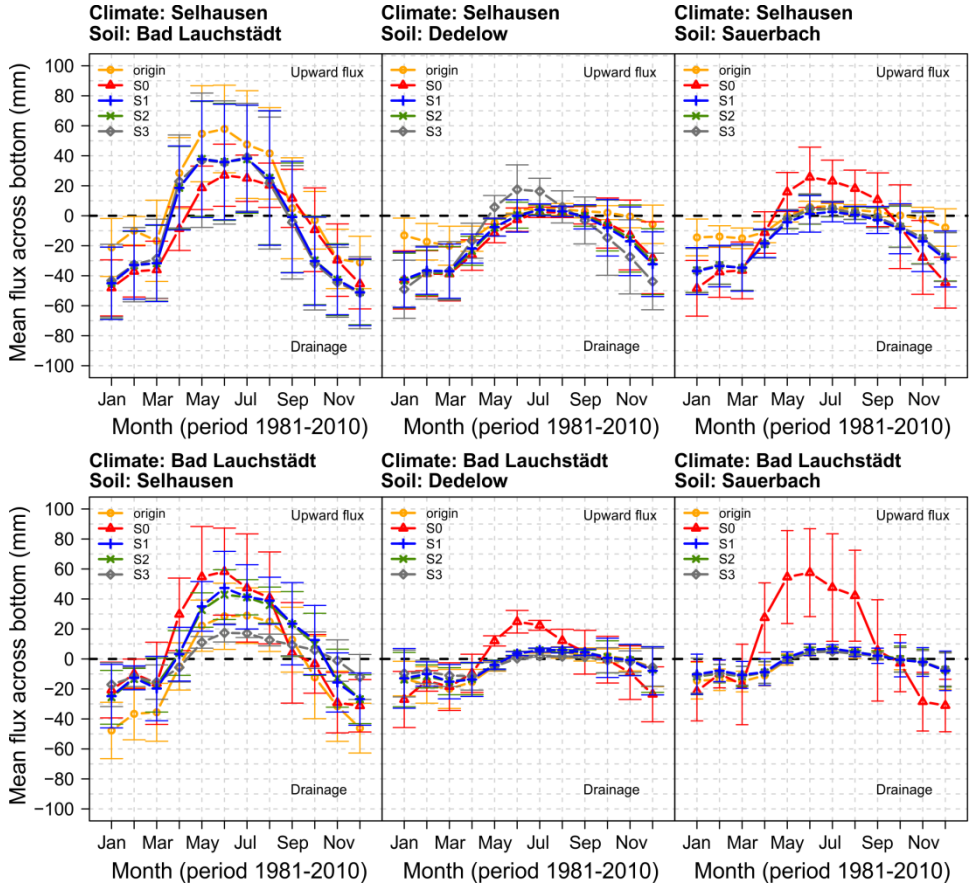

Figure II. 4: Monthly averaged water flux across the bottom boundary of lysimeter that remained at their original location (origin) and lysimeter that were transferred from BL, Dd, Sb and Se to the central test sites BL and Se and in which the matric potentials at the bottom boundary are prescribed by scenario S0, S1, S2, and S3. Positive values represent upward water fluxes (capillary rise), and negative values represent downward water fluxes (drainage). Error bars represent the standard deviation of the monthly averaged fluxes in different years.

The opposite is true for lysimeters that are transferred to a site with a lower groundwater table (e.g. BL lysimeter transferred to Se). The climatic boundary conditions at the top of the lysimeter influence the time course of the fluxes at the bottom of the lysimeter (see difference between the origin and the other scenarios). But, for the differences in climate conditions between the original sites and the sites where the lysimeters were transferred to, the effect of the different climate conditions on the matric potentials that are used to control of the bottom boundary was not large (see Figure II. 2 and the difference between S1 and S2). Consequently S1 and S2 hardly led to differences in simulated monthly averaged water fluxes at 1.4-m depth.

The results indicate additionally that at sites with a relatively shallow groundwater table and silty soils, upward water fluxes during summer can be considerable. Tension-controlled

lysimeters are required to reproduce these fluxes so that the soil water balance in the field can be mimicked in the lysimeter system. But an inappropriate control of the matric potential based on matric potentials that are obtained for a nonrelevant water table depth (e.g. from a site that is not related to the site where the lysimeters were taken from) can lead to large deviations of these fluxes.

With the water that flows back into the lysimeter system, also dissolved chemical substances are transported. A correct mimicking of the water fluxes at the bottom of the lysimeter is therefore also of importance for a correct representation of the chemical balance, for example, nitrogen balance (Klammler and Fank 2014) or tracer experiments in the lysimeter. Seasonal changes in saturated conditions at the lysimeter bottom can impact chemical processes, for example, the denitrification rate (Anderson et al. 2014) or the estimation of solute transport parameters (Rühle et al. 2015). Within the SOILCan lysimeter setup, we assume that chemical reactions and temperature in the leachate tank, where the leachate is stored, are comparable with that in the surrounding soil at the corresponding depth of 1.4-m. However, when biogeochemical gradients are present in the soil profile, the chemical composition of the water that flows back into the soil profile will differ from that that leaches from the profile. How the water composition of the water that flows back into the system needs to be controlled so that the chemical balance of the lysimeter system corresponds with that of the field profile requires further investigation. In case of a negative water balance over the year, additional water has to be added with a similar chemical composition of the seasonal outflow (e.g. prepared in laboratory) for a correct chemical balance. The importance of bottom boundary conditions in zero tension lysimeter systems to represent pesticide balances in field soil profiles has been demonstrated by Boesten (2007). But similar studies for tension-controlled lysimeters are still missing.

II.3.3 Impact of different controls of the bottom boundary on the water contents in the lysimeters

In Figure II. 5, time-averaged water contents and the standard deviations of the temporal fluctuation at a certain depth are shown for the different approaches. Again, the depth of the water table in the soil profiles that were considered to define the control of the lysimeter bottom boundary played an important role for the vertical water content profile (Chen and Hu 2004). The S0 (groundwater table at the location where the lysimeters were transferred to) led to considerably different water content profiles than those of other approaches (based on

groundwater tables at locations where the lysimeters were taken). Besides affecting the mean water content, the groundwater table depth also influenced the temporal variability of the soil water content with smaller variability when the water table depth was high (e.g., S0 for lysimeters transferred to BL) and higher variability when the groundwater table was lower (e.g., S3 for Se lysimeters transferred to BL). The effect of the climate on the soil moisture in the soil columns can be evaluated by comparing the moisture contents at the original locations with those using S2 to control the lysimeters bottom boundary, as both control matric potentials are simulated in a soil profile with the same water table depth and soil properties as at the original site, but using climate of the location where the lysimeters were transferred to.

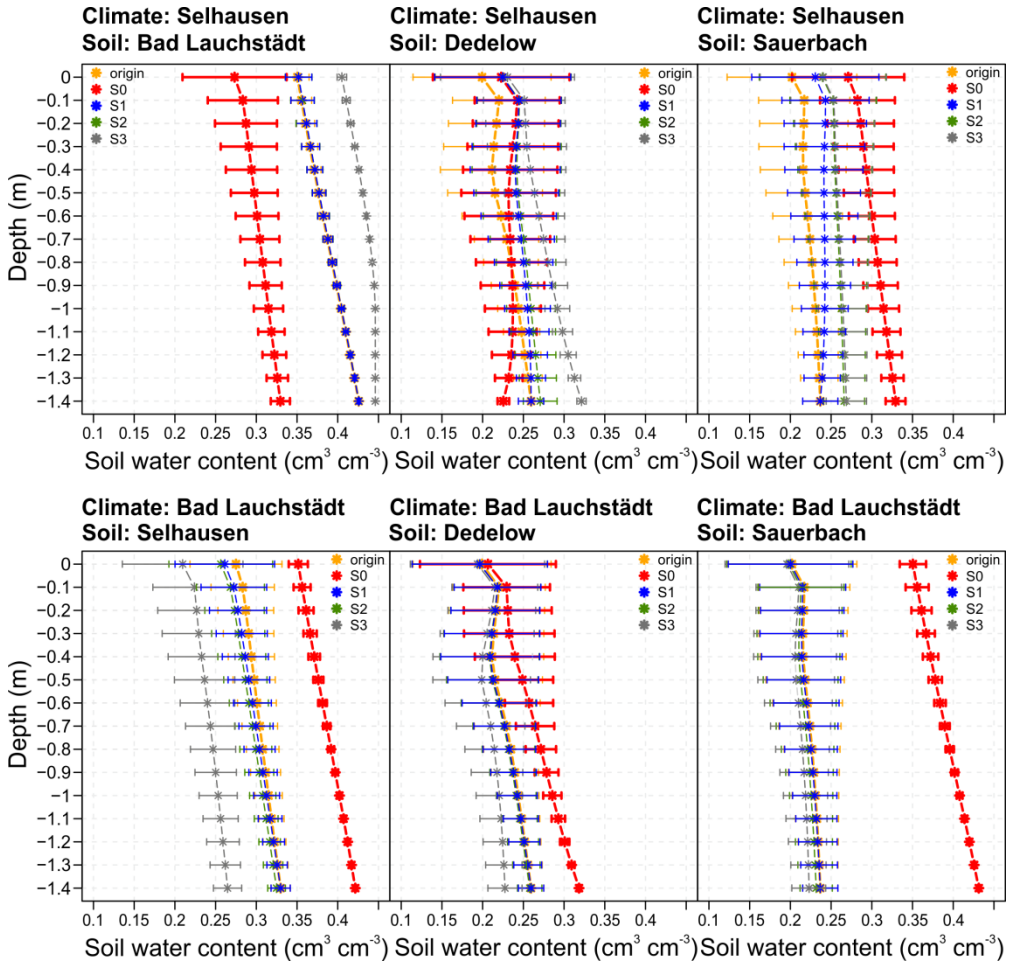

Figure II. 5: Time-averaged water contents in lysimeters that remained at their original location (origin) and in lysimeters that were transferred from BL, Dd, Sb and Se to the central test sites BL and Se and in which the matric potentials at the bottom boundary are prescribed by S0, S1, S2, or S3. Error bars represent the standard deviation of the temporal variations of the soil water content. The water contents of the soil from BL at Se (climate) are identical for S1 and S2.

II How to control the lysimeter bottom boundary to investigate the effect of climate change on soil processes?

The Dd and Sb lysimeters that were transported to Se (wetter climate) showed higher water contents in the top of the soil profiles than at the original location. For the BL lysimeter transferred to Se, the water content profile seems to be completely dominated by the shallow water table depth in BL so that there was hardly an influence of the climate on the water content profile in this soil. The Se lysimeter that was transferred to BL (drier climate) showed lower water contents at the top of the soil profile than at the original location. The Dd and Sb lysimeters that were transferred to BL did not show a difference in soil water content profile with the profile at the original location since the climate at those locations was similar to that in BL. A comparison between the water content profiles in the lysimeter from S1 and S2 shows the impact of using matric potentials at the bottom of the lysimeter that were observed at the site where the lysimeter were taken (S1) and the test site where the lysimeter were transferred to (S2). Only for the Sb lysimeter that was transferred to Se was a noticeable effect present. But the effect vanishes closer to the soil surface where the water content profiles of S1 and S2 were closer to each other than the profiles from S1 and S0.

Finally, when comparing S3 (groundwater table changes compared with the depth at the original location) and S2, lowering of the water table in the Se and Dd profiles led to lower water contents in the lysimeters that were transferred to the drier BL site. For the Sb lysimeter, the effect of further lowering the groundwater table on the water content profiles was small since the water table at the original location was already quite deep and did not influence the water dynamics in the soil profile a lot. For the lysimeters that were translocated to Se, an increase in water table height led to wetter soil profiles except for the Sb profile, where the groundwater table was deep.

When we compare the different approaches, it seems that the groundwater table depth in the soil profile was more important for the control of the bottom boundary conditions of the lysimeter than the climate. This implies that using matric potentials that are measured in the soil profile at the site where the lysimeters are transferred to for controlling the bottom boundary of the lysimeters may lead to considerable artefacts in the lysimeters water balance. The main focus of the translocation concept in SOILCan is to observe changes in water and matter fluxes in the same soil under different climate conditions. The artefacts from the current bottom boundary control (S0) will lead to a nonclimate change related alteration of the water balance in the considered transferred terrestrial ecosystem. A better option seems to use matric potentials that are measured at the sites where the lysimeters originate from. This bottom boundary control setup for transferred lysimeters allows a direct comparison of

changes in soil processes and soil functions under different climate regimes with identical bottom boundary conditions.

The important role of the groundwater table on the soil water balance is further discussed in the following sections, where the sensitivity of drainage or upward flux to the groundwater table depth and feedbacks between drainage and groundwater table are evaluated.

II.3.4 Sensitivity of water fluxes toward a changing water table depth

Figure II. 6 illustrates the ET and drainage- upward flux as a function of depth to groundwater table for all soils under the climatic conditions of both central test sites (Se and BL). The drainage generally increases, whereas the ET decreases with increasing groundwater table depth. The ET and drainage or upward flux simulations were sensitive to groundwater table depth changes. The sensitivity vanishes for a deep groundwater table when ET becomes water limited and in the silt loam soils (all except Dd) and also for shallow groundwater tables when ET becomes energy limited. It should be noted that we did not consider groundwater table depths above 1 m. In these cases, simulated ET decreased with decreasing water table depth because too wet soil conditions also induce a transpiration reduction. Kollet and Maxwell (2008) named the region with strong correlations between water table depth and land surface energy fluxes as “critical zone”. The lower boundary of the critical zone represents the point where the water table is disconnected from the land surface (Maxwell and Kollet 2008). In their study, this zone was defined for the Little Washita watershed in Central Oklahoma (soil: loam–loamy sand) and ranged between 1 and 5 m. Following the concept of a critical zone from Kollet and Maxwell (2008), we defined the upper and lower limits of the sensitive water table (GWT) region (critical zone) as the depth where $|dET/dGWT| > 5$ mm m^{-1} $year^{-1}$. The threshold value for |dET/dGWT| was chosen arbitrarily but represents the region where drainage-upward flux was sensitive to the groundwater table depth and enables an estimation of a soil specific critical zone.

The thickness of the critical zone from Figure II. 6 (colored bars at the subplot bottom) showed a strong dependence on soil texture as well as on climatic conditions. Soils with a finer texture showed a significantly thicker and deeper located critical zone than coarser textured soils. The simulation was in a good agreement with studies by Soylu et al. (2011), who showed that soil properties (texture) affect the depth and the thickness of critical zone. A change in climate regime from wetter to drier conditions, with a smaller P-to-PET ratio, resulted for the soils with the silt and the sandy loam texture in a thicker critical zone. Finer

textured soils showed a much larger increased thickness of critical zone by a change in climate regime than the coarser textured soil. Additionally, we can see from Figure II. 6 the effect of changing the water table at one site to the water table at the corresponding central test site. All soils, where a change of the two water tables was within the soil specific critical zone (horizontal colored bars at the bottom), showed a considerable change in the drainage or upward flux and ET in the soil profile.

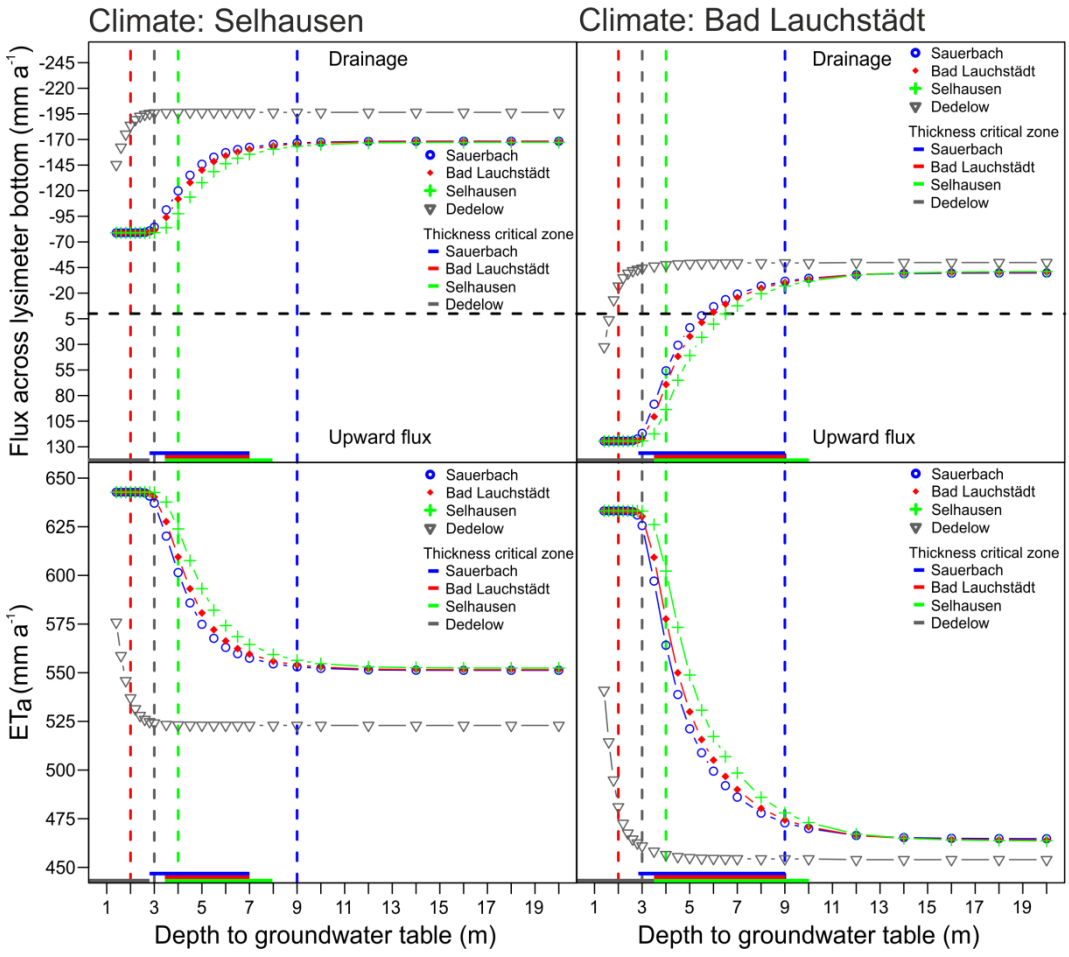

Figure II. 6: Yearly water flux across the lower (drainage-upward flux) and upper boundary (evapotranspiration) of a soil profile, which represents the corresponding soil texture class from BL, Dd, Sb, and Se, averaged over 30 years under the respective climatic conditions at the central test site Se and BL. Horizontal colored bars at the bottom of each subplot represent the thickness of the soil texture specific critical zone. Vertical colored lines represent the water table depth at the site where the lysimeter were taken from.

When the water table change was not in the critical zone (soil Dd in Se) there was no effect of the groundwater table depth on the change or drainage-upward flux due to a change of the net P. This explains the low sensitivity of water balance components toward a water table change

in the scenarios of a coarser soil (Dd) in Figure II. 3. The larger change of drainage-upward flux and ET due to changing groundwater tables in BL indicates a higher sensitivity of water table changes on the water fluxes in the soil profiles under drier climatic conditions. But the question that needs to be answered is how the groundwater levels will change when the net P changes.

II.3.5 Feedback between groundwater change, climate change, and drainage

In our scenario S3, we used a fixed and preset drop of the groundwater table of 2 m to evaluate the potential effect of the climate change (wet to drier conditions) on groundwater table depths and its feedback on drainage. This drop was arbitrarily chosen but could, as we demonstrate in this section, be estimated if the hydrogeological settings of the site are considered.

The averaged water table depth, drainage and water table drop as a function of the drain depth are shown for two different climate conditions: BL and Se (Figure II. 7). The water table depth was under wetter conditions (Se) generally higher and showed until 14 m larger seasonal fluctuations than under drier conditions (BL). Under the BL climate, drainage emerged for drain depths (or impermeable layer depths) deeper than 6 m. It should be noted that this threshold depth corresponds with the groundwater table depth in Figure II. 7 where the drainage becomes zero. Drier climate conditions prevented the buildup of a water table and the generation of drainage for drain depths or impermeable layer boundaries shallower than 6 m. Under these conditions, water that perched on the impermeable layer could be completely consumed by ET without saturating the soil and generating drainage. Additionally, we have to remark that with simulations under wetter conditions (Se) runoff occurred when drain depth distance between impervious layer and soil surface was smaller than 8 m.

The calculated drop of the water table, when the climate shifts from wet to drier conditions, was maximal (around 2.9 m) for the threshold drain depth of 8 m when a groundwater table emerged under the BL conditions. For deeper drain depths, the groundwater table drop decreased to about 2 m for a drain depth of 20 m. The simulation results for a defined fixed hydrogeological setting indicate that a change in climate conditions will affect the average position and the seasonal behavior of water table depth. A change in water table depth and the seasonal variability goes along with a modified matric potential in the soil at 1.4 m, which impacts the water flux across the boundaries of transferred lysimeters. As an example from simulations with drain spacing of 200 m, considering a groundwater table of 7 m under wet

climate conditions and assuming that it remains constant when the conditions change to drier conditions, the simulated drainage under dry conditions (S2, Figure II. 7 red dashed line) would be 9 mm year^{-1}. When a drop in groundwater table due to changing climate conditions from 7 to 9 m is considered (S3, Figure II. 7 red dashed line), the drainage under dry conditions would be 34 mm year^{-1}. Also, the effect of the change of the groundwater table depth when the climate changes from drier to wetter conditions could be evaluated from Figure II. 7. If the groundwater table is at 7 m under dry conditions and assumed to be the same under wet conditions (S2, Figure II. 7 black dashed line), the drainage under wet conditions would be 151 mm year^{-1}. When the groundwater table rise due to the wetter conditions on 6 m is considered (S3, Figure II. 7 black dashed line), the drainage under wet conditions would be 136 mm year^{-1}. The relevance of these changes on the boundary conditions will alter the water flux and cause significant changes on the measured water balance components in transferred lysimeter.

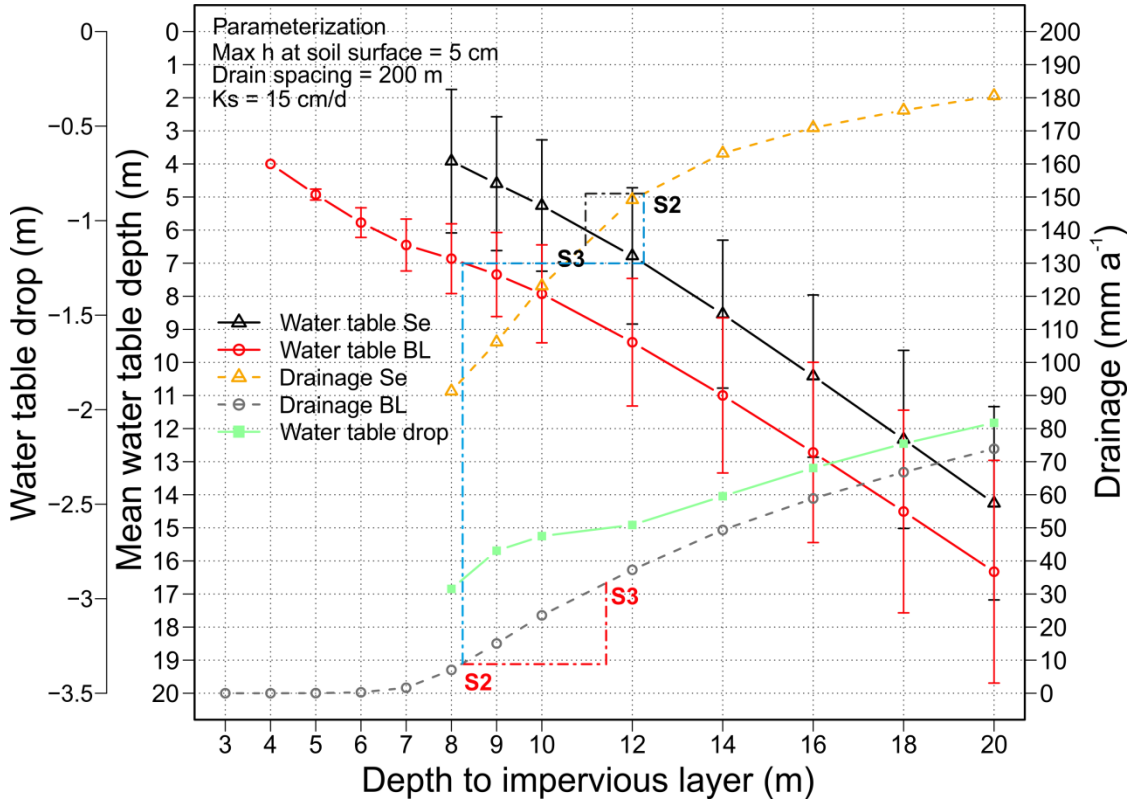

Figure II. 7: Sensitivity of mean water table depth, standard deviation and mean drainage (lateral flow) on top of an impervious layer for the soil from Se with a fixed hydrogeological setting under different climate conditions (Se, triangles; BL, circles). The green line represents the water table drop by a shift from a wetter to a drier and hotter climate.

II How to control the lysimeter bottom boundary to investigate the effect of climate change on soil processes?

II.4 Conclusion

We used tension-controlled lysimeter systems to study the effect of climate change on soil hydrology. Lysimeters with a similar soil texture were transferred to other locations to simulate the soil water balance under different climatic regimes. With the transfer of lysimeters and/or soils in the simulation setup, not only the atmospheric but also surrounding subsurface conditions changed and influenced the measured matric potentials that are used to control the bottom boundary of transferred lysimeters. We found that the use of nonappropriate matric potentials, which do not correspond with water table depths and soil textural properties from the site where the lysimeters originated from, can lead to large biases in soil water fluxes and seasonal water flux dynamics across the lysimeter bottom and lead to nonclimate change-related alteration of water availability and fluxes in the considered terrestrial ecosystem. Feedback mechanisms between changing climate conditions (principle weather parameters and net P), groundwater dynamics, and bottom boundary conditions, which are used to control the bottom boundary of transferred lysimeters, can lead to an additional amplification or diminishing of climate change effects on the terms of the water balance in lysimeters. We found that the effect of a changing water table in the field under a different climate regime was rather small in comparison to the difference between the current control approach (S0), which is based on water table depths at the sites where lysimeters are transferred to and which may differ considerably from the conditions at the sites where the lysimeters originate from, and the approach which used measured matric potentials at the site where the lysimeter was taken from (S1). However, the effects from water table change on the water flux in lysimeters were noticeable when the water table was located within a specific critical water table depth range. This region, where land surface and subsurface processes are coupled, was called critical zone. A sensitivity analysis investigating the impact of different water table depths on the water flux in lysimeters showed a strong dependence of the thickness and depth of the critical zone on soil textural properties and climatic conditions.

The simulation results confirm that not only are aboveground conditions relevant for lysimeter measurements but, moreover, surrounding subsurface conditions are highly important for lysimeters with a tension-controlled bottom boundary. We found that local field conditions led to considerable artifacts on the water balance of transferred and tension-controlled lysimeters when they do not match with the conditions of the sites where the lysimeters were extracted from. These findings are also relevant for future lysimeter

installations with a tension-controlled bottom boundary system. Changes in soil textural properties and water table depth between the location of excavation and installation can lead to a strong bias in water fluxes across the lysimeter boundaries.

Theoretically, the control of the bottom boundary that includes the effect of changing climate conditions on the matric potentials that are used to control the bottom of the lysimeter (S2 or S3) would be better for studying the effect of climate change on flow and transport processes in transferred soils. However, these bottom boundary conditions can only be derived by simulations which imply uncertainties. In contrast, the bottom boundary control from S1 can be based on actual measurements and shows to be a reliable representative of the bottom boundary control from S2 and S3, unless the change in climate and water table depth are substantial. Therefore, we suggest, for studies with a transfer of soil, managing the bottom boundary by matric potentials that are measured at the place where the lysimeter was taken from (S1). This control setup allows a direct comparison of changes in soil processes and soil functions between soils under rainfall and temperature regimes with identical bottom boundaries conditions.

III Determining dew and hoar frost formation for a low mountain range and alpine grassland site by weighable lysimeter

This chapter is based on a journal article submitted as:

Groh, J.*****, Slawitsch, V.*, Herndl, M., Graf, A., Vereecken, H., and Pütz, T., Determining dew and hoar frost formation for a low mountain range and alpine grassland site by weighable lysimeter, *Journal of Hydrology* (submitted).

*Shared first co-authorship

III Determining dew and hoar frost formation for a low mountain range and alpine grassland site by weighable lysimeter

III.1 Introduction

Dew forms when the temperature of a surface is lower than or equal to the dew-point temperature, such that water vapor of the ambient air condenses at the colder surface. Free water on the soil or surface of plants can originate from separate processes. We distinguish between i) dew formation and direct water vapor adsorption in case that condensed water originate from the atmosphere (Monteith 1957), ii) distillation if the source of water vapor comes from the soil, and iii) guttation if the water comes from the plant itself (Singh 2014). However, the latter both represent only a redistribution of water within the soil-plant-atmosphere system and hence do not really contribute to the water balance. Please note, we followed the terminology of Agam and Berliner (2006) and used in our investigation the term dew formation instead of dew deposition or dewfall. This prevents, that one may misinterpret from the terms dew deposition or dewfall that droplets of water were formed in the air and not at the surface. Dew is a natural phenomenon and results from a phase transition between the gaseous and liquid state when moist air comes in contact with a surface (Agam and Berliner 2006) and hence heterogeneous nucleation with a growth of water droplets starts (Beysens 1995). In case that surface temperature falls below the frost point of the air, we can observe the formation of hoar frost rather than dew (Monteith and Unsworth 2013). So, dew and hoar frost formation can be seen in the absence of fog and P as a mechanism by which water can be added to the soil-plant system.

The physical phenomena of dew formation is ecologically and biologically important as the non-rainfall water directly impact the productivity of mosses and lichens (Csintalan et al. 2000; Gauslaa 2014; Goetz and Price 2016), provide sufficient water for the growth of microbiotic crusts (Kidron et al. 2002), is a major water source for plants in many arid- and semi-arid regions (Hanisch et al. 2015; Guo et al. 2016), influence barren landscapes and their micrometeorological conditions by enhancing the moisture cycle of bare soils (Graf et al. 2004) and is in drylands often the only water source for small animals (Guadarrama-Cetina et al. 2014; Wang et al. 2017). Dew is also from an economical perspective beneficial and improve the water use efficiency of plants (Ben-Asher et al. 2010), serve in water scarce regions as supplement irrigation demand for reforestation and agriculture (Tomaszkiewicz et al. 2017), can negatively affect yields, because they may lead to a spread of plant disease (Agam and Berliner 2006), affect the efficiency of agrochemicals (Saab et al. 2017) and thus impact on crop yield. Modern dew harvesting can supply water for human consumption and

reduce the water scarcity in many parts of the world (Muselli et al. 2009; Tomaszkiewicz et al. 2015; Beysens 2016).

Some studies emphasized, that dew is not a significant component as it contributes only small amounts to the total annual water balance in humid areas (Malek et al. 1999), as such quantities are often an order of magnitude smaller than PET fluxes (Monteith and Unsworth 2013). Thus most studies on dew formation focused on arid and semi-arid regions (Kidron 2000; Agam and Berliner 2006), because here the impact of non-rainfall water can be considered as most significant for the water balance and the survival of various plant species (Price and Clark 2014). But during short periods, even small amounts of water from dew formation can be highly beneficial for plants not only for arid regions, but also for humid regions (Xiao et al. 2009).

Only few studies were conducted in humid areas for arable or grassland and the amount of dew was determined with artificial devices e.g. passive dewfall collector (Jacobs et al. 2008), filter papers (Hughes and Brimblecombe 1994; Kabela et al. 2009), or dewmeter (Price and Clark 2014). However, the properties of these artificial devices differed considerably from those of a natural soil-plant system. Beysens (1995) emphasized, that the formation of dew under appropriate atmospheric conditions depends mainly on the temperature and wetting properties of the substrate, which control the nucleation rate. Additionally, the wetting properties affect the form and growth of the droplet patterns (Beysens 1995). Also, the seasonal development of the land surface will impact the formation of non-rainfall water (i.e. dew and hoar frost formation), as canopy height, thermal regime, and the plant as well as soil surface will change. Thus, the dew yield of artificial devices used to collect dew or hoar frost will differ from that of dynamic and heterogeneous natural land surface coverages. All mentioned techniques to quantify the amount of dew cannot detect direct-adsorption, as their artificial surfaces properties are not able to adsorb vapour (Agam and Berliner 2006); at the same time they record not only water from dew formation but also from distillation (Xiao et al. 2009). High-precision weighable lysimeters do not have such issues, because they are filled with natural soils which can reproduce direct water adsorption and measure at the same time only the formation of dew or hoar frost, since the distilled water comes from the lysimeter interior and does not lead to a change of weight.

Earlier lysimeter studies (Meissner et al. 2007; Fank 2013) showed that such measuring systems are suitable to detect the formation of dew. However, the precision of lysimeter measurements and the temporal resolution have to be high enough in order to record such

small amounts of water on the land surface. Recent developments in lysimeter technology improved not only the precision and the temporal resolution of the measurements, but also provide a more dynamic and field related flow across the bottom of the lysimeter (Unold and Fank 2008), which is important for the temperature profile in the soil. Also, the recent study from Peters et al. (2017) showed that not only the measuring system needs certain requirements; also the pre- and post-processing of the noise-prone lysimeter balance data is of crucial importance. Xiao et al. (2009) investigated with lysimeters, which are located in the central German dry area (dryness index ~ 0.92; Meissner et al. 2009), that the seasonal vegetation cover influences the annual amount and seasonal formation of dew. It is still a research gap, how much dew and hoar frost formation contributes to the seasonal and annual water balance and how ecologically relevant those amounts are for grasslands under humid climate conditions.

In this framework, our study presents a comparison of annual and seasonal amounts of dew and hoar frost for two distinct grassland sites from Austria (alpine) and Germany (low mountain range).

Main objectives of our study are:

(1) To quantify the amount and the temporal distribution of dew and hoar frost formation over a period of two hydrological years for a low mountain range and alpine grassland.

(2) To estimate the ecological relevance of dew and hoar frost formation for a low mountain range and alpine grassland.

(3) To evaluate the use of meteorological variables to quantify the seasonal amount of non-rainfall water from dew and hoar frost formation

III.2 Material and Methods

III.2.1 Site descriptions

The study was conducted at two test sites in humid regions (see Table III. 1), one is located at the Agricultural Research and Education Centre Raumberg-Gumpenstein (GS) in the Enns Valley of Styria in Austria (Herndl et al. 2011), the other site is located in Rollesbroich (RO) in the TERENO Eifel/Lower Rhine Valley observatory in Germany (Pütz et al. 2016). At both test sites, six weighable lysimeters were established (METER Group, Munich, Germany; Figure III. 1), where at GS three lysimeters (GS1, GS2, GS6) and at RO six lysimeters (RO1 – RO6) were used to quantify amounts of water from dew and hoar frost formation.

Figure III. 1: Lysimeter station at Gumpenstein (A) and Rollesbroich (B).

Beside the lysimeters at GS, an agrometeorological station, operated by the University of Natural Resources and Life Sciences, provided standard meteorological data of air temperature, air pressure, wind speed and relative humidity. P was measured with a tipping-bucket rain gauge (Young GWU, Erftstadt, Germany). The surface temperature was measured since April 2014 at GS with an infrared radiometer sensor (SI-111, apogee Instruments, Logan, USA). Beside the lysimeters at RO, a weather station (WXT510, Vaisala Oyj, Helsinki, Finland) logged the same meteorological parameters. Measurements of P were taken from a tipping bucket rain gauge (ecoTech, Bonn, Germany). At each station, a net radiation sensor (LP Net07, Delta OHM S.rL., Caselle di Sevazzano, Italy) was installed above one lysimeter.

Table III. 1: Experimental sites, coordinates, elevation, mean values of air temperature and precipitation of both experimental sites (Gumpenstein: 1971 - 2000, Rollesbroich: 2005 - 2015), main grassland species and soil types.

Site	**Coordinates**	**Elevation**	**Mean value**		**Main species**	**Soil type**[1]
		(m a.s.l.)	air temp. (°C)	precip. (mm)		
Gumpenstein (GS)	47°29`40`` N/ 14°06`11`` E	710	7.9	1014	*Arrhenatherum elatius; Festuca pratensis*	Stagnic Cambisol
Rollesbroich (RO)	47°29`40`` N/ 14°06`11`` E	515	8.2	1150	*Lolium perenne; Trifolium repens*	Stagnic Cambisol

[1] Soils were classified through the US soil taxonomy (FAO soil type).

The grassland vegetation at the GS lysimeters is dominated by *Arrhenatherum elatius* and *Festuca pratensis*. The management of the grassland during the observation period consisted of three cuts per year where the fertilization was carried out mineral-based. The plant community of RO was classified according to Schubert et al. (2001) as ryegrass "*Lolio perennis-Cynosuretum cristati*" and the main species are *Lolium perenne* and *Trifolium repens*. The grassland vegetation on the lysimeter and the surrounding field is extensively managed with three to four cuts and two to three liquid manure applications (~1.6 l m^{-2}) per growing season during the observation period from 2013-11-01 until 2015-10-31.

III.2.2 Lysimeter set up

The set of lysimeters, with 1 m² surface area and 1.5 m depth each are regularly arranged around a central service well. The lysimeters have a controlled bottom boundary condition that enables an upward- and downward directed water flux across the lysimeter bottom, and ensures that the lysimeter water dynamics are adjusted to observed field dynamics (Groh et al. 2016). The weighing system of the lysimeter and the seepage tank allowed minutely recording water flux changes at a resolution of 10 g (0.01 mm) and 1 g (0.001 mm), respectively. The total weight measured by the lysimeter range in the observation period between 2918 and 3300 kg and 2811 and 3013 kg at RO and GS, respectively. The measurement accuracy of each lysimeter was routinely checked by a loading and unloading experiment, as proposed by Nolz et al. (2013). The matric potential at the bottom of the lysimeter is controlled and adjusted to measured matric potentials from an undisturbed soil profile nearby. All lysimeters consists of a housing area with field identical temperatures (Unold and Fank 2008; Hertel and von Unold 2014; Pütz et al. 2016). The installation depth of the time domain reflectometry probes (PICO32, IMKO GmbH, Ettlingen, Germany at GS; CS610, Campbell Scientific, North Logan, USA at RO) for soil moisture determination and the tensiometers combined with temperature sensors (T8-30 at GS, TS1 at RO both from METER Group, Munich, Germany) to determine matric potential are 0.1, 0.3 and 0.5 m. Further details of the lysimeter design can be taken from Herndl et al. (2011) and Pütz et al. (2016).

III.2.3 Quantification of dew and hoar frost formation from lysimeter data

The high temporal resolution and high measurement precision of the lysimeter balance systems are the prerequisite to quantify soil water balance components with high resolution and precision on the natural surface (grassland) and especially dew, fog or hoar frost. The

changes of the lysimeter weight are in general prone to external forces e.g. exerted by wind, management operations or animals. Hence, lysimeter data require an appropriate data processing scheme to reduce the impact of noise and errors on the determination of land surface water fluxes i.e. P and ET (Marek et al. 2014; Hannes et al. 2015; Herbrich and Gerke 2016). In a first step the raw data underwent an extensive manual and automated plausibility control (Pütz et al. 2016; Küpper et al. 2017). Subsequently, a smoothing of lysimeter data was necessary in order to further reduce the impact of noise. The AWAT-filter applies an adaptive smoothing window size and an adaptive threshold value to lysimeter weight data to improve the data reliability (Peters et al. 2014; Peters et al. 2016). A piecewise cubic Hermitian spline interpolation was carried out between anchor points and the 75^{th} percent quantile was used for the implemented snap routine (Peters et al. 2017). This filter has shown to be able to identify precisely even small land surface fluxes, e.g. low ET or dew formation (Peters et al. 2017). Processed data were finally used to calculate P and ET from lysimeter weight changes. We assume, that no ET can occur during P events (1 minute interval) and hence every increase or decrease in lysimeter mass change can be attribute to P or ET, respectively. A comparison of P measured with weighable lysimeters compared with P measured by rain gauges (tipping bucket method) tends to differ by up to 22 % (Fank 2013; Hoffmann et al. 2016; Herbrich et al. 2017; Groh et al. 2018c). One reason might be that weighable lysimeters detect P not only as rainfall, but also in form of dew, fog and hoar frost. Another part of the difference might be related to evaporation and wind errors of rain gauges (Richter 1995; Graf et al. 2014). However, during night the influence of evaporation is small and wind speed are in general much lower than at daytime.

Consequently, lysimeter data were surveyed for periods with mass increases between sunset and sunrise. These periods with mass increases of a lysimeter were subsequently compared with P from a tipping-bucket measurement. Mass increases not concurrent with rain or snow were classified as dew (Fank and Unold 2007; Meissner et al. 2007; Xiao et al. 2009) or hoar frost. Aggregated hourly amounts of dew and hoar frost were limited by the maximum rate of dew formation during clear nights (0.07 mm/h; Monteith and Unsworth 1990). Furthermore, air temperature was used to differentiate between dew and hoar frost formation. During times with air temperature below or equal to the freezing point, were related to the formation of hoar frost. Vice versa times with air temperature above zero were attributed to dew formation. This approach might lead to a slight overestimation of dew and underestimation of hoar frost, since the surface can be frozen under dew conditions (positive temperature profile) even when

the air temperature is somewhat above zero. As in many other studies, we could not differentiate between dew formation and fog (e.g. Brown et al. 2008; Xiao et al. 2009). To disentangle between fog and dew or hoar frost formation, further measurements of P droplet size, stable water isotopes, camera or light transmittance observations could be used (Meunier and Beysens 2016; Kaseke et al. 2017).

To quantify the possible ecological relevance during the above-mentioned soil and atmospheric conditions, we counted days with dew, when the water content in the topsoil (0 - 0.1 m) was below the permanent wilting point and days with hoar frost. The soil water content at the permanent wilting point was estimated according to the method proposed by Ad-hoc-Arbeitsgruppe-Boden (2005) from soil texture and bulk density data. Both can be used as indicators to quantify the ecological relevance of non-rainfall events and represent distinct ecological functions. Dew can be helpful during droughts, because the non-rainfall water reduces both plant water stress and ET. The formation of hoar frost can thermally protect the vegetation and reduced the risk of low temperature injuries of plants.

III.2.4 Estimation of potential dew and hoar frost formation from environmental variables

Dew amounts can be measured with different methods such as dew collector, dew condenser, eddy-covariance observations, blotting, drosometer, and lysimeter (Richards 2005; Meissner et al. 2007; Kabela et al. 2009; Muselli et al. 2009; Guo et al. 2016), but there is still no standard procedure and device. The same can be said for the estimation of dew and hoar frost from environmental variables. There are different approaches to assess the dew and hoar frost formation from meteorological data with: i) the energy balance, ii) the turbulent vapour transport, iii) the Bowen ratio energy balance and iiii) the Penman-Monteith (PM) equation (Neumann 1956; Jacobs et al. 1990; Madeira et al. 2001). In general, all four methods can be used to quantify dew, but differ in terms of needed variables, e.g. soil heat flux or surface temperature. The equation of the energy balance, turbulent vapour transport and the Bowen ratio energy balance require measurements of the surface temperature to estimate dew formation, which is usually not a standard meteorological variable. Hence, in our investigation the PM model will be used to assess dew and hoar frost formation. The PM equation accounts with its diabatic and adiabatic terms for the transport of energy and vapour within the atmosphere. It was applied to study dew formation over a range of different vegetation forms and regions with artificial devices (Garratt and Segal 1988; Sudmeyer et al.

1994; Jacobs et al. 1996; Jacobs et al. 1999; 2000; Luo and Goudriaan 2000; Jacobs et al. 2006; Jacobs et al. 2008). Hourly potential dew and hoar frost formation can be estimated by the FAO-PM equation (Food and Agriculture Organization) according to Allen et al. (2006):

$$PET = \frac{0.408\,\Delta\,(R_n - G) + \gamma \frac{C_n}{T_{air}+273} W_s (e_s - e_a)}{\Delta + \gamma(1 + C_d u_2)} \quad \text{[III.1]}$$

where Δ describes the increase of the saturation vapour pressure with temperature (MJ m^{-2} h^{-1}), R_n the net radiation (MJ m^{-2} h^{-1}), G the soil heat flux (MJ m^{-2} h^{-1}), γ the psychrometric constant (kPa C^{-1}), C_n and C_d are constants that changes with reference type (grass; alfalfa) and calculated time step, T_{air} the mean hourly air temperature (°C), W_s the mean hourly wind speed at 2 m height (m s^{-1}), e_s the saturation vapour pressure (kPa), and e_a the mean actual vapour pressure (kPa). Estimated values from the equation are mainly larger than zero and thus represent PET from a grass reference surface. However, occasionally nighttime PET are negative, indicating the formation of dew or hoar frost (ASCE-EWRI 2005). The necessary meteorological variables were derived from the external weather stations beside the test sites, G and R_n were obtained from direct lysimeter observations, and C_n was set according to Allen et al. (2006) to 37 and C_d to 0.24 and 0.96 for day- (R_n> 0) and nighttime. Negative nocturnal PET values were defined as potential dew or hoar frost, when T_{air} was above or below the freezing point.

III.3 Results and Discussion

III.3.1 Amount of dew and hoar frost measured with lysimeters

Figure III. 2 A and B illustrate exemplary for one lysimeter the formation of dew and hoar frost overnight and the prevailing meteorological conditions at the lysimeter station in GS. Subplot A in Figure III. 2 shows the lysimeter weight, surface temperature, air temperature (mean and range), and humidity from 2015-09-10 11 am to 2015-09-11 10 am. Before sunset and after sunrise, the lysimeter weight decreased due to ET by in total 1.19 mm, and both air and surface temperature increased. However, after sunset the lysimeter weight started to increase from 7 pm (2015-09-10) until 8 am of the following day, whereas the temperature of the surface decreased below the dew point temperature of the surrounding air. At the same time, we assume that the vapour contained in the thin layer of air above the plant starts to condense on the surface and the relative humidity was close to 100 %, which was visible with

a delay from relative humidity measurements at 2 m above the grass canopy. The external rain gauge did not detect any rain during this time period. Under such meteorological conditions, the slow increase of lysimeter weight can be related to formation conditions of dew, as the air and surface temperature stayed above zero. Hence, the increase in lysimeter weight between sunset and sunrise corresponds to the formation of dew by 0.3 mm. In the subplot B from Figure III. 2, the lysimeter weight increased between sunset and sunrise and thus corresponded to the formation of hoar frost, as surface and air temperature were below the freezing point of water. The hoar frost formation was 0.24 mm during 2014-12-09 4 pm and 2014-12-10 8 pm.

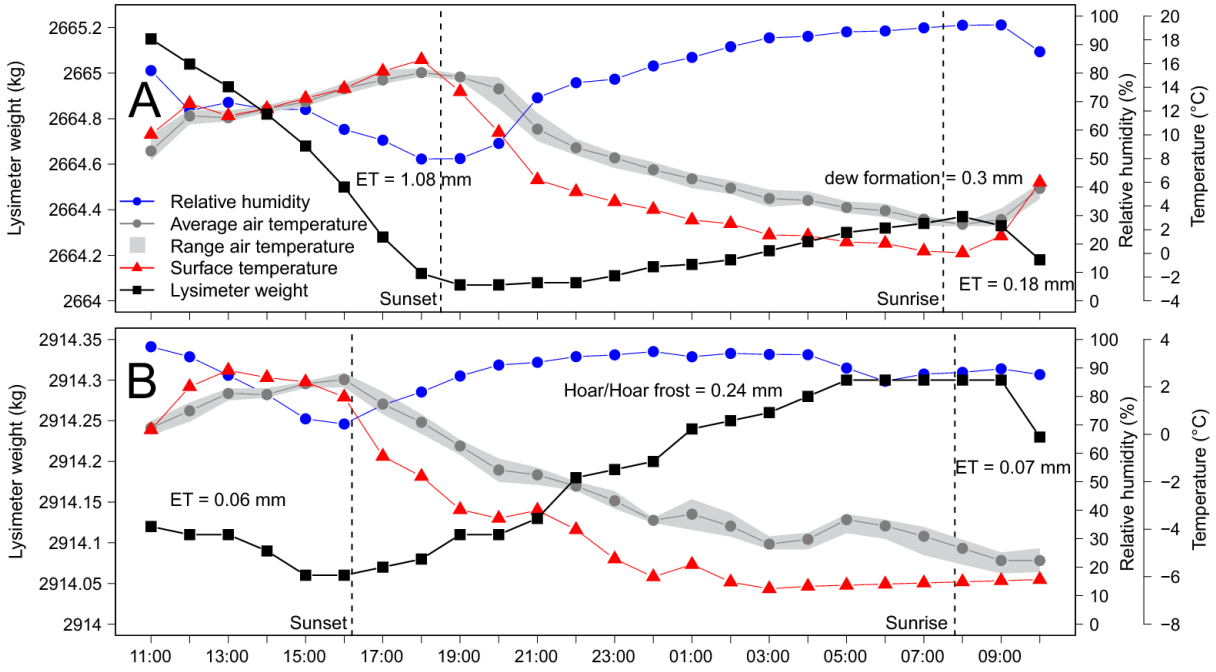

Figure III. 2: Exemplary formation of dew (A) and hoar frost (B) measured with a lysimeter (GS6) at the station Gumpenstein. Subplot A and B depict additionally the meteorological variables: relative humidity, surface and air temperature for the time period 2015-09-10 11 am until the 2015-09-11 10 am (A) and 2014-12-09 11 am and 2014-12-10 10 am (B).

The average monthly amounts of P, dew and hoar frost formation at GS and RO during two consecutive hydrological years 2013/2014 (HY-13/14) and 2014/2015 (HY-14/15) are summarized in Table III. 2. The P amount during the first hydrological year 2013/2014 was 1132.2 mm and 1126.9 mm at RO and GS, respectively. The corresponding amount of dew of 61.9 mm at RO was larger than at GS (52.1 mm). The highest monthly amount of dew formation was obtained in November at both test sites. Dew formation followed at RO in

comparison to GS a seasonal pattern with overall higher average monthly amounts of dew during autumn and winter than during spring and summer months. The dew formation reached 5.5 % and 4.6 % of the annual P at the low mountain range and alpine grassland site respectively. The spatial variability at the annual scale, which was observed between the different lysimeters at the corresponding station, was small with respect to measurement accuracy of the system, with 4.4 mm at RO and 3.6 mm at GS.

Larger average monthly amounts of hoar frost formation were achieved at both sites between November (2013) and March (2014). The total amount of water from hoar frost during the HY-13/14 was with 5.8 mm and 12.6 mm for RO and GS, respectively - clearly lower than those from dew. But in months with low air temperatures and few P, monthly values of hoar frost were up to 7.18 mm (Dec-2013), which corresponded to nearly 29 % of the monthly P amount at test site GS. The hoar frost formation contributed with 0.5 % (RO) and 1.1 % (GS) at the annual scale (HY-13/14), a rather small amount in comparison to dew. However, the spatial variability of hoar frost formation, with 0.7 mm and 0.5 mm, was clearly higher than for dew.

During the second hydrological year 2014/2015, the P amounts were 1036.8 mm at RO and 991.5 mm at GS, and thus were clearly lower than the P for the HY-13/14. At RO, the measured amount of dew was higher with 56.9 mm than at GS (38.8 mm) and the spatial variability was small with 1.9 mm and 5.2 mm at both sites. The highest monthly amount of dew formation in this HY-14/15 was achieved in December at both test sites. The average monthly contribution of dew on the P amount reached values between 2.5 -15.5 % and 1.6 - 16.3 % at RO and GS, respectively, and showed a seasonal tendency with higher contributions during winter and autumn months.

In the months January and February 2015, very few or no dew was measured at GS. During this time, the lysimeter surface was covered with a 15 cm thick snow layer for 40 days and records of lysimeter weight changes were unreliable. In HY-14/15, the dew formation reached with 5.5 % and 3.9 % of the total P similar values than for the HY-13/14 at RO and GS, respectively. The measured total water amount from hoar frost was 8.5 mm at RO and therefore larger than the year before. However, at GS hoar frost formation was with 3.3 mm clearly smaller than in HY-13/14. Hoar frost amounts reached in December 2014 with 2.57 mm a peak at RO. Dew formation in RO was in this month also large (6.8 mm) and thus both dew and hoar frost contributed together more than 10 % of the monthly amount of P. The long snow cover in the winter reduced the formation of hoar frost at GS.

Table III. 2: Monthly average amount of precipitation (P), dew and hoar frost formation obtained from lysimeter measurements for a low mountain range and alpine grassland in Rollesbroich (RO) and Gumpenstein (GS) during two consecutive hydrological years (2013/2014, 2014/2015).

Time	P		Dew						Hoar frost					
	RO	GS	RO	GS	RO	GS	RO	GS	RO	GS	RO	GS	RO	GS
	mm	mm	Mean (mm)		Stdv (mm)		% of P		Mean (mm)		Stdv (mm)		% of P	
Nov-2013	145.8	82.1	9.15	7.90	0.37	1.31	6.3	9.6	1.24	0.76	0.13	0.08	0.9	0.9
Dec-2013	76.0	25.0	7.07	2.32	0.71	0.26	9.3	9.3	1.33	7.18	0.15	2.30	1.8	28.7
Jan-2014	83.8	24.0	6.81	4.29	0.64	0.25	8.1	17.8	1.94	2.95	0.31	1.04	2.3	12.3
Feb-2014	60.3	63.8	6.51	4.40	0.65	0.6	10.8	6.9	0.28	1.33	0.10	0.51	0.5	2.1
Mar-2014	30.3	87.1	2.59	4.37	0.48	0.37	8.5	5.0	0.89	0.29	0.12	0.05	2.9	0.3
Apr-2014	52.0	93.8	3.60	4.92	0.79	0.7	6.9	5.2	0.09	0.05	0.08	0.03	0.2	0.1
May-2014	74.5	136.3	3.55	5.76	0.60	1	4.8	4.2	0.03	0.00	0.01	0.00	0.0	0.0
Jun-2014	94.2	91.9	2.85	1.62	0.48	0.23	3.0	1.8	0.00	0.00	0.00	0.00	0.0	0.0
Jul-2014	202.6	135.4	4.01	2.58	0.36	0.89	2.0	1.9	0.00	0.00	0.00	0.00	0.0	0.0
Aug-2014	169.1	151.1	4.52	4.18	0.49	0.03	2.7	2.8	0.00	0.00	0.00	0.00	0.0	0.0
Sep-2014	59.7	136.4	4.05	5.46	0.73	0.21	6.8	4.0	0.00	0.00	0.00	0.00	0.0	0.0
Oct-2014	84.0	99.9	7.23	4.28	0.40	0.17	8.6	4.3	0.00	0.06	0.00	0.03	0.0	0.1
ΣHY13/14	**1132.2**	**1126.9**	**61.9**	**52.1**	**4.4**	**3.6**	**5.5**	**4.6**	**5.8**	**12.6**	**0.7**	**0.5**	**0.5**	**1.1**
Nov-2014	57.4	32.0	7.42	4.70	0.30	0.66	12.9	14.7	0.22	0.19	0.03	0.03	0.4	0.6
Dec-2014	123.5	33.2	8.44	5.42	0.70	0.11	6.8	16.3	2.57	1.56	0.20	0.15	2.1	4.7
Jan-2015	122.9	120.8*	5.30	#	0.50	#	4.3	#	1.61	#	0.98	#	1.3	#
Feb-2015	63.1	19.1*	3.12	#	0.39	#	5.0	#	2.09	#	0.79	#	3.3	#
Mar-2015	102.9	33.2	4.96	3.55	0.18	0.70	4.8	10.7	1.10	0.87	0.22	0.19	1.1	2.6
Apr-2015	67.4	45.7	3.05	3.31	0.27	1.72	4.5	7.2	0.54	0.61	0.10	0.30	0.8	1.3
May-2015	49.7	140.7	3.25	3.63	0.24	0.33	6.6	2.6	0.13	0.00	0.01	0.00	0.3	0.0
Jun-2015	79.8	120.6	2.39	3.55	0.07	0.12	3.0	2.9	0	0.00	0.00	0.00	0.0	0.0
Jul-2015	101.8	171.8	2.55	2.75	0.21	0.28	2.5	1.6	0	0.00	0.00	0.00	0.0	0.0
Aug-2015	89.5	49.4	4.70	2.62	0.30	0.34	5.2	5.3	0	0.00	0.00	0.00	0.0	0.0
Sep-2015	138.7	133.3	5.50	4.26	0.21	1.08	4.0	3.2	0	0.00	0.00	0.00	0.0	0.0
Oct-2015	40.2	91.7	6.25	4.98	0.34	1.08	15.5	5.4	0.24	0.04	0.02	0.03	0.6	0.0
ΣHY14/15	**1036.8**	**991.5**	**56.9**	**38.8**	**1.9**	**5.3**	**5.5**	**3.9**	**8.5**	**3.3**	**1.9**	**0.3**	**0.8**	**0.3**
# no or missing lysimeter data during times with closed snow cover														
***** daily value obtained from external reference measurement device														

Our results are in line with previous studies, which showed that dew contributes on a yearly base between 4.5 % - 6.9 % of the total P for different grassland sites under regional climate conditions in Croatia, Germany, and the Netherlands (Jacobs et al. 2006; Xiao et al. 2009; Heusinger and Weber 2015). Dew formation for arid- and semi-arid climates were reported for various continents, e.g. Africa, Australia, South and North America and ranged for different land cover forms from 2 % up to 48 % of the total P (Baier 1966; Evenari et al. 1971; Sharma 1976; Malek et al. 1999; Kalthoff et al. 2006; Hanisch et al. 2015). Kalthoff et al. (2006) reported for an arid valley in Chile, located south of the hyper-arid Atacama Desert, that dew formation, which ranged between 5 mm to 10 mm, can even reach the dimension of yearly P amounts in extreme dry years. It suggests that the contribution of dew on the annual P amount is much larger under drier climatic conditions. Most studies on non-rainfall events were conducted in arid to semi-arid regions. Thus, very little data exists on the quantification of water added to soil-plant system by hoar frost formation on the yearly basis. While hoar frost does not occur during the main vegetation period, it can be of ecological relevance for the plant, as will be shown in the following section.

III.3.2 Ecological relevance of dew and hoar frost

The indicator to quantify the ecological relevance of dew formation is summarized in Table III. 3 and describes the average number of days per month with dew during water stress. The critical soil water content at the permanent wilting point was set according to texture and bulk density information from the topsoil on $0.22\ m^3\ m^{-3}$ and $0.12\ m^3\ m^{-3}$ at RO and GS, respectively. Plant water stress can occur in dependence on vegetation type much earlier than at the permanent wilting point, but verifying this requires leaf water potential measurements of the grassland ecosystem. In the first hydrological year, no water stress occurred and hence the ecological relevance of dew was due to relatively humid conditions negligible at both test sites. This was also the case for the second HY 14/15 at GS. However, for RO in months June, July and August 2015, 5 to 11 days per month were observed where dew occurred during times with water stress in the upper soil layer. The standard deviation for those months was relatively high and ranged between 3 to 6 days. This suggests that the ecological relevance of dew varied over space. This is mainly related to pronounced differences in soil water contents at the same depth in different locations caused by spatial variations in hydraulic parameters and is in line with a study at the catchment scale from a soil moisture sensor network (Qu et al. 2014). The dry conditions in those months agreed well with a large

scale investigation, which demonstrated that most parts of Europe were affected by a drought (Ionita et al. 2016), which was after the exceptional drought in 2003 one of the most severe droughts in the region (Laaha et al. 2016). Thus, dew is also under humid climate conditions an important water supply during periods of drought, when plants have only limited access to available water resources in the effective root zone (Agam and Berliner 2006; Ben-Asher et al. 2010).

Table III. 3: The ecological relevance of dew and hoar frost at both grassland sites (RO: Rollesbroich; GS:Gumpenstein) are expressed as number of days with hoar frost or days with water stress and dew formation per month.

Time	Dew during water stress				Days with hoar frost			
	RO		GS		RO		GS	
	Mean	Stdv	Mean	Stdv	Mean	Stdv	Mean	Stdv
Nov-2013	0.0	0.0	0.0	0.0	10.8	0.9	7.0	1.4
Dec-2013	0.0	0.0	0.0	0.0	10.8	0.4	24.3	0.5
Jan-2014	0.0	0.0	0.0	0.0	12.5	0.5	18.0	0.8
Feb-2014	0.0	0.0	0.0	0.0	6.5	1.1	18.0	1.2
Mar-2014	0.0	0.0	0.0	0.0	8.0	1.2	10.0	1.4
Apr-2014	0.0	0.0	0.0	0.0	2.3	0.7	2.0	0.0
May-2014	0.0	0.0	0.0	0.0	1.0	0.0	1.0	0.5
Jun-2014	1.0	1.8	0.0	0.0	0.0	0.0	0.0	0.0
Jul-2014	0.0	0.0	0.0	0.0	0.0	0.0	0.0	0.0
Aug-2014	0.0	0.0	0.0	0.0	0.0	0.0	0.0	0.0
Sep-2014	0.0	0.0	0.0	0.0	0.0	0.0	0.0	0.0
Oct-2014	0.0	0.0	0.0	0.0	0.0	0.0	1.3	0.5
Σ-HY13/14	**1.0**	**1.8**	**0.0**	**0.0**	**51.9**	**4.2**	**81.6**	**2.1**
Nov-2014	0.0	0.0	0.0	0.0	5.8	0.4	6.7	0.5
Dec-2014	0.0	0.0	0.0	0.0	11.5	0.8	15.0	0.8
Jan-2015	0.0	0.0	0.0	0.0	8.5	0.8	0.0	0.0
Feb-2015	0.0	0.0	0.0	0.0	10.8	0.4	0.0	0.0
Mar-2015	0.0	0.0	0.0	0.0	13.0	0.0	11.7	2.6
Apr-2015	0.0	0.0	0.0	0.0	12.0	1.2	6.3	1.7
May-2015	0.0	0.0	0.0	0.0	2.0	0.0	0.0	0.0
Jun-2015	10.7	3.9	0.0	0.0	0.0	0.0	0.0	0.0
Jul-2015	11.3	6.0	0.0	0.0	0.0	0.0	0.0	0.0
Aug-2015	5.3	2.7	0.0	0.0	0.0	0.0	0.0	0.0
Sep-2015	0.0	0.0	0.0	0.0	0.0	0.0	0.0	0.0
Oct-2015	0.0	0.0	0.0	0.0	3.0	0.0	1.0	0.0
Σ-HY14/15	**27.3**	**12.1**	**0.0**	**0.0**	**66.6**	**1.4**	**40.7**	**2.9**

A second ecological function of dew could be a suppression or reduction of transpiration rates during early morning hours, which prevents higher water loss due to transpiration especially at times with a high atmospheric ET demand during drought periods. A recent study by Gerlein-Safdi et al. (2017) confirmed this and showed, that dew formation induced suppression of plant transpiration processes of a tropical plant *Colocasia esculenta*.

The indicator to quantify the ecological relevance of hoar frost formation also is summarized in Table III. 3 and describes the days with hoar frost. For hoar frost, Table III. 3 shows, that during November until April, depending on the seasonal meteorological conditions average monthly days with hoar frost ranged between 1 and 13 days at RO and between 1 and 24 days at GS. On the annual scale, we can see that in HY-13/14 on more than 52 and 82 days and in HY-14/15 on 67 and 41 days hoar frost at RO and GS, respectively. During the formation process of hoar frost ("white frost") heat is released, when liquid water vapour freezes to ice on the plant surface and thus, naturally protected plant tissues from freezing and causes less damage on plants than the so-called black frost, which forms under drier atmospheric air conditions (Snyder et al. 2005; Pessarakli 2014). The lower values of days with hoar frost in GS HY-14/15 can be explained by the closed snow cover in January and February, which provides in addition to hoar frost an optimal insulation from lethal freezing temperatures (Thorsen et al. 2010).

Our study results indicate that dew and hoar frost formation fulfils an important ecological function for grassland and thus might be of ecological relevance during periods of drought and wintertime, but further plant specific observations are of need to directly quantify the ecological relevance and impact of non-rainfall water on the development of plant communities and their functional traits.

III.3.3 Comparison of actual and potential dew and hoar frost formation

Figure III. 3 depicts the measured and estimated monthly amounts of dew and hoar frost formation at both test sites. Estimates of potential dew achieved values of 25.0 mm and 17.3 mm at RO and 38.7 mm and 32.2 mm at GS for the HY-13/14 and HY-14/15. Thus, the PM model underestimated the formation of dew on average on a yearly scale by 64.4 % (38.0 mm) and 22.0 % (10.4 mm) at RO and GS, respectively. The seasonal patterns of dew formation were captured well at both sites with the PM model (see Figure III. 3 A and C). An underestimation of potential dew formation at GS by the PM model was notable for November 2013 and during the months January until May.

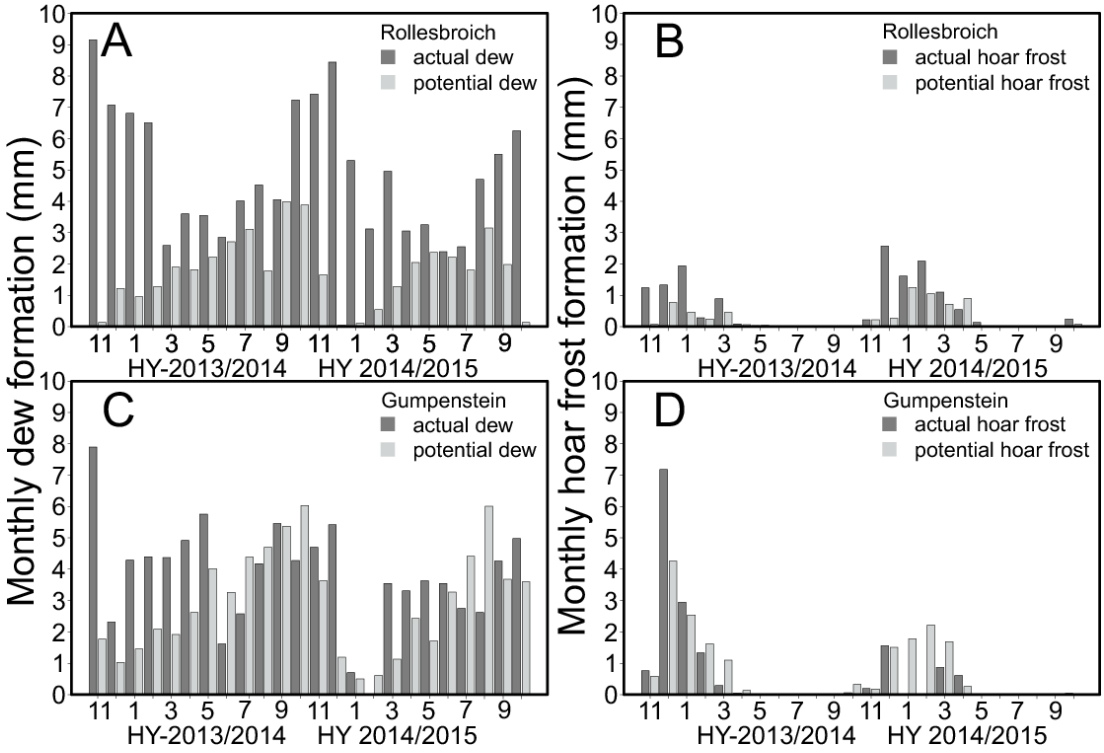

Figure III. 3: Monthly amount of actual and potential amount of dew formation at Rollesbroich (A) and Gumpenstein (C). Monthly amounts of actual and potential hoar frost formation at the Rollesbroich (B) and Gumpenstein (D) test site.

For RO, we observed a general underestimation of dew by the PM model. This was more pronounced during autumn to winter (SONDJF) than in spring to summer months (MAMJJA). The larger deviations during this period of time at the test site RO might be related to nighttime transpiration. The average diurnal cycle of PET during both periods is depicted in Figure III. 4 for both sites. Decreasing surface temperature (radiative cooling) combined with sufficient moisture in the air in the night with a small adiabatic term results in negative values of PET, which indicate the formation of dew (ASCE-EWRI 2005). This is more pronounced during spring to summer (MAMJJA), because of higher radiative cooling (clear nights, fewer clouds) and the fact that vapour holding capacity of air increases exponentially with air temperature. Thus, average hourly PET rates during the vegetation period (MAMJJA) are much lower than during autumn and winter time (SONDJF; see Figure III. 4). Dew formation started at both sites during period MAMJJA in the late evening (8 pm) and lasted until early morning hours (5 pm). However, for the autumn to winter period (SONDJF) PET during nighttime showed only at the GS test site the formation of dew or hoar frost. The corresponding values of PET during night at RO were on average above zero and predicted the occurrence of nighttime PET. Recent investigations with lysimeters at RO

nevertheless confirmed the occurrence of nighttime ET (Groh et al. 2018a). However, investigation also reveals that larger nighttime PET rates are related to relative high wind speeds during night in periods SONDJF (on average >3 m s^{-1}), which consequently enlarged the adiabatic term and exceeded the diabatic component in the PM equation. This suggests that the PM model tends to underestimate dew formation at test sites with large wind speeds at night.

The estimates of potential hoar frost achieved on average 3.3 mm and 9.1 mm at the annual scale at RO and GS, respectively. The seasonal monthly tendency was captured well for both sites with the PM model. However, single months especially at the beginning of November until December showed a clear underestimation of hoar frost with the PM model. For the second hydrological year the PM model showed an overestimation by in total 4.4 mm at GS. This can be related mainly to missing information on hoar frost formation during the time from January until February 2015, where the lysimeter surface was covered by snow. Thus, our results showed that the PM model is in general able to capture well the seasonal tendency of dew and hoar frost formation at both sites. But our investigation also demonstrates that the PM model underestimated dew and hoar frost formation during colder time of the year and under specific meteorological conditions like high wind speeds at night.

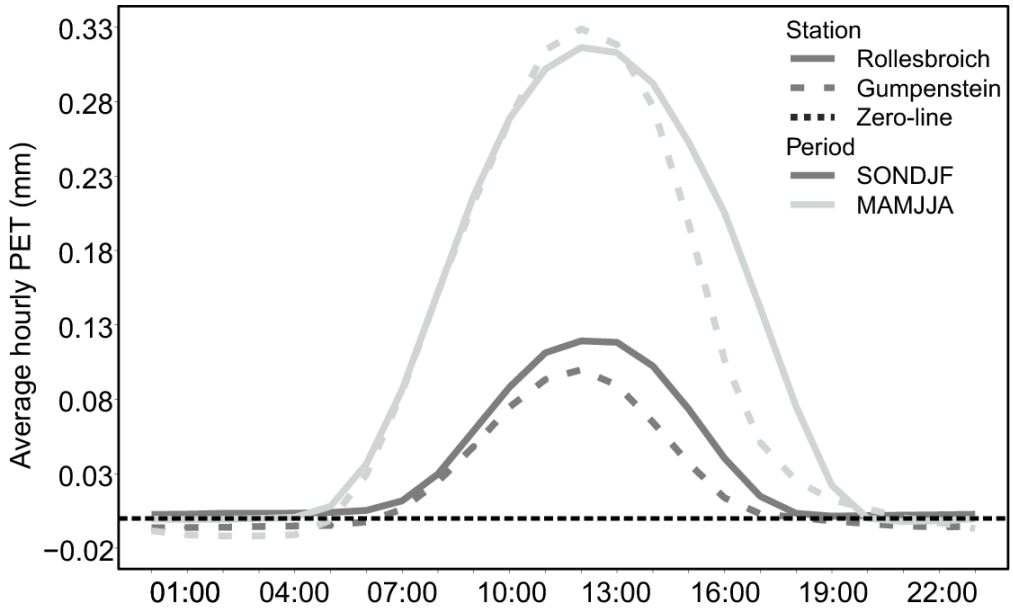

Figure III. 4: Average hourly potential evapotranspiration (PET) at the lysimeter station in Rollesbroich and Gumpenstein during autumn to winter (SONDJF) and spring to summer months (MAMJJA).

III.4 Conclusion

Our analysis provides observations of dew and hoar frost formation for two distinct grassland ecosystems at a low mountain range and alpine site over two consecutive hydrological years. The dew and hoar frost formation ranged between 42.1 - 67.7 mm, which corresponds to 4.2 – 6.0 % of the P on a yearly basis. Seasonal patterns of dew and hoar frost amounts were in general larger during autumn and winter months. In winter months, with lower P events, dew and hoar frost formation contributed together substantially to the total monthly P amount (up to 38 %). Moreover, our investigation showed that dew was an ecologically important source of water during periods of drought, when plants had only a limited access on water resources in the effective root zone. During colder periods of the year, hoar frost formation took over an ecological function at both grassland sites as it thermally protected crops and thus potentially reduced the risk of low temperature injuries of plants.

The estimates of potential dew and hoar frost formation with the PM model were underestimated, but showed in general promising results to capture the observed seasonal patterns and amount of additional P water. The mean underestimation between calculated and measured dew and hoar frost on a yearly scale were 63.2 % and 16.6 % at RO and GS, respectively. Using the PM model might thus enable to account for dew and hoar frost at large scales (e.g. catchment, landscape, continents). However, the PM model underestimated dew and hoar frost formation during colder periods and specific meteorological conditions (i.e. high wind speeds at night).

The study revealed that dew and hoar frost formation contribute substantially to the water budgets of a low mountain range and alpine grassland site. Non-rainfall water can be of relevance, when quantifying water budget components at larger scales, as it might impact the transport of contaminants (transit time), nutrient budgets, alter ET, change the water use efficiency and consequently affect the seasonal crop growth. The urgency to account for such water fluxes is even more important for studies in arid- semiarid regions, where water scarcity often occurs during the year and which might be more sensitive to climate variability and climate change. Recent investigations for the Mediterranean region indicate, that climate change will lead to a substantial reduction of dew yields and thus amplify water scarcity (Tomaszkiewicz et al. 2016). This demonstrates the overall importance to precisely quantify low P fluxes, such as dew and hoar frost formation, in the water and nutrient cycling of ecosystems, especially in the context of climate change and occurrence of droughts. However,

there is still a lack of information, how different vegetation types and soils affect the formation of dew and hoar frost, as most recent dew studies were conducted with devices, which have artificial surface (e.g. dew condenser), because their main research focused was to increase dew yield for human consumption. These substrates largely differ in terms of wetting properties from natural surface and thus might amplify the bias to estimate dew and hoar frost formation for different ecosystems. Additionally, dew condensers often not only quantify the amount of dew, but also from dew condensation, which complicates to distinguish between different water sources of dew observed with an artificial and natural measurement device. However, water from soil distillation matters only close to ground under strong humidity and temperature gradients, and typically during low wind speed (Monteith 1957).

IV Quantification of nighttime evapotranspiration for two distinct grassland ecosystems

This chapter is based on a journal article submitted as:

Groh, J.*, Pütz, T., Vanderborght, J., and Vereecken, H., Quantification of nighttime evapotranspiration for two distinct grassland ecosystems, *Water Resources Research* (submitted)

IV.1 Introduction

In the past, models often assumed that nighttime transpiration is negligible as the widespread stomatal optimization theory suggested that plants try to maximize their carbon gain while minimizing the water loss (Cowan and Farquhar 1977). Therefore, scientists traditionally assumed that at the leaf level stomata are closed during non-photosynthetic periods to prevent water loss through transpiration. Various observations at the leaf level showed an incomplete stomatal closure or sap-flow during the night for a range of C3 and C4 species (Caird et al. 2007a; Rogiers et al. 2009; Forster 2014; Coupel-Ledru et al. 2016; O'Keefe 2016), which involves a loss of water at night without carbon assimilation. Investigations reported that nighttime ecosystem transpiration could account in arid to semi-humid conditions for 10 – 55 % of the daytime transpiration and hence it contributes substantially to the total ET (Caird et al. 2007a; Skaggs and Irmak 2011; Wang and Dickinson 2012; Schoppach et al. 2014; Resco de Dios et al. 2015). A recent simulation study with a global land-surface model (CLM4.5SP) considering updated nighttime stomatal conductance values showed that such an extension increased the transpiration by up to 5 % globally and reduced soil moisture (Lombardozzi et al. 2017). This overnight increase in water use can result in a major reduction of water use efficiency WUE at the single plant and landscape level (Chaves et al. 2016). Moreover extreme weather conditions like warm spells or heat waves, which frequency are expected to increase due to climate change (Fischer and Schar 2010), could affect nighttime transpiration and WUE. This increasing evidence suggests that nighttime transpiration significantly contributes to the water cycle. Resco de Dios et al. (2015) pointed out that nighttime water loss could have a higher impact on the global ET than current changes of ET by global warming.

Nighttime stomatal conductance or sap-flow measurements have been reported for a wide range of climate conditions (arid, humid), species and ecosystem, but the environmental factors that regulate such nighttime water losses are still poorly understood (Zeppel et al. 2014). Eddy covariance observations for three distinct ecosystems showed that the ratio of nighttime evapotranspiration (ET_N) to daytime evapotranspiration (ET_D) were not only dependent on the land surface cover type but also on the seasonal environmental conditions (Novick et al. 2009). Leaf gas exchange, nocturnal stomatal conductance or sap-flow, which are associated with ET_N, were found to respond to exogenous drivers like wind speed (Karpul and West 2016), air temperature (Fisher et al. 2007), and vapor pressure deficit (Fisher et al. 2007; Novick et al. 2009; Doronila and Forster 2015), and to depend on soil water (Howard

and Donovan 2007) and nutrient availability (Eller et al. 2017). But, counteracting effects of different drivers prevented some authors from observing clear effects from single drivers (Fisher et al. 2007; Howard and Donovan 2007). Therefore, a better understanding and quantification of nighttime water loss in different ecosystems and for different environmental conditions is still an important research topic in land surface hydrology.

The reported estimates of ET_N were often derived from measurements over a relatively short period, on a single plant, or under partially controlled atmospheric and soil conditions (e.g. Liu et al. 2015; Resco de Dios et al. 2015; Coupel-Ledru et al. 2016) and with different, often indirect methods. For instance, sap-flow in trees during night may also be a result of recharge of depleted stem internal water storage (Dawson et al. 2007), so additional measurements e.g. leaf gas exchange and correction methods (e.g. Karpul and West 2016) are necessary to estimate nighttime transpiration from sap flow. Sap flow measurements are not necessarily related to transpiration (Wang et al. 2012), observations can differ according to the technology used to measure sap flow (Forster 2014). The disadvantage of using gas exchange measurements to estimate nighttime transpiration is that the measurements disturb the leaf surrounding environment, are limited in time, and samples represent only a relative small area of the ecosystem specific canopy (Ewers 2013). Concerning eddy-covariance, stable atmospheric and low wind conditions paired with relative small ET fluxes during night (Pattey et al. 2002) makes this method often unsuitable to estimate nighttime ET.

High precision weighing lysimeters offer an alternative to obtain estimates of nighttime transpiration over a long time period, under natural outdoor conditions, for non-woody plants and a representative number of plants. Recent developments in lysimeter science improved the precision of measurements, the temporal resolution of measurements, and the control of the lower boundary (Unold and Fank 2008). The use of a tension controlled lower boundary condition provides a more dynamic control, is based on field tension measurements and thus enables upward directed water fluxes. This is important and improves ET estimations with lysimeters, as upward directed water fluxes from shallow groundwater tables or deeper soil layers enhance ET processes (Schwaerzel and Bohl 2003; Karimov et al. 2014; Groh et al. 2016). Also the pre- and post-processing to reduce the impact of noise on lysimeter balance data has been improved substantially (Marek et al. 2014; Peters et al. 2014; Pütz et al. 2016; Küpper et al. 2017; Peters et al. 2017). Hence we used state of the art weighable lysimeter systems with a high temporal resolution and precision to quantify nighttime ET and to investigate the following points:

(1) What is the contribution of ET_N to the total ET on the seasonal and annual time scale in a natural and in an extensively used grassland ecosystem in a humid and temperate climate?
(2) Which atmospheric and soil related drivers control nighttime and daytime ET?
(3) Can approaches that are used to predict ET based on meteorological variables and that are based on land surfaces energy balances predict ET_N and its contribution to the total ET?
(4) To what extent is ET_N increased during heat waves and can this increase be predicted?

IV.2 Material and Methods

IV.2.1 Site descriptions

The study was carried out at the grassland stations in Rollesbroich (50°37′12”N, 6°18′15”E, 515 m a.s.l.) and Wüstebach (50°30’10”N, 6°19’41”E, 625 m a.s.l.). Both are located in the TERENO Eifel/ Lower Rhine Valley observatory in Germany and belong to the German wide lysimeter network SOILCan (Bogena et al. 2015; Bogena et al. 2016; Pütz et al. 2016). The vegetation on and around the lysimeters in Wüstebach, which is located in the Eifel National Park, corresponds to a natural forest meadow with no active land use. Main species are *Agrostis capillaris* and *Galium saxatile*. Beneath the grass and shrub canopy a 5 – 10 cm thick moss layer (*Rhytidiadelphus squarosus*) covers the lysimeter surfaces. The grassland vegetation on the lysimeters and the surrounding field at Rollesbroich is extensively managed with three to four cuts per growing season during the observation period from 1 January 2013 until 31 December 2016. In accordance to the local agricultural management of the surrounding grassland, liquid manure was applied (~1.6 L m^{-2}) two to three times per growing season. The plant community consists mainly of *Lolium perenne* and *Trifolium repens*. Both sites have a humid temperate climate with a mean annual P of 1150 mm and 1200 mm and a mean annual temperature of 8°C and 7.5°C for Rollesbroich and Wüstebach, respectively (Pütz et al. 2016).

Since December 2010, stations composed of six weighable, cylindrical, high precision lysimeters (METER, Munich) each with a surface of 1 m² and a depth of 1.5 m were installed at both sites. Each lysimeter was placed on three load cells with a 10 g resolution, which corresponds to water depth of ≈ 0.01 mm. The lysimeters have controlled bottom boundaries, which permit down- and upward directed water fluxes. The water flux across the bottom boundary is controlled by field measurements of soil water potentials at the corresponding

depth (1.4 m) and hence contributes to a better representation of land surface fluxes (Groh et al. 2016). At both sites, the lysimeters contain undisturbed soil monoliths of a Stagnic Cambisol. The lysimeters were equipped with time domain reflectometry probes (CS610, Campbell Scientific, North Logan, UT, USA) to measure soil moisture at 0.1 m and heat fluxes plates (HFP-01, Hukseflux Thermal Sensors B.V., Delft, the Netherlands) to measure heat flux in 0.1 m. At each station, a net radiation sensor (LP Net07, Delta OHM S.r.L., Caselle di Sevazzano, Italy) was installed above one lysimeter. Beside the lysimeter stations, a weather station (WXT510, Vaisala Oyj, Helsinki, Finland) provides standard meteorological parameters on wind speed, air temperature, relative humidity, air pressure and P.

Meteorological parameters were used to calculate the hourly PET for a hypothetical grass surface with the Penman-Monteith PM equation (Allen et al. 1998). Time series of sensed net radiation and soil heat flux were used in the equation to estimate hourly PET. According to Allen et al. (2006), surface resistance, r_s, was set to 50 s m^{-1} for daytime, i.e. when the net radiation $R_n > 0$, and 200 s m^{-1} for nighttime calculations. The larger resistance for nighttime calculations is used to represent the effect of stomatal closure at night.

IV.2.2 Lysimeter data and statistical analysis

Lysimeter weight measurements are in general prone to external disturbances like animals, management operations and wind. These can have a significant impact on land surface water flux rates derived from lysimeter weights (Marek et al. 2014). The separation of P and ET from lysimeter weight changes requires an appropriate data pre- and post-processing scheme to minimize the effect that external errors and noise have on the determination of land surface water fluxes. The lysimeter raw data first underwent an extensive manual and automated plausibility check (more details see Groh et al. 2015; Pütz et al. 2016; Küpper et al. 2017). In the next step we used the “adaptive window and threshold” filter (AWAT; Peters et al. 2017) to further reduce the impact of noise from the lysimeter weight changes on the determination of land surface water fluxes. The parameters of the AWAT filter were set to 31 min for the maximum window width, 0.2 mm for the maximum threshold, and 0.75 for the quantiles of the snap-routine (see Peters et al. (2014) and Peters et al. (2017) for the definition of these parameters). A recent study by Peters et al. (2017) showed that a combined use of the AWAT-filter and the implemented snap-routine can quantify low water fluxes, such as dew formation (e.g. 0.008 mm/h).

We analyzed the land surface flux data for both sites and for four consecutive years (1 January 2013 until 31 December 2016) to quantify the amount of water loss due to nighttime

ET. The photoperiod length and the intensity of light might affect the degree and velocity to which plants close their stomata during the night (Schwabe 1952; Caird et al. 2007a) and impact ET. Hence ET was calculated for the following periods:

- dawn evapotranspiration (ET_{dawn}) during the period from nautical dawn (when the geometric center of the sun is 12° below the horizon) and sunrise (when the geometric center is at 0° relative to the horizon),
- dusk evapotranspiration (ET_{dusk}) during the period between sunset (0° relative to the horizon) and nautical dusk (geometric center of the sun is 12° below the horizon),
- nocturnal evapotranspiration (ET_{noc}) between nautical dusk and nautical dawn.

The sum of ET_{dawn}, ET_{dusk}, and ET_{noc} was the total ET_N. The functions "*sunriset*" and "*crepuscule*" from the R software package "*maptools*" V0.9-2 (Bivand and Lewin-Koch 2016), which are based on astronomical algorithms of Meeus (1991), were used to obtain the time of nautical dawn, sunrise, sunset and nautical dusk for every day. The measured annual amounts of ET_{dusk}, ET_{dawn} and $ET_{noctural}$ were compared with the PET calculated using the FAO PM equation, to clarify how well the widely used approach can account for water losses during nighttime. In a next step averaged monthly ET amounts and rates during dawn, dusk and nocturnal periods were compared to investigate their intra-annual variability.

Linear correlations between monthly averaged rates of ET_D, ET_{dusk}, ET_{dawn} and ET_{noc} and corresponding calculated PET's were investigated. Subsequently, stepwise linear regression were carried out to identify relations between monthly averaged measured ET rates and soil and meteorological variables: like soil moisture (θ; vol.- %), soil heat flux (G; MJ m^{-2}), air temperature at 2 m (T_{air}; °C), air pressure (P_a; hPa), relative humidity (RH; %), wind speed at 2 m (W_s; m s^{-1}), vapor pressure deficit (VPD; kPa), and net radiation (R_n; MJ m^{-2}).

Diagnostic plots for linear regression analysis (q-q-plot, residual plot) were used to check the assumption of normality and homogeneity. The functions "*step*" and "*lm*" from the R software package "*stats*" (R-Core-Team 2016) were used to perform a stepwise linear regression model (direction = both). Regression was carried out for the entire data set and for a split data set in which the observation period was divided into two different seasons: Non-growing season during autumn and winter (NGS; October - February) and growing season during spring and summer (GS; March - September).

IV.3 Results and Discussion

IV.3.1 Environmental conditions and annual nighttime evapotranspiration

The total annual amounts of P, obtained from six lysimeters respectively, for four consecutive years across the two grassland locations ranged between 1048 - 1239 mm for Wüstebach and between 1024 - 1133 mm for Rollesbroich. Differences in annual land surface fluxes were notably larger for ET fluxes than for P between both grassland ecosystems. Annual ET values ranged between 393 - 440 mm for Wüstebach and 620 - 685 mm for Rollesbroich (see Figure IV. 1 e). Also nighttime ET was higher in Rollesbroich (36.5 - 60.6 mm) than in Wüstebach (11.6 - 17.9 mm, Figure IV. 1 d). The relative difference of the nighttime ET between the two sites was considerably larger than the difference in total ET. Annual ET during dusk ranged between 1.6 - 2.6 mm for Wüstebach and 7 - 10 mm for Rollesbroich (Figure IV. 1 b) and was larger than the ET during dawn which ranged for Wüstebach between 1.2 - 2.3 mm and for Rollesbroich between 4.1 - 5.5 mm (Figure IV. 1 a). Annual ET during nocturnal periods ranged between 8.5 - 13.1 mm for Wüstebach and 25.5 - 45.0 mm for Rollesbroich (Figure IV. 1 c). The average ET rates decreased from dusk to nocturnal periods to dawn from 0.0158 mm h^{-1} to 0.0094 mm h^{-1} at Rollesbroich and from 0.0042 mm h^{-1} to 0.0037 mm h^{-1} at Wüstebach. Long term annual averaged ET_N was 7.6 % and 3.7 % of the daytime ET and ranged annually between 6.3 - 10.1 % and 3 - 4.4 % at Rollesbroich and Wüstebach, respectively. This result demonstrated that water loss between sunset and sunrise significantly contributes to total ET at the annual scale and might thus reduce the WUE of the ecosystem. Our findings are in line with previous observations from Novick et al. (2009), which showed for a grassland ecosystem in Durham (North-Carolina, USA) that ET_N at the annual scale were on average 8 % of the ET_D. Please note lysimeter observations provide combined information on evaporation and transpiration. Thus despite the large evidence of nighttime transpiration (Caird et al. 2007a; Forster 2014), we cannot exclude that nighttime water losses stems partially from evaporation processes from the soil or plant surface (dew-rise, guttation, canopy intercept) or the plant itself (stomata, cuticula).

Both annual ET_D and ET_N were much smaller in Wüstebach than in Rollesbroich. The lysimeter station in Wüstebach is located on a clearing with natural forest meadow and the surrounding area is covered by Norway Spruce (Picea abis L.). Thus, the station exposure and surrounding land use type in Wüstebach might reduce the ET. The differences in annual ET measurements between the two sites were well reproduced by the annual PET estimates (see

Figure IV. 1 e) so that these differences were mainly due to different meteorological conditions at the two sites whereas differences in vegetation and management did not play an important role. The measured daily ETs were also close to the calculated PET which indicates that at these humid sites, there was hardly water stress (Figure IV. 1 f).

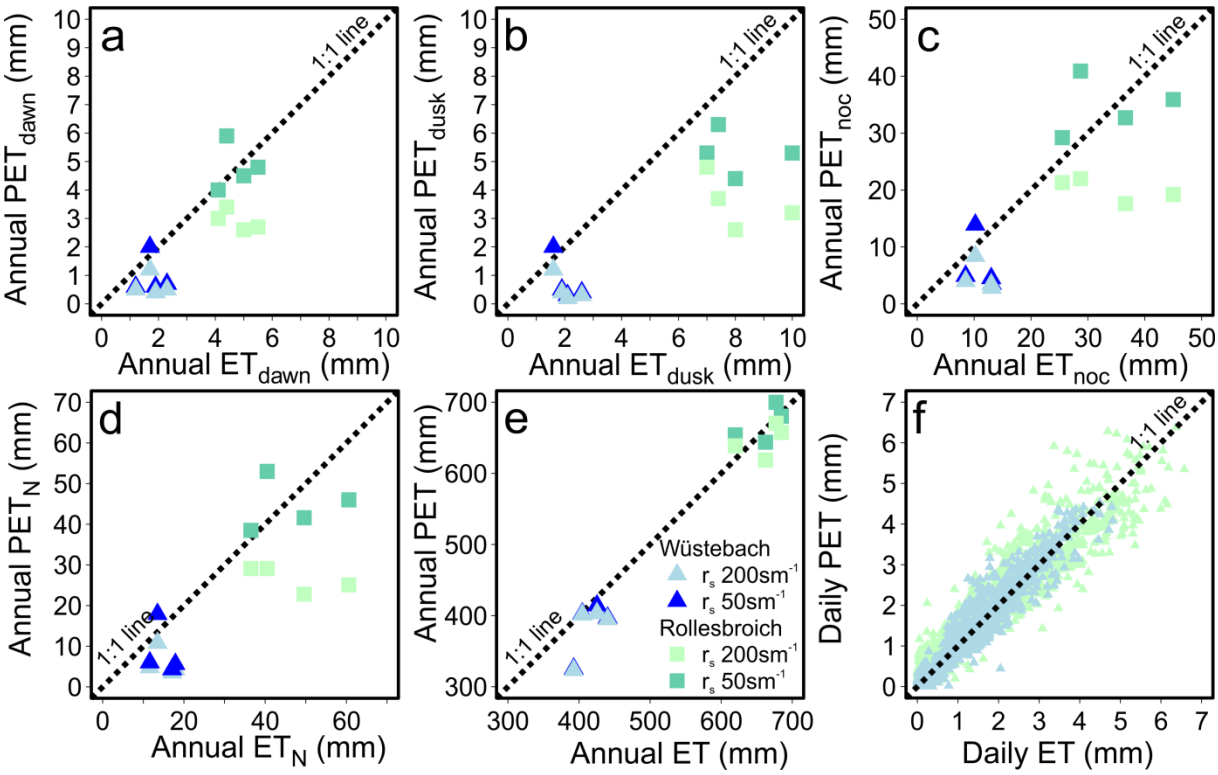

Figure IV. 1: Scatterplot of calculated PET and measured ET during dawn (a), dusk (b), nocturnal periods (c), nighttime (d), and day and night (e) at the annual scale in Rollesbroich (square) and Wüstebach (triangle). Subplot f represents daily values of calculated PET and measured ET values (2013 - 2016). Daily PET was derived from hourly PET which was estimated with r_s parameter for nighttime with 200 s m^{-1}.

However, the calculated PET during dawn, dusk, and nocturnal periods were in general much smaller than corresponding ET values derived from lysimeter observations. Hence the recommended approach to estimate hourly PET according to Allen et al. (2006) underestimated PET during different nighttimes (PET_N) considerably. Calculated PET_N were 41 % and 60 % of the observed ET_N for Wüstebach and Rollesbroich, respectively. This might be related to the r_s parameter during nighttime, which represents the bulk surface resistance in the FAO PM equation for hourly PET. Using a smaller r_s value (50 s m^{-1}) during night which corresponds to the daytime r_s value reduced for Rollesbroich the difference between modeled and measured ET_N significantly (see Figure IV. 1 d). For Wüstebach,

reducing r_s did not have a large effect on PET_N. Although the relative differences between modeled and measured ET_N at Wüstebach remained large, it must be noted that the nighttime ET values at this site were very small. The absolute deviations modeled and measured ET_N values in Wüstebach were however not larger than in Rollesbroich. The estimation of the small ET_N values in Wüstebach from energy balances seemed therefore to be limited by the accuracy with which the different components of the energy balance can be measured or estimated. The differences in PET between the stations can be explained by the diabatic and adiabatic component of latent heat loss in the FAO PM formula. During night, the hourly diabatic component turns normally into to a negative value, because the system is dominated by the outgoing terrestrial radiation. The decrease in surface temperature (radiative cooling) combined with sufficient moisture in the air leads thus at times to a small adiabatic term during night (low wind speeds, low vapor pressure deficit) and thus to a negative PET, indicating the formation of dew (ASCE-EWRI 2005). This is more pronounced during the growing season, because of a higher radiative cooling (clear nights, fewer clouds), higher air temperatures and corresponding higher water holding capacity of the air. Thus, the average hourly PET during night at the Wüstebach site showed more negative values during the growing season than during the non-growing season (see Figure IV. 2).

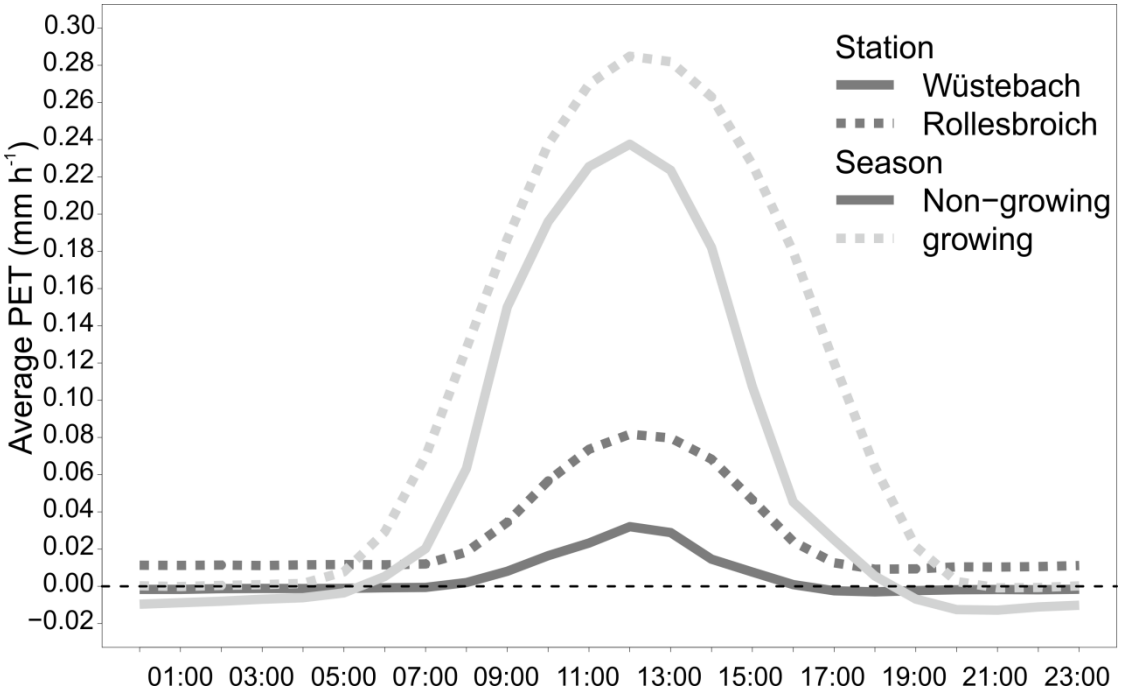

Figure IV. 2: Average daily pattern of hourly PET rates during the non-growing (October – February) and growing season (March – September) for Wüstebach and Rollesbroich.

However at the Rollesbroich site, PET remained mostly positive, also during the growing season, which can be explained by the larger adiabatic term due to the higher wind speed at this site (Figure IV. 2). It must be noted that the average hourly rates shown in Figure IV. 2 include both ET and dew formation. For the Wüstebach site, the average negative PET rates during night indicate that at this site, there would be a net input of water during nighttime due to dew formation. However, for the calculation of ET_N from the lysimeter weights, only time periods when the lysimeter weights decreased were considered so that time periods when dew was formed were excluded. Therefore, the annual PETs shown in Figure IV. 1 were calculated excluding the time periods when the calculated PET was negative. In the following, all calculated PET amounts and rates are calculated for time periods when PET was positive excluding times when negative PET was calculated.

A comparison between seasonal average hourly meteorological variables showed that both station differ mainly by the variable wind speed and air pressure. Higher wind speeds combined with smaller r_s parameter value during night reduced the denominator of the adiabatic term in the PM-equation, which then exceeded the diabatic term and thus agreed in the end better to measured nighttime ET´s. This is in line with earlier investigations by Irmak et al. (2005), who showed that a use of higher r_s values during night (200 s m^{-1}) in the ASCE-PM equation tends to reduce nighttime PET estimates in comparison to a use of r_s 70 s m^{-1}.

These results confirmed that the FAO PM equation to calculate PET on an hourly basis could be used to account for water losses during night, but require using the daytime surface resistance value of vapor flow through the evaporation soil surface and the transpiring crop at night. Hence, we assume that this modification for nighttime calculations of hourly PET in the FAO PM equation may be able to account for the effect of soil evaporation, an incomplete stomatal closure or transpiration through the cuticle at night under the suitable meteorological conditions.

IV.3.2 Seasonal patterns of nighttime evapotranspiration

Figure IV. 3, 4 and 5 depict average monthly amounts of ET, average daily duration, and average ET and PET rate during different nighttime periods for both grassland ecosystems. ET rates during dawn (Figure IV. 3) showed in comparison to the average monthly water fluxes (< 0.6 mm) no clear seasonal patterns. Average rate of ET during dawn was 0.0037 mm h^{-1} and 0.0094 mm h^{-1} for Wüstebach and Rollesbroich, respectively. The highest average rate of ET was achieved during spring and November at Rollesbroich (0.013 mm h^{-1}) and during summer and November at Wüstebach (0.005 mm h^{-1}). In contrast the rate of PET

showed a seasonal tendency with higher rates during the non-growing season at both sites, because of the smaller radiative cooling and less impact of temperature on the water holding capacity of the air. PET rates in this and the following section represent results from the hourly PET, calculated with r_s value of 50 s m^{-1} at night.

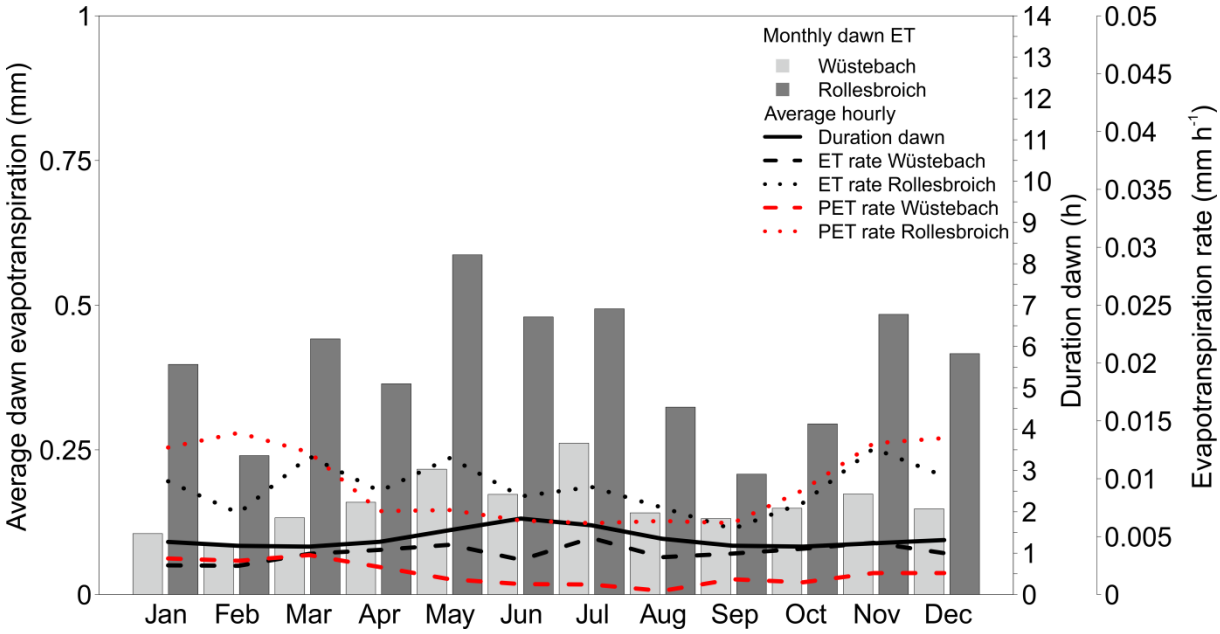

Figure IV. 3: Average monthly evapotranspiration during dawn for two different grassland ecosystems at Wüstebach and Rollesbroich. The observation period comprised observation from four consecutive years (2013 – 2016). The second y-axis depicts the seasonal course of the average daily duration of dawn (hours), the average rate of evapotranspiration and potential evapotranspiration (mm/hours) per month.

For the ET amounts and rates during dusk (Figure IV. 4), we observed a clear seasonal behavior with larger values during the growing and smaller values during the non-growing season. The highest average rates were achieved for both grassland ecosystems in May (Wüstebach: 0.006 mm h^{-1}; Rollesbroich: 0.026 mm h^{-1}) and for Rollesbroich these rates were clearly higher than corresponding ET rates during dawn. Average rate of ET during dusk was 0.0042 mm h^{-1} and 0.0158 mm h^{-1} for Wüstebach and Rollesbroich, respectively. PET rates for both sites were clearly smaller and showed with higher values during the non-growing season an opposite seasonal tendency than the measured ET rates.

The average monthly ET_{noc} amounts are depicted in Figure IV. 5 and showed for both grasslands a seasonal tendency with higher average monthly values during the non-growing season. Also for ET_{noc} the extensively used grassland showed much higher monthly values and average ET and PET rates than the forest meadow in Wüstebach. Average rate of ET

during the nocturnal period was with 0.0037 mm h^{-1} and 0.0102 mm h^{-1} rather similar to average ET rates during dawn for Wüstebach and Rollesbroich, respectively. The PET rates showed a clear seasonal pattern with higher values during autumn and winter months but this pattern was not observed in the measured ET rates.

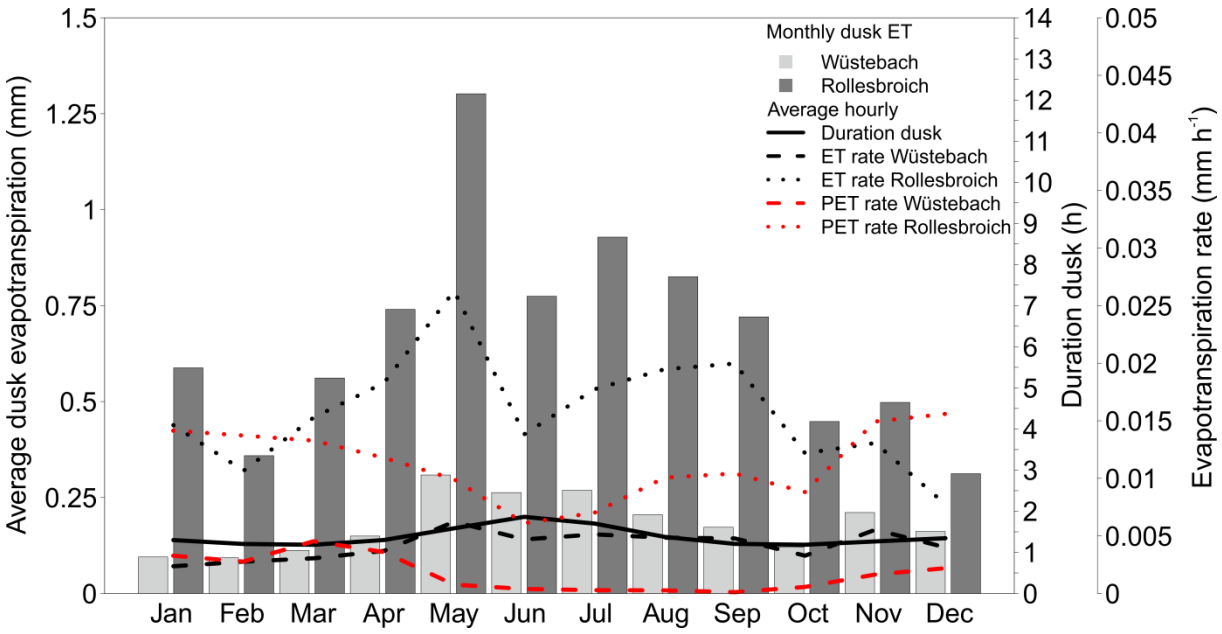

Figure IV. 4: Average monthly evapotranspiration during dusk for two different grassland ecosystems at Wüstebach and Rollesbroich. The observation period comprised observation from four consecutive years (2013 – 2016). The second y-axis depicts the seasonal course of the average daily duration of dusk (hours), the average rate of evapotranspiration and potential evapotranspiration (mm/hours) per month.

Meanwhile the overall duration of dusk and dawn was relatively short; nearly 25 % of the annual water loss during night occurred during twilight hours. This could be potentially related to an unstable reduction of stomatal conductance between light and dark time of the day. Various studies reported an increased endogenous stomatal opening during twilight hours (e.g. Bucci et al. 2005; Dodd et al. 2005; Caird et al. 2007a). However average ET rates during dawn were clearly smaller than during dusk. Smaller ET rates during dawn might be explained by the formation of dew during the early morning hours. Recent studies confirmed a dew-formation induced suppression of plant transpiration of a tropical plant, *Colocasia esculenta* (Gerlein-Safdi et al. 2017). Groh et al. (2018c), Groh et al. (2018b) and Gebler et al. (2015) showed that at both grassland sites dew formation is a relevant process that substantially contributes to the water balance.

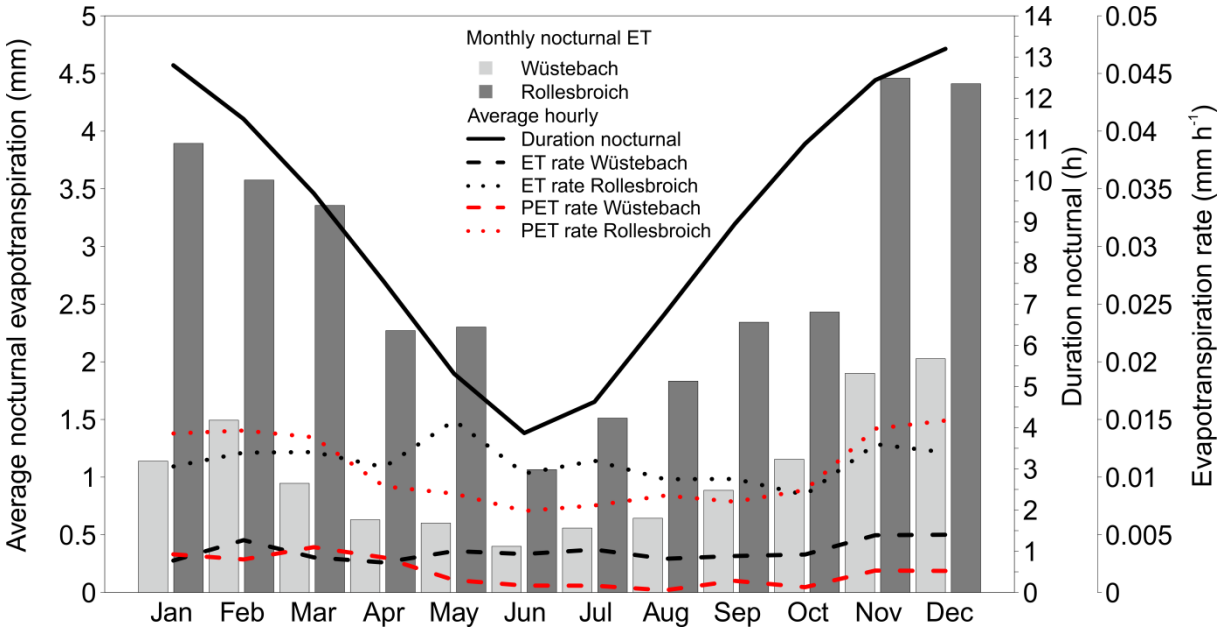

Figure IV. 5: Average monthly nocturnal evapotranspiration (dusk to dawn) for two different grassland ecosystems at Wüstebach and Rollesbroich. The observation period comprised observation from four consecutive years (2013 – 2016). The second y-axis depicts the seasonal course of the average daily nocturnal duration (hours), the average rate of evapotranspiration and potential evapotranspiration (mm/hours) per month.

IV.3.3 Heat wave impact

In July 2016 the region suffered from two main heat waves from the 8th until the 10th and from the 18th until the 20th of July, which carried warm air masses with high vapor pressure deficits combined with relative high wind speeds. We followed the recommendations of the WMO TT-DEWCE and defined a heat wave as a marked unusual hot weather that persisted at least two consecutive days during the hot period of the year, when daily thermal conditions (maximum air temperature) exceeded a certain average local threshold (WMO-TT-DEWCE 2015). Frequently an average maximum air temperature threshold of 5°C is used, but in absence of long-term observations (2012 -2016) the threshold value was set onto 3.5°C. In order to account for the impact of daily maximum temperature on the following night, the first day after the heat wave was included additionally into our analysis (i.e.11 July 2016 and 21 July 2016). Figure IV. 6 depicts exemplarily the hourly ET and P rate for the first heat wave at Rollesbroich from lysimeter Ro1. The subplot from Figure IV. 6 shows the relative hourly ET from 12 am until 11 am of the following day. Days with enhanced ET during nighttime periods are marked in green. During this time, the total daily ET was relative large and reached on the 10th of July 2016 a maximum value of 8.3 mm, which was nearly 33 % larger than the calculated PET value of 5.6 mm.

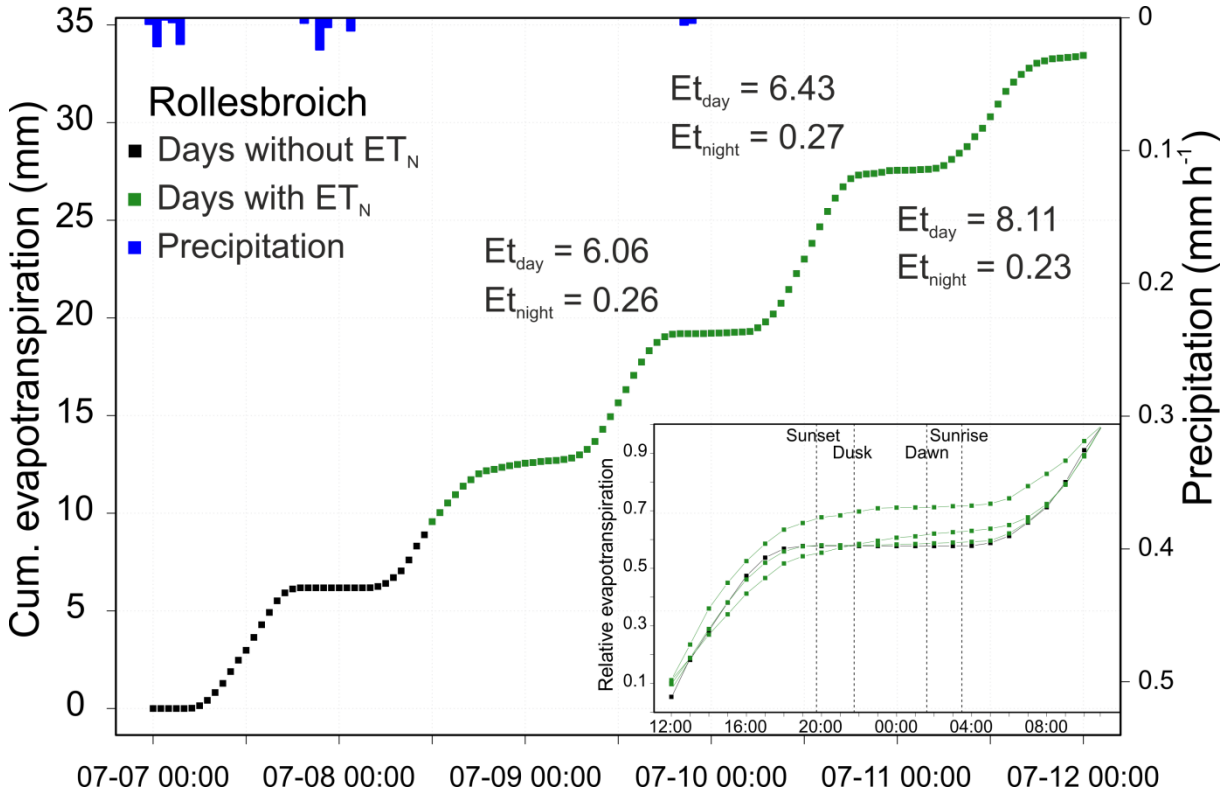

Figure IV. 6: Cumulative evapotranspiration and precipitation rate for the first heat wave period in July 2016 for Rollesbroich of lysimeter Ro1. The subplot depicts the relative cumulative evapotranspiration from 12 am until 11 am of the following day from 7 July 2016 until 11 July 2016. The vertical lines in the subplot represents the starting time of sunset, dusk, dawn, and sunrise.

The average ET rates during the heat waves in July (AV-heat-wave), average July 2016 (AV-July2016) and July 2013-2016 (AV-July) can be taken from Table IV. 1 for dusk, dawn and nocturnal periods. For both grassland ecosystems ET rates were in general the highest during dusk and the lowest during dawn. Comparing the ET rates during AV-heat-wave and AV-July2016 showed generally higher values during all three nighttime periods of the heat wave. Moreover, we have to note that AV-July2016 ET rates were still influenced by the two heat waves in July; hence a comparison with AV-July is more appropriate to evaluate the influence of a heat wave on ET rates. Comparing the long-term values (AV-July) with the heat wave period (AV-heat-wave) showed that ET rates during the specific nighttime were up to twice as high as long-term average rates, at least for Rollesbroich. This was less pronounced for the grassland ecosystem at Wüstebach during dawn and nocturnal periods, where AV-July ET rates were only slightly smaller than during the AV-heat-wave. But average ET rate during dusk were, similar to ET rates from Rollesbroich, significantly higher for the period under heat wave influence than long-term average July ET rate. Higher nighttime ET rates during

heat waves appear counter intuitive, as we might expect that nighttime ET should decrease with progressive soil drying. However recent investigation with wheat showed, that nighttime transpiration even increased in response to progressive soil drying, which might be related to the fact that cuticular transpiration and incomplete stomatal closure are not driven by hydraulic or hormonal signals (e.g., absicic acid; Claverie et al. 2017). These results showed that heat waves clearly affected the rate of nighttime ET for both grassland ecosystems.

During these eight days in July the ET_N reached values up to 0.1 mm and 0.34 mm per night for Wüstebach and Rollesbroich, respectively. This is in line with earlier findings from De Boeck et al. (2016) who showed for a single event that ET_N ranged between 0.12 – 0.32 mm for grassland influenced by heat waves. Doronila and Forster (2015) showed that nocturnal sap-flow during a heat wave accounted up to nearly 28 % of the total daily flow of different Eucalyptus species. During the seven days in July influenced by heat waves measurements showed a total ET_N of 0.38 mm and 1.77 mm at Wüstebach and Rollesbroich, respectively. The relative short period corresponds to 38 % and 49 % of the total monthly ET_N amount at Wüstebach and Rollesbroich and demonstrates how heat waves will impact the increase of monthly ET_N. Additionally, our observations showed that during such heat waves the water loss during twilight hours contributed on average more than 50 % of the ET_N and was twice as high as on the annual scale.

Table IV. 1: Average hourly evapotranspiration rate for dawn, dusk, and nocturnal periods at different days during the heat waves at Rollesbroich and Wüstebach. Moreover average ET rate for the period with heat wave influence (AV-heat-wave), average July 2016 (AV-July2016), and long-term July values (AV-July) are given at the end of the table.

Day	Wüstebach (mm/h)			Rollesbroich (mm/h)		
	ET_{dawn}	ET_{dusk}	ET_{noc}	ET_{dawn}	ET_{dusk}	ET_{noc}
08.07.2016	0.000	0.023	0.010	0.000	0.089	0.023
09.07.2016	0.020	0.000	0.016	0.042	0.016	0.039
10.07.2016	0.000	0.008	0.000	0.015	0.066	0.023
11.07.2016	0.009	0.017	0.001	0.021	0.079	0.035
18.07.2016	#	#	#	0.000	0.007	0.002
19.07.2016	0.000	0.009	0.001	0.000	0.022	0.003
20.07.2016	0.006	0.018	0.004	0.004	0.037	0.019
21.07.2016	0.008	0.011	0.006	0.021	0.029	0.032
AV-heat-wave	**0.006**	**0.012**	**0.005**	**0.013**	**0.043**	**0.022**
AV-July2016	**0.003**	**0.007**	**0.003**	**0.010**	**0.025**	**0.013**
AV-July	**0.005**	**0.005**	**0.004**	**0.009**	**0.018**	**0.011**

Conditions of heat wave not fulfilled

The differences in ET rates during dusk, dawn and nocturnal periods suggest either that stomatal conductance were not stable through the whole night, which is in line with previous findings for other plant species (Caird et al. 2007a) or that water evaporates from the soil (Agam et al. 2012). Another explanation could be transpiration through the leaf epidermis and cuticle (Ledford 2017) at night. Recent investigation in a sunflower leaf showed that even when stomata was closed at night that water losses remained on a lower level from transpiration stream through the cuticle (Hanson et al. 2016). Konarska et al. (2016) reported for urban areas that tree transpiration significantly increased the cooling rate shortly after sunset. Higher ET rates between sunset and sunrise during heat waves could indicate that leaves try to fix carbon during low-light conditions or in dark while atmospheric conditions in terms of air temperature and vapor pressure deficit are still low (Chaves et al. 2016). To clarify the reason for water losses during night micro meteorological measurements and observations of stomatal and leaf conductance during heat waves at daytime, twilight and night would help to clarify these findings.

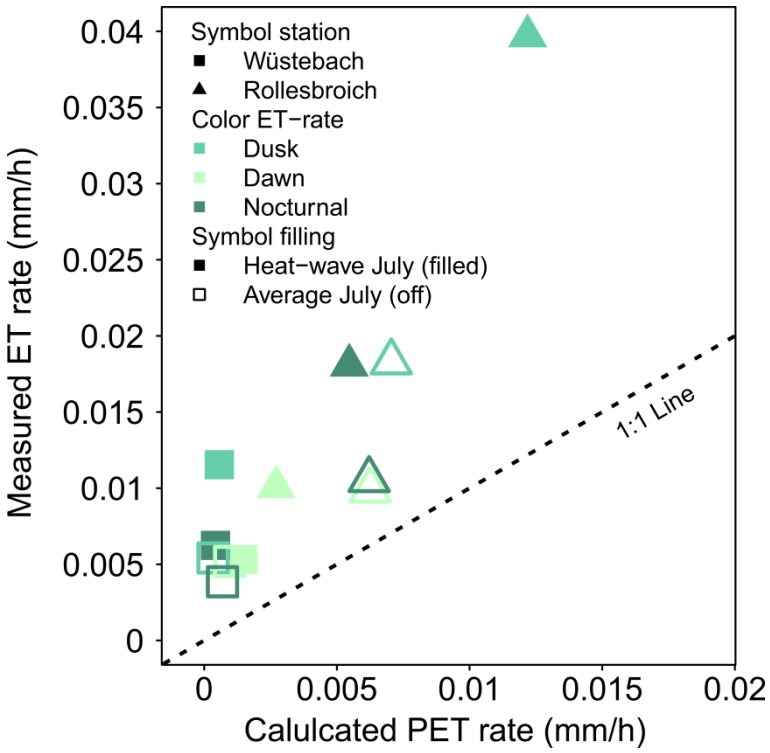

Figure IV. 7: Average actual (lysimeter) and potential evapotranspiration rate (PET, r_s = 50 sm^{-1}) for a period which was under heat wave influence (filled symbols) and long-term average ET rate in July (not filled symbols, 2013 – 2016). The different colors correspond to the ET rate during different nighttimes i.e. dusk, dawn, and nocturnal. The symbols reflect the different stations (Rollesbroich (triangle); Wüstebach (square)).

Figure IV. 7 shows a scatterplot of average ET and PET (r_s = 50 sm^{-1}) rates during a period subjected to a heat wave (AV-heat-wave) and long-term average values (AV-July). Average ET rates during AV-heat-wave were largely underestimated by the modified FAO-PM model. Especially during dusk, measured average ET rates was an order of magnitude higher at Wüstebach and with 0.043 mm h^{-1} nearly four times larger than calculated PET rates at Rollesbroich. The results for AV-July ET rates were similar, but less pronounced with an overall smaller distance to the 1 to 1 line. This demonstrated the limitation of the modified FAO-PM model to estimate the nighttime ET rate during times affected by heat waves and thus suggests that other factors such as the aerodynamic resistance and other terms of the heat balance (net radiation, soil heat flux) are not well represented during heat waves.

IV.3.4 Relationship between average rates of nighttime evapotranspiration and environmental variables

The relationship between monthly average rates of ET, obtained from six lysimeter respectively, during different daytimes and environmental drivers can be taken from Table IV. 2. The regression results with the split data set achieved higher R^2 values than using the entire data set (except daytime, see supporting information Table IV.A 1). This indicates that monthly average ET rates during night were driven by distinct environmental drivers during the non- and growing season. Hence we will discuss only the results from regression analysis with the split data set. Different environmental drivers controlled the ET during dawn. ET during dawn at Rollesbroich was mainly controlled by incoming energy (T_{air}; R_n) and P_a during both seasons. But results for Wüstebach showed, that mainly θ (N-GS) and P_a (GS) were related to ET during dawn. The grassland ecosystem at Wüstebach might be less affected by the thermal sources between dawn and sunrise, because the surrounding spruce population limited the incoming earlier morning energy. At both sites the reduction of P_a was correlated significantly with increasing rates of ET.

During the day, monthly average ET rates were mainly governed by the environmental variables R_n and VPD which agrees well with previous studies (Wang et al. 2012; Pereira et al. 2014; Liu et al. 2015). ET rates during dusk were mainly governed by G and P_a and by T_{air}, W_s and G during the N-GS and GS season at Rollesbroich and Wüstebach respectively. For both seasons during nocturnal periods, ET rates were mainly driven by W_s at both sites and the R^2 values were higher during the months of the N-GS. These results agreed well with previous studies which showed that water losses during night were significantly related to W_s (Malek 1992; Novick et al. 2009; Phillips et al. 2010; Irmak 2011; Skaggs and Irmak 2011).

We observed an increase of ET_{noc} with higher wind speed for both grassland ecosystems. This is in line with Monteith and Unsworth (1990), who remarked that with higher wind speeds the rate of evaporation of a wet surface always increases, as the resistance of heat transfer by convection and water vapor in general decrease. Our study did not confirm any significant influence from vapor pressure deficit or air temperature on nighttime ET of both grassland ecosystems, which were reported in previous studies (Bucci et al. 2005; Dawson et al. 2007; Fisher et al. 2007; Howard and Donovan 2007).

Measured ET and calculated PET rates during different day times were only during day (both sites) and partially during nocturnal periods (Rollesbroich) significantly ($p < 0.001$) correlated. The analysis showed that environmental variables can be used in general to estimate average ET rate during different nighttimes and season. The PM-model, which is the standard approach to estimate PET, didn´t correlate well with monthly averaged ET rates during different nighttimes (see low R^2 in Column ET~PET Table IV. 2). This result was not surprising, as the PM-model already showed a different seasonality of PET than ET rates during night (Figure IV. 3, 4, and 5). The reason for it might be that the PM-model estimate more frequently formation of dew (larger diabatic term) in the growing season during clear nights, higher air temperatures and corresponding higher water holding capacity of the air.

Table IV. 2: Results of a stepwise linear regression analysis to identify which environmental variables drive the average evapotranspiration rates during different day times (dawn, day, dusk, nocturnal periods) on a monthly basis for a split data set. Environmental variables are the following: air temperature (T_{air}), net radiation (R_n), vapor pressure deficit (VPD), air pressure (P_a), relative humidity (RH), wind speed (W_s), soil heat flux (G), and soil water content 0.1 m (θ). Linear correlation analysis between average monthly ET and PET rates at different daytimes (ET~PET).

Station	Daytime period	Non-growing season					Growing season				
		Environmental factors	ET		ET~PET		Environmental factors	ET		ET~PET	
			R^2	P	R^2	P		R^2	P	R^2	P
Rollesbroich	Dawn	P_a ‘*’;T_{air} ‘***’	0.61	‘**’	-0.03	‘ ’	P_a ‘**’;R_n ‘*’	0.42	‘*’	0.15	‘.’
	Day	VPD‘***’;R_n ‘**’	0.86	‘***’	0.93	‘***’	R_n ‘***’;VPD‘**’;G ‘*’	0.90	‘***’	0.85	‘***’
	Dusk	G‘**’	0.38	‘**’	-0.03	‘ ’	P_a ‘*’;R_n ‘.’	0.22	‘.’	0.10	‘ ’
	Nocturnal	W_s ‘***’;P_a ‘.’	0.63	‘**’	0.59	‘***’	W_s ‘***’;G‘.’	0.45	‘*’	0.33	‘.’
Wüstebach	Dawn	θ‘**’	0.46	‘**’	0.03	‘ ’	P_a ‘*’	0.28	‘*’	0.23	‘.’
	Day	R_n ‘***’;VPD‘***’	0.89	‘***’	0.94	‘***’	R_n ‘***’;VPD‘**’	0.87	‘***’	0.92	‘***’
	Dusk	T_{air} ‘**’;W_s ‘*’	0.41	‘*’	0.01	‘ ’	G‘*’	0.19	‘.’	0.02	‘ ’
	Nocturnal	T_{air} ‘.’;W_s ‘**’	0.49	‘*’	-0.02	‘ ’	T_{air} ‘.’;W_s ‘**’	0.35	‘.’	0.03	‘ ’
P-signif. Codes: 0 ‘***’ 0.001 ‘**’ 0.01 ‘*’ 0.05 ‘.’ 0.1 ‘ ’ 1											

IV.4 Conclusion

Our analysis provides long-term observations of nighttime ET for two distinct grassland ecosystems. We showed that nighttime ET ranged on a yearly basis between 3 - 4.4 % and 6.3 - 10.1 % of the total daily ET at Wüstebach and Rollesbroich grassland sites, respectively. Seasonal patterns of nighttime ET were closely related to the length of the corresponding twilight and nocturnal phase. The analysis revealed that nearly 25 % of annual water loss during night occurred shortly after sunset or before sunrise and hence highlights the importance to differentiate between ET processes. Moreover, the magnitude of seasonal nighttime ET patterns was closely related to meteorological conditions and the surrounding land use. Thus, nighttime ET significantly contributes to the seasonal water cycle of a natural as well as an extensively used grassland ecosystem. Without any increase of biomass, this additional loss of water during night will reduce the WUE of ecosystems and was exemplarily shown for grapevines in Medrano et al. (2015). Thus, reducing nighttime water loss might be an important factor for breeding crops with a higher WUE (Caird et al. 2007b; Coupel-Ledru et al. 2016). The amount and rate of nighttime ET increased partly considerably during periods that were subjected to heat waves. These results are especially of high importance for scientists and decision makers, as we expect that the frequency of such extreme weather conditions will be enlarged by climate change. The relationship between ET rate and environmental variables at different daytimes revealed that wind was the most significant driver for nocturnal ET, while during twilight hours other, station and season dependent, environmental variables governed ET rates of both grassland ecosystems. ET rates during the day were mainly controlled by the available energy and gradient in vapor pressure between plant and atmosphere. Further comparisons between measured ET and calculated PET during nighttime showed at least for the station Rollesbroich the ability of a modified PM-model, modified to the use of a nighttime r_s value that equals that for daytime conditions, to predict ET during different nighttime periods from standard meteorological parameters.

Our study results revealed that nighttime ET is an important contributor for the total ET and impacts the WUE and adds to a further reduction of available soil moisture in the root zone. Thus, when quantifying water budgets, carbon balance and energy fluxes from plot to landscapes or continents, it is urgent to use realistic constraints of minimum stomatal conductance, transpiration through leaf cuticle or soil evaporation to account for nighttime ET.

V Inverse estimation of soil hydraulic and transport parameters of layered soils from water stable isotope and lysimeter data

This chapter is based on a accepted journal article:

Groh, J.*, Stumpp, C., Lücke, A, Pütz, T., Vanderborght, J., and Vereecken, H., 2018, Inverse estimation of soil and transport parameters of a layered soils from water stable isotope and lysimeter data, *Vadose Zone Journal* (accepted).

V Inverse estimation of soil hydraulic and transport parameters of layered soils from water stable isotope and lysimeter data

V.1 Introduction

Quantification of water fluxes and fluxes of dissolved substances in the vadose zone is important to resolve a number of environmental issues. These issues comprise (i) the protection of groundwater resources, which is the main source of drinking water in many regions of the world (Aeschbach-Hertig and Gleeson 2012; Taylor et al. 2013a), both in terms of groundwater quantity and quality; and (ii) optimizing crop production making efficient use of water and fertilizers and plant protection products. Simulation models are used to link known fluxes at the upper boundary of the vadose zone with fluxes at different depths in the vadose zone and related state variables such as water contents, matric potentials and solute concentrations. These simulation models require accurate and precise information about the properties of the vadose zone that link fluxes with state variables, such as the soil water retention curve, the unsaturated soil hydraulic conductivity, and the solute dispersion coefficient. Typically, these properties are determined from laboratory experiments, and the precision of the estimated properties has increased considerably over the last decade by improving the experimental and estimation procedures (Peters and Durner 2006; 2008; Peters et al. 2015). However, these lab-scale estimated properties may have low accuracy describing field scale processes due to spatial variability at the field scale, which is not captured by limited sampling; small sampling volumes (e.g. soil cores or columns) subjected to specific boundary conditions that differ from real world conditions; and scale dependent solute transport parameters (Hopmans et al. 2013). The inability of lab scale determined soil hydraulic and solute transport parameters to describe field and larger scale water flow and transport processes under natural conditions is an issue in many hydrological applications (Mertens et al. 2005; Wöhling et al. 2008; Iiyama 2016).

In situ observations of state variables and fluxes at the scale of interest and inverse modeling have been shown to be promising approaches to estimate soil hydraulic parameters (Peters and Durner 2006; Puhlmann and von Wilpert 2012; Stumpp et al. 2012; Ries et al. 2015; Sprenger et al. 2015). However, inverse modeling requires the specification of boundary (e.g. actual ET, drainage flux, capillary rise) and initial conditions (e.g. water content, matric potential, solute concentration) which are often not available or associated with large uncertainties in outdoor experiments (Vrugt et al. 2008a; Li et al. 2009; Mannschatz and Dietrich 2017). For example, various studies have shown that standard devices to measure P (tipping bucket) frequently underestimate the amount of rain (Gebler et al. 2015; Groh et al.

2015; Hoffmann et al. 2016; Herbrich et al. 2017) and affect the estimation of soil hydraulic properties (Peters-Lidard et al. 2008). Also boundary conditions at the bottom of the soil profile can have an important impact on the water fluxes and state variables within the investigated system (Groh et al. 2016) and hence need to be correctly represented. In the past, mainly free-drainage (zero-gradient) or a seepage-face boundary were used in inverse modeling studies. The latter boundary condition can be applied to lysimeters with a seepage face at the bottom across which water and solutes can leave the soil profile when the seepage face is saturated with water. Although this boundary condition can be accurately represented in the simulation model, water and solute fluxes observed from lysimeters with a seepage-face at the bottom are not representative for field scale conditions (Flury et al. 1999; Boesten 2007; Kasteel et al. 2007). Breaking the capillary connection between the soil profile and deeper soil layers affects drainage, the movement of solutes, ET and prevents capillary rise (Schwaerzel and Bohl 2003; Abdou and Flury 2004; Stenitzer and Fank 2007). Alternatively, time series of state variables, for example matric potential, could be used as a bottom boundary condition. However, this leads to a loss of information, since the temporal evolution of the state variable is not used to derive information about the system properties but is prescribed as a boundary condition.

The majority of field scale inverse modeling studies used solely information about water content (e.g. Qu et al. 2014; Fang et al. 2015; Seki et al. 2015; Lai and Ren 2016; Le Bourgeois et al. 2016). However, since water fluxes in the soil are driven by gradients in matric potential, *in situ* observations of water content do not necessarily provide sufficient information to accurately parameterize the field-scale hydraulic properties (Vereecken et al. 2008; Scharnagl et al. 2011; Wöhling and Vrugt 2011). When aiming at inversely estimating transport parameters, concentrations of artificial or of environmental tracers can be used. Particularly water stable isotopes were shown to give information about water transit times and dispersivities (Stumpp et al. 2012; Sprenger et al. 2015; Stockinger et al. 2015; Stockinger et al. 2016).

Surprisingly little attention was given to combining different observation types to calibrate water flow and transport models. In some studies, estimate soil hydraulic parameters and/or longitudinal dispersivity were estimated from inverse modeling using a combination of *in situ* observation variables, e.g., water content and matric potential (Wöhling and Vrugt 2011; Caldwell et al. 2013; Groh et al. 2013), water content and ET data (Foolad et al. 2017), water

content and $\delta^{18}O$ isotope ratio profiles (no continously monitoring; Sprenger et al. 2015; Sprenger et al. 2016a), deuterium enriched water (Stumpp et al. 2009), or bromide (Abbasi et al. 2003). Only few studies were found that used a combination of water content, solute concentration, and matric potential (Mishra and Parker 1989; Jacques et al. 2002; Stumpp et al. 2012). Soil layering, which corresponds to the vertical variation of soil properties, is often not considered when estimating hydraulic and transport parameters using inverse modeling and it is assumed that the soil profile can be represented by a homogenous profile with one set of effective parameters. Such an effective approach can be used to describe averaged state variables and fluxes when hydraulic properties are described by random space functions. However, when soil layers are relatively thick compared to the soil profile depth that is considered in simulations and when the properties of the layers vary considerably, the vertical variation in soil properties cannot be represented by a random space function but is rather a deterministic variation. In such a case, homogenous effective parameters are of little meaning to describe the vertical variation of state variables and fluxes. This implies that the properties of the different layers need to be determined. Schelle et al. (2012) showed, using synthetic data that soil layer specific observations of state variables, e.g. matric potentials, were prerequisite to inversely determine soil hydraulic parameters of different layers in a layered soil profile. Stumpp et al. (2012) and Jacques et al. (2002) used a stepwise and sequential approach to derive parameters layer by layer to avoid non-uniqueness of parameter estimates when a larger number of parameters has to be estimated. However, this approach ignored possible parameter interaction between corresponding soil layers (Wöhling and Vrugt 2011). Hence, simultaneous estimation of the full parameter-set for a layered soil using various observation types including water content, matric potential, and water isotope data is therefore promising. Since tracer concentrations depend also on water flow and root water uptake, these measurements not only constrain parameters for solute transport but also for water flow and root water uptake (Sprenger et al. 2015). Mishra and Parker (1989) used a synthetic data set of a simple infiltration-evaporation scenario to demonstrate that the information on water content, matric potential, and solute concentration at the corresponding soil layer were beneficial to identify simultaneous layer specific soil hydraulic and solute transport properties. However, no systematic verification was conducted within their numerical study and thus it is still unclear which variables are necessary to adequately describe soil hydraulic

properties as well as the transport behavior of layered soils in outdoor experiments under variable boundary conditions.

Using state of the art weighable lysimeter systems can help overcome the above mentioned limitations at the field scale, because all relevant surface and bottom boundary water fluxes can be determined with a high temporal resolution and high precision (Unold and Fank 2008). Hence, lysimeters equipped with matric potential, soil water content sensor and devices for soil water sampling are ideal experimental systems to obtain high-resolution observation data for the inverse estimation of water flow and solute transport parameters under realistic transient boundary conditions (Schelle et al. 2013a). However, observations of state variables within the lysimeters at a specific depth are still local measurements (Garré et al. 2011; Cai et al. 2016) raising the question to what extent such local observations are representative for a given depth within the lysimeter. Our hypothesis is that using the average value of several local measurements from one depth in several lysimeters can be used to derive a layer specific effective parameterization and help to identify soil hydraulic properties and dispersivities which describe water and matter fluxes at the field scale.

In this framework, our study presents a comparison of different inverse modeling strategies (stepwise and simultaneous) including the use of water stable isotope data to identify soil hydraulic and solute transport properties of a layered soil profile. The software HYDRUS-1D (Šimůnek et al. 2016) was used to simulate water and solute fluxes and a global optimization algorithm to calibrate the vadose zone model.

Different inverse modelling strategies were carried out:

(1) to investigate which state variables, are necessary to estimate soil hydraulic properties as well as solute transport parameter (dispersivity) of a layered soil.

(2) to identify effective hydraulic properties and longitudinal dispersivities of a layered soil using horizontally averaged state variables from four large scale lysimeters.

(3) to use bromide concentrations from an artificial tracer experiment to validate the calibrated dispersivity parameters of the vadose zone model.

V.2 Material and Methods

V.2.1 Study site Wüstebach

The experimental site Wüstebach (50°30’10”N, 6°19’41”E, 630 m a.s.l.) is located within the Eifel National Park and is part of the lower Rhine Valley-Eifel observatory of TERENO and

the German wide lysimeter network SOILCan (Bogena et al. 2015; Bogena et al. 2016). The vegetation cover and plant growth on the lysimeter and the surrounding area correspond to a forest meadow with no agricultural activities (Knauer et al. 2017). The area belongs to the humid temperate climate zone with a mean annual P of 1200 mm and a mean annual temperature of 7.5°C (Pütz et al. 2016). Since December 2010, six weighable lysimeters (Wu4 – Wu9, METER GROUP, Munich) each with a surface of 1 m² and a depth of 1.5 m were installed at the research test site. The Wüstebach catchment is covered with a 1 to 3 m thick periglacial solifluction layer and the bedrock is fractured Devonian shale and Sandstone (Rosenbaum et al. 2012). The cylindrical lysimeters contain undisturbed soil monoliths of a Stagnic Cambisol, which is the dominant soil type in the western part of the Wüstebach catchment. A soil description and soil samples were taken from two soil profiles during the lysimeter excavation process (see Table V. 1). The profiles were taken beside (south-east, north-west) the place of lysimeter excavation and showed a similar layering. Only the soil texture of layer four differed significantly (south-east: sand >75 % and north-west: loam >69 %).

Table V. 1: Soil analysis from two profiles in Wüstebach (south-east and north-west), which were taken beside the location of lysimeter excavation. Stone content was estimated according to Ad-hoc-Arbeitsgruppe-Boden (2005). The depths of the north-west profile were used to define the model layers. Layer II Bv 1 and II Bv 2 were grouped into one model layer.

Soil horizon		Layer depth		Texture (Sand/Silt/Clay)		Stone content	
South-east	North-west	South-east	North-west	South-east	North-west	South-east	North-west
		m		%		%	
Of, Oh	Of, Oh	+0.02 - 0	+0.02 - 0	-	-	-	-
Ah-Sew	Ah	0 - 0.21	0 - 0.15	40/28/32	35/24/41	0	20
II Bv 1	Sew-Ssw	0.22 - 0.43	0.16 - 0.31	61/18/21	47/19/34	30	20
II Bv 2	II Bv 1	0.44 - 0.68	0.32 - 0.59	81/13/6	22/70/8	40	20
II Bv 3	II Bv 2	0.69 - 1.00	0.59 - 1.10	75/17/8	23/69/8	50	50
III Cv	III Cv	1.01 - 1.50	1.11 - 1.50	64/17/19	65/17/18	70	80

The lysimeters are located annularly around a central service pit, which houses the measurement equipment and data recording devices. The lysimeters have a tension controlled bottom boundary system that adjusts the matric potential at 1.4 m depth in the lysimeter to measured matric potentials (tensiometer TS1, METER Group, Munich, Germany) at the same depth in the field. Hence, we can assume that water and solute fluxes in the lysimeter are directly transferable to the surrounding field. Each lysimeter was equipped with tensiometers

(TS1, METER Group, Munich, Germany), time domain reflectometry probes (CS610, Campbell Scientific, North Logan, UT, USA) and suction cups (SIC20, METER Group, Munich, Germany) at 0.10, 0.30, 0.50, 1.40 or 1.45 m soil depth. The weighing precision is 10 g (≙ 0.01 mm) for the lysimeter and 1 g (≙ 0.001 mm) for the water reservoir tank in which the effluent from a lysimeter was collected and from which water was pumped back into the lysimeter during periods of upward flow at the bottom of the lysimeter. Weight measurements were logged every minute. Further information about the general design and setup of the SOILCan lysimeter network can be taken from Pütz et al. (2016).

Lysimeter weight changes are not only related to water storage changes because these are also affected by external factors like management operations, animals or wind. The separation of P and ET from lysimeter weight changes requires thus an appropriate data processing scheme to reduce the impact of external errors and noise on the calculation of water fluxes (Schrader et al. 2013; Hannes et al. 2015). The raw data of lysimeter measurements were subjected to extensive manual (visually, software DIAdem, National Instruments, Austin, TX, USA) and automated plausibility checks to ensure the quality of the observation dataset (more details see Pütz et al. 2016; Küpper et al. 2017). Subsequently, the "adaptive window and threshold" filter (AWAT; Peters et al. 2017) was used to further smooth the noise prone lysimeter weight changes. Daily P and ET amounts were calculated from the smoothed lysimeter signal. We assumed that any increase or decrease in mass during a one minute time period can be related, to respectively, P or ET. Meteorological parameters were used to calculate the hourly PET of a hypothetical grass surface with the Penman-Monteith equation (Allen et al. 1998). To capture the seasonal vegetation development, measurements of grass length and leaf area index (LAI) were conducted with a measuring stick and a LAI-2200 device (Plant Canopy Analyzer, LI-CORE, Lincoln, USA).

The salt tracer experiment started on December 4th, 2013. On each of five lysimeters (Lys-Wu4, Lys-Wu6 – Lys-Wu9) ~ 1 liter KBr solution (~25 g Br^-) was sprayed, followed by 0.5 liter of pure water for flushing the application device. Lysimeter Lys-Wu5 received no Br^- and was used as a reference. We used a frame to avoid Br^- loss during the application because of wind drift. The inner side of the frame was covered (per lysimeter) with aluminum foil to collect splashing tracer water. The loss of Br^- due to splashing was determined in the lab. After the tracer application of the corresponding lysimeter and flushing, the application device was washed; water was collect and analyzed in the lab. The setup guarantees to recalculate the

exact amount of Br^- applied to each lysimeter. The amount of applied Br^- was 25.08 g for Lys-Wu4, 24.83 g for Lys-Wu6, and 25.30 g for Lys-Wu8. We did not measure $\delta^{18}O$ ratios in Lys-Wu7 and Lys-Wu9. Hence measurements of bromide concentrations and water fluxes from Lys-Wu7 and Lys-Wu9 were not part of this study. Since a tracer solution enriched in δ^2H was applied to Lys-Wu8, we used the $\delta^{18}O$ ratio as tracer in our investigation since more comparable time series were available for this isotope.

Soil water samples from suction cups at 0.1, 0.3, 0.5 m depth and from the seepage water (1.45 m) were collected every two weeks. At the beginning of the tracer experiment and after heavy rainfall events (>~30 mm d^{-1}) water samples were collected weekly or twice a week. Since December 2013, soil water samples were analyzed for $\delta^{18}O$, δ^2H and Br^- for lysimeter Lys-Wu4, Lys-Wu5, Lys-Wu6 and Lys-Wu8. P samples were collected during the observation period from January 2012 to April 2016 with a wet deposition collector (cooled) and sampled weekly. The isotopic analysis was carried out with a laser based cavity ringdown spectrometer (L2130-i Analyzer, Picarro Inc., Santa Clara, CA, USA). Isotope values are given in the δ notation relative to the Vienna Standard Mean Ocean Water (V-SMOW). The measurement accuracy was ≤ 0.1 ‰ for $\delta^{18}O$ and ≤ 1.0 ‰ for δ^2H. The Br^- concentration of soil water samples were determined with an ion chromatography system (ICS-3000, DIONEX, Thermo Fisher Scientific Inc., Waltham, MA , USA), which had an relative measurement error of 3.2 % for concentrations ≥ 0.5 μg ml^{-1}.

V.2.2 Model setup

V.2.2.1 Water flow

The one dimensional water flow model HYDRUS-1D (Šimůnek et al. 2016), which solves numerically the Richards equation, was used to simulate the transient water flow in the lysimeters. The Mualem-van Genuchten model (MvG; van Genuchten 1980) was selected to describe the water retention characteristic θ(h) and the unsaturated hydraulic conductivity function K(h):

$$\theta(h) = \begin{cases} \theta_r + \frac{\theta_s - \theta_r}{(1+|\alpha\Psi|^n)^m} & h < 0 \\ \theta_s & h \geq 0 \end{cases} \quad [V.1]$$

$$K(h) = K_s \left(\frac{\theta-\theta_r}{\theta_s-\theta_r}\right)^{\tau} \left[1 - \left(1 - \left(\frac{\theta-\theta_r}{\theta_s-\theta_r}\right)^{\frac{1}{m}}\right)^{m}\right]^2 \quad [V.2]$$

where θ, θ_s and θ_r are the actual, saturated and residual volumetric water contents [cm^3 cm^{-3}], respectively; α [cm^{-1}] is related to the reciprocal of the air entry value, n [-] to the width of the pore size distribution, m = 1 – 1/n, τ [-] is the pore connectivity parameter, and K_s is the saturated hydraulic conductivity [cm d^{-1}].

The upper boundary condition was defined as a time dependent atmospheric boundary with surface runoff. The ET, measured from the corresponding lysimeter, was used as boundary condition instead of the PET to further constrain the parameter estimates. We set the parameter of hCritA, which describes the minimum allowed matric potential at the soil surface, onto a value of -10^8 cm. This value guarantees that the actual evaporation rate was decreased from the potential value only during extreme dry conditions (matric potential < -10^8 cm). No reduction of actual transpiration due to plant water stress was observed in the grassland lysimeter under the relative wet climate conditions. The actual evaporation and transpiration were calculated from ET according to Beer´s law using LAI and the canopy radiation extinction constant (0.463) for the partitioning. The seasonal development of the forest meadow LAI per lysimeter was approximated by a linear interpolation of the LAI measurements. The root water uptake was simulated using the model of Feddes et al. (1978) with the vegetation specific stress response function for grass, which is available in the HYDRUS-1D software (Šimůnek et al. 2013). The root water uptake was restricted until the maximum rooting depth of 0.6 m, which was determined during the soil profile sampling. Root water uptake decreased linearly between 0.05 m and the maximum rooting depth, where it reached zero. To account for a delay of infiltration during times with snow in the catchment area a simple approach according to Jarvis (1994) was used. The snow melt and sublimation constant were set to 0.43 [cm $days^{-1}$ C^{-1}] and 0.06, respectively.

V.2.2.2 Isotope transport

The solute transport of $\delta^{18}O$ was calculated with the advection-dispersion equation, which is the most widely used model to predict solute transport under transient natural boundary conditions (Vanderborght and Vereecken 2007).

$$\frac{\partial(\theta C)}{\partial t} = \frac{\partial}{\partial z}\left(\theta D \frac{\partial C}{\partial z}\right) - \frac{\partial(qC)}{\partial z} - SC \quad [V.3]$$

where θ is the volumetric water content [cm^3 cm^{-3}], z the vertical coordinate [cm], C [mg l^{-1}] the tracer concentration in the soil water, D is the dispersion coefficient [cm^2 d^{-1}], and S is the root water uptake [d^{-1}]. D is given by (Bear 1972):

$$\theta D = D_L|q| + \theta D_w \tau_w \quad [V.4]$$

where D_L is the longitudinal dispersivity [cm], D_W is the molecular diffusion coefficient in free water [cm^2 d^{-1}], and τ_W [-] is a dimensionless tortuosity factor in the liquid phase. A modified version of HYDRUS-1D (Stumpp et al. 2012; Šimůnek et al. 2016) was used to simulate the transport of stable isotopes. The module neglects fractionation processes due to evaporation and was successfully applied in various studies (Huang et al. 2015; Sprenger et al. 2015; Sprenger et al. 2016a; Sprenger et al. 2016b). The modified code prevents an accumulation of isotopes (i.e. equivalent to increase in isotope ratios) at the soil surface when evaporation occurs and assumes a passive uptake by roots, so that water and tracer ($\delta^{18}O$) can leave the system via evaporation and transpiration. The solute transport boundary conditions at the top boundary were described as a time variable solute flux boundary (Cauchy boundary) when the water flow was directed into the system (P) and by a zero concentration gradient (Neumann boundary) when the water flux was out of the system (evaporation). At the bottom boundary a zero concentration gradient (Neumann boundary) was used when the water flux left and entered the system.

V.2.2.3 Data used for boundary and initial conditions

The simulated time period was from 2012-01-01 until 2016-04-30. For this period, isotope ratios in the P were available and daily P, ET, discharge and upward directed water flow were derived from lysimeter and effluent reservoir weights. Measurements of internal states of the lysimeters (water contents, water potentials, $\delta^{18}O$ ratios) were available for a shorter period from 2013-12-04 until 2016-04-30. Therefore, initial conditions for the water flow and isotope transport simulations had to be estimated and a spinup phase of 703 days was considered to minimize the effect of chosen initial conditions on the calibration of the model parameters against measurements of the internal states of the lysimeters. A linear decrease of pressure head between the top (-70 cm) and the bottom boundary nodes (-50 cm) were chosen as initial conditions for the water flow. The initial $\delta^{18}O$ ratios in the soil profile were estimated by averaging measured $\delta^{18}O$ ratios derived from the soil water samples at 0.1 m and

1.45 m depth over the entire observation period. We assumed a linear decrease of the $\delta^{18}O$ ratios between top and bottom of the soil profile; please note that all isotope values were transferred into positive numbers by adding an arbitrary value for the simulation only because it is not possible to use negative numbers in the modeling procedure.

V.2.2.4 Definition of soil layers in the simulation model

Figure V. 1 shows both soil profiles, the position of the measurement devices and the conceptual representation of the layering in HYDRUS-1D for all four lysimeters. The layering of both profiles was rather similar; hence the conceptual representation of the layering in the simulation was based on the north-west profile. In total seven parameters had to be estimated/optimized for four soil horizons to simulate the water (θ_r, θ_s, α, n, K_S, τ) and solute transport (D_L).

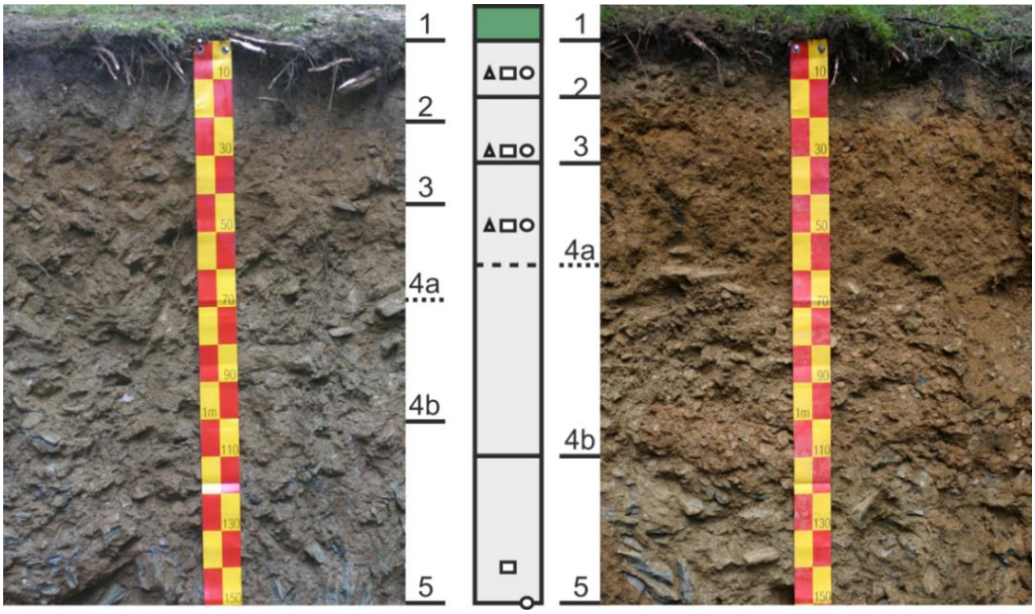

Figure V. 1: The two soil profiles from the Wüstebach catchment. The figure shows the two soil profiles (south-east, north-west), the conceptual representation of the layering in HYDRUS-1D simulation (which was based on the north-west profile) and the position of the measurement devices and observation points in the simulation. The location of the measurement devices are: TDR-probe (triangle), TS1 tensiometer (rectangle) and suction cups (circle).

The lysimeters in Wüstebach were covered with a few centimeter thick moss layer. Previous studies showed that internal water fluxes in mosses affect the drainage behavior across the

moss layer and change the rate of evaporation (Price and Whittington 2010), as the physiology of moss differs from that of other plants (Suzuki et al. 2007) or bare soil conditions (Blok et al. 2011). To represent moss in our hydrological model the hydraulic and transport properties of the moss layer were set to 0.01 (cm^3/cm^3; θ_r), 0.92 (cm^3/cm^3; θ_s), 0.4373 (cm^{-1}; α), 1.405 (-; n), 175 (cm/day; K_S), -2.31 (-;τ), and 5 (cm; D_L) according to McCarter and Price (2014) and Stofberg et al. (2016). The thickness of the moss layer was 0.05 m.

V.2.2.5 Parameter optimization and model efficiency

To reduce the amount of data, daily averages of matric potentials and water contents were calculated from the measurements. These were compared with daily values of water contents and matric potentials that were simulated by HYDRUS-1D. The $\delta^{18}O$ ratios in the collected effluent from the lysimeter were compared with a flux weighted average of $\delta^{18}O$ ratios that were simulated in the pore water at the bottom of the lysimeter over the time period that the effluent was collected. The same procedure was used to compare the $\delta^{18}O$ ratios in the pore water with simulated ratios at the depth of the soil water samplers. Parameter values for θ_s in layer 2 – 4 were estimated from the measured soil water retention characteristic using RETC (Van Genuchten et al. 1991) to reduce the amount of optimization parameters. The parameter search space of water flow and solute transport parameter during the optimization is summarized in Table V. 2. The lower boundary for the parameter τ was defined according to Peters et al. (2011).

Table V. 2: Lower and upper boundaries of soil hydraulic properties and dispersivity parameter for the inverse parameter optimization strategies. Measured minimum and maximum leaf area index (LAI).

Parameter	Unit	Lower bound	Upper bound
LAI	$cm^2\ cm^{-2}$	0.2	3.7
θ_r	$cm^3\ cm^{-3}$	0	0.36
θ_s	$cm^3\ cm^{-3}$	0.25	0.55
α	cm^{-1}	0.001	0.3
n	-	1.001	3
K_S	$cm\ day^{-1}$	1	1500
τ		$\tau > -2/(1-1/n)$	6
D_L	cm	0.1	30

We used the “Shuffled Complex Evolution Metropolis algorithm” (SCEM; Vrugt et al. 2003) to determine for each lysimeter and soil layer the soil hydraulic parameters and the

longitudinal dispersivity. SCEM is a global optimization algorithm that has been applied for a wide range of hydrological problems at different scales (Heimovaara et al. 2004; Raat et al. 2004; Ries et al. 2015). The algorithmic variables that need to be specified are the number of complexes q (e.g. 25 = number of parameters), and the population size s (e.g. q x 10). We considered four different optimization strategies that included different sets of observations:

- Bi-objective optimization strategy (BOS1): water content and $\delta^{18}O$ data at all available soil depths (0.1, 0.3, 0.5, and 1.45 m) are used to calibrate the soil hydraulic parameter and D_L of the HYDRUS-1D model.
- Bi-objective optimization strategy (BOS2): used in comparison to BOS1 matric potential instead of water content data.
- Two-step optimization strategy (2SOS): soil hydraulic parameters were estimated from layer specific measurements of water content and matric potential in a first optimization run with SCEM. In a next step, the transport parameters D_L were estimated for each soil layer from the $\delta^{18}O$ data using the optimized hydraulic parameter obtained in the first run.
- Multi-objective optimization strategy (MOS): uses water content, matric potential and $\delta^{18}O$ ratios simultaneously to calibrate 25 parameters of the advection-dispersion and the Richards equation.

Strategies with only one measured state variable (e.g. $\delta^{18}O$ ratios) or pedotransfer functions were not considered because earlier investigations by Sprenger et al. (2015) showed that such a strategy failed to match observations of state variables which were not included in the objective function (water content) during the inverse model calibration. The objective function that was minimized using the SCEM algorithm was based on Nash-Sutcliffe efficiencies (NSE). NSE coefficients were calculated per depth and observation variable to evaluate model behavior and performance:

$$NSE_{i,v} = 1 - \frac{\sum_t^N \left(x_{v,s,t,i} - x_{v,o,t,i}\right)^2}{\sum_t^N \left(x_{v,o,t,i} - \mu_{v,o,i}\right)^2} \quad [V.5]$$

where N is the total number of time-steps, t is the time step, $x_{v,s,t}$ and $x_{v,o,t}$ are the simulated and observed values of the variable v, and $\mu_{v,o}$ is the mean observed value. NSE values range between 1 (perfect fit) and -∞. Values below zero imply that the mean of the observations is a

better predictor than model simulations. Since the SCEM algorithm minimizes an OF, the average NSE coefficient was defined as NSE -1. To evaluate and compare between all four strategies, we calculated based on the optimal parameter set an average NSE coefficient (AV-NSE) that lumps NSE coefficients for all the observation depths and variables. No water content measurements were available for Lys-Wu4 in layer 4 (0.5 m) and for all lysimeters at 1.4 m depth. At depths were no water content were available, matric potential measurements were used instead of water content in the OF.

V.2.3 Effective parameters and boundary conditions

V.2.3.1 Effective parameters

We used averaged water fluxes at the boundaries of the lysimeters, combined with averaged values of water contents, matric potentials, and $\delta^{18}O$ ratios from four lysimeter to estimate effective soil hydraulic parameters and D_L. These parameters were compared with results for each single lysimeter considering uncertainty caused by parameter equifinality (Beven 2006). The range of parameter uncertainty was defined as the set of parameter values for which AV-NSE was less than 0.01 smaller than the optimized AV-NSE.

V.2.3.2 Impact of precipitation accuracy on the simulation of water and solute transport

To quantify exemplarily the impact of a less accurately defined upper boundary condition on simulated state variables (that is water content, matric potential, and $\delta^{18}O$ ratios), we compared simulations that used daily amounts of P measured with a rain gauge (tipping bucket method) with simulations in which P was derived from the lysimeter weights. When using rain gauge data, the boundary condition for water fluxes at the bottom had to be changed to free drainage (zero gradients) since the measured effluent fluxes in combination with measured ET rates and the rain gauge P values led to a long term decline of stored water in the soil profile. Simulation results for the two cases were compared to measured average water contents, matric potentials, and $\delta^{18}O$ ratios in the four lysimeters.

V.2.4 Validation of dispersivity parameters

To validate our soil depth and lysimeter specific dispersivity parameters, we used the optimal parameter-set from the best inverse parameter optimization strategy to simulate the Br^- breakthrough curve (BTC) of the conducted tracer experiment in a forward simulation run

with HYDRUS-1D. Uptake of bromide by plants was reported in various studies (Kung 1990; Schnabel et al. 1995; Magarian et al. 1998; Xu et al. 2004). We assumed during the forward simulations a passive uptake of Br^- by plants.

V.3 Results and Discussion

V.3.1 Lysimeter observation data

Table V. 3 summarizes the P measured by a rain gauge, PET and P, ET, discharge, and capilary upflow during the entire observation period (2013-12-04 – 2016-04-30) derived from lysimeter measurements. Daily surface fluxes (P; ET) derived from lysimeters measurements correlated well with respectively, rain gauge measurements and calculated reference ET (P: $R^2 = 0.7$; ET: $R^2 = 0.83$). However, P sums derived from the lysimeters weights were on average 23 % (670 mm) larger than the rain gauge measurements. Since water flow in the soil is driven by P, it is evident that these differences in P estimates will lead to important differences in simulated water fluxes in the soil which may have an important impact on the cailbration of the soil hydraulic and solute transport properties. Similar deviations between standard meteorological P measurement devices (tipping bucket rain gauge) and lysimeters have been reported in literature (e.g. Groh et al. 2015; Hoffmann et al. 2016; Herbrich et al. 2017). These differences in P between both methods may be caused by the fact that lysimeters account for the presence of dew, fog and rime (Gebler et al. 2015). According to Xiao et al. (2009) and Fank and Unold (2007), dew can be derived from lysimeter mass increase measurements between sunset and sunrise, when rain gauges do not detect P. However, weather station exposure or wind effects on rain gauges still can cause an additional underestimation of P. A threshold of maximum possible rate of dew formation on clear nights was used (Monteith and Unsworth 1990) and dew formation rates larger than 0.07 mm h^{-1} were excluded from the analysis. From our measurements we found that dew formation accounted for ~4.7 % of the total lysimeter derived P, which is in line with previous studies (Xiao et al. 2009; Heusinger and Weber 2015; Guo et al. 2016), but still explains only a small fraction of the difference in P amounts measured by lysimeters and rain gauges. Weather station exposure or wind effects are another important cause of the underestimation of P by rain gauges (Richter 1995; Hagenau et al. 2015). The measured cumulative ET was 72 % of the calculated reference PET. This indicates that the stomatal conductance and aerodynamic conductance of the boundary layer above the canopy were smaller than those of the reference

crop and/or that evaporation was reduced due to the high insulating capacity of mosses. The variability of daily P, ET, and capillary upflow between the different lysimeters was relative small and increased with larger daily water fluxes (see Figure V.A 1 Appendix). However, for drainage, we observed in comparison to the other daily water fluxes a larger spatial variability (up to ± 6 mm d^{-1}), which might be related to the spatial variability of soil hydraulic properties.

Table V. 3: Cumulative water balance components derived from the weather and lysimeter station at the Wüstebach SOILCan test site from 2013-12-04 – 2016-04-30. The reference precipitation and evapotranspiration corresponds to precipitation derived from tipping bucket and the potential ET, respectively.

	Precipitation	Evapotranspiration	Discharge	Capillary rise	Storage change
	mm	mm	mm	mm	mm
Rain gauge/ Reference	2337	-1144	-	-	-
Lys-Wu4	2982	-907	-2131	38	-18
Lys-Wu5	3033	-882	-2217	31	-35
Lys-Wu6	3015	-923	-2142	32	-18
Lys-Wu8	2997	-869	-2186	39	-19
Average	3007	-895	-2169	34	-23

Figure V. 2 shows the isotopic compostion (δ^2H and $\delta^{18}O$) of P and of soil water sampled at different depths from lysimeter Lys-Wu4, Lys-Wu5 and Lys-Wu6. Stable isotope values in soil water samples from all depths (e.g. water line WL in 0.1 m in Figure V. 2) plot close to the local meteoric water line (LMWL) demonstrating no significant impact of fractionation processes due to evaporation or condensation. This implies that the assumption of no fractionation due to evaporation at the soil surface, which we made to define the boundary condition of the isotope transport model, will cause no significant bias between the simulated and measured isotope ratios in the soil. The lack of observable fractionation indicates low evaporation losses from the moss covered soil surfaces in the wet climate. The high insulating capacity of mosses (low thermal conductivity) can reduce the transfer of energy into the soil (Blok et al. 2011), dew formation declines water demand from the soil, and consequently, the moss layer restricts evaporation from the ground surface (Suzuki et al. 2007).

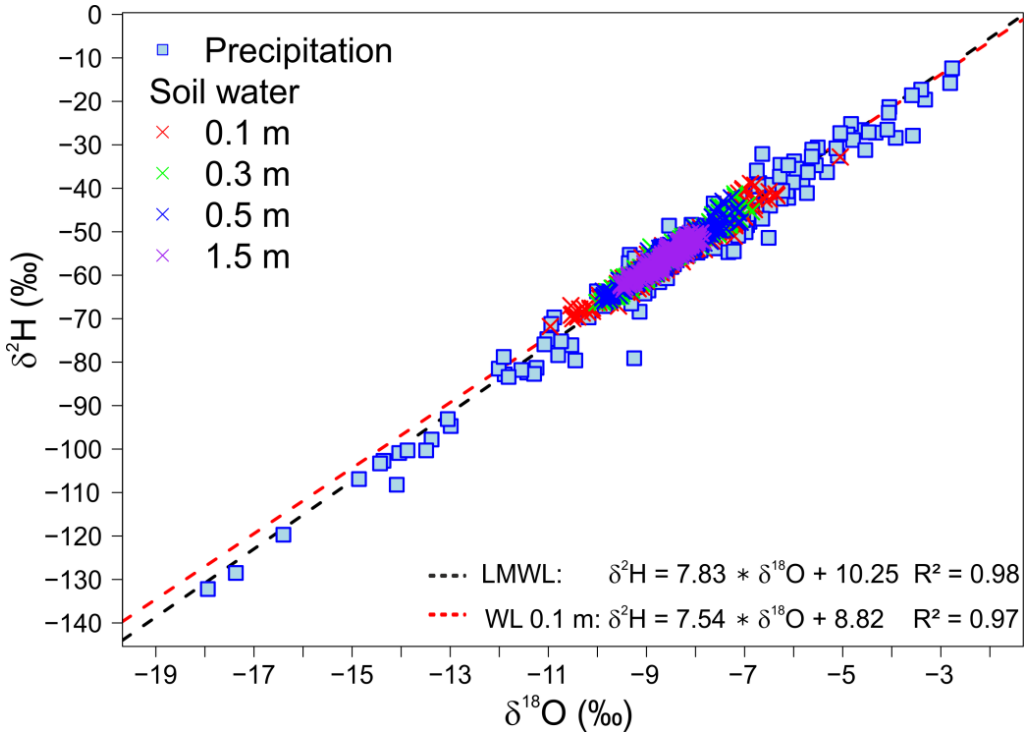

Figure V. 2: Isotopic composition of precipitation, soil water from three lysimeters at different soil depths, the local meteoric water line (LMWL) and water line in 0.1 m soil depth (WL).

V.3.2 Parameter optimization strategies

In this section, results of the four inverse optimization strategies BOS1, BOS2, 2SOS and MOS obtained for each lysimeter are discussed. The model performance per observation variable (NSE-θ, NSE-Ψ, NSE-18O) and AV-NSE efficiency criterion are summarized in Table V. 4. Additionally, information on the model performance for single observations variables ($NSE_{\theta,i}$, $NSE_{\Psi,i}$, $NSE_{18O,i}$) and depths (i) can be taken from Table V.A 2 (see Appendix). The observed water retention data and the simulated hydraulic conductivity curves, which varied largely between lysimeters, are shown in Figure V. 3 and Figure V. 4. Further details on the simulated and observed water content, matric potential, and isotope ratios of $\delta^{18}O$ can be taken from Figure V.A 2, Figure V.A 3, and Figure V.A 4 (see Appendix).

V.3.2.1 Model performance BOS1

The NSE values that were obtained with the BOS1 method for each lysimeter using water content and $\delta^{18}O$ ratios ranged between 0.52 and 0.65, -2.06 and 0.31, and -0.15 and 0.37, respectively for water content, matric potential and $\delta^{18}O$ data (Table V. 4). The smaller NSE-

Ψ values and the larger deviation between simulated and measured matric potentials (Figure V.A 3) compared to other state variables is obviously the consequence of not including the NSE-Ψ values in the OF as was found in previous studies by Wöhling and Vrugt (2011) and Groh et al. (2013). Hence, water retention functions obtained from BOS1 deviate from field observations (Figure V. 3). The simulated hydraulic conductivity varied between the lysimeters and the soil layer (Figure V. 4), and the strategy BOS1 achieved an average NSE value of -0.18, which describes the average NSE criterion between all lysimeters (see Lys-average Table V. 4).

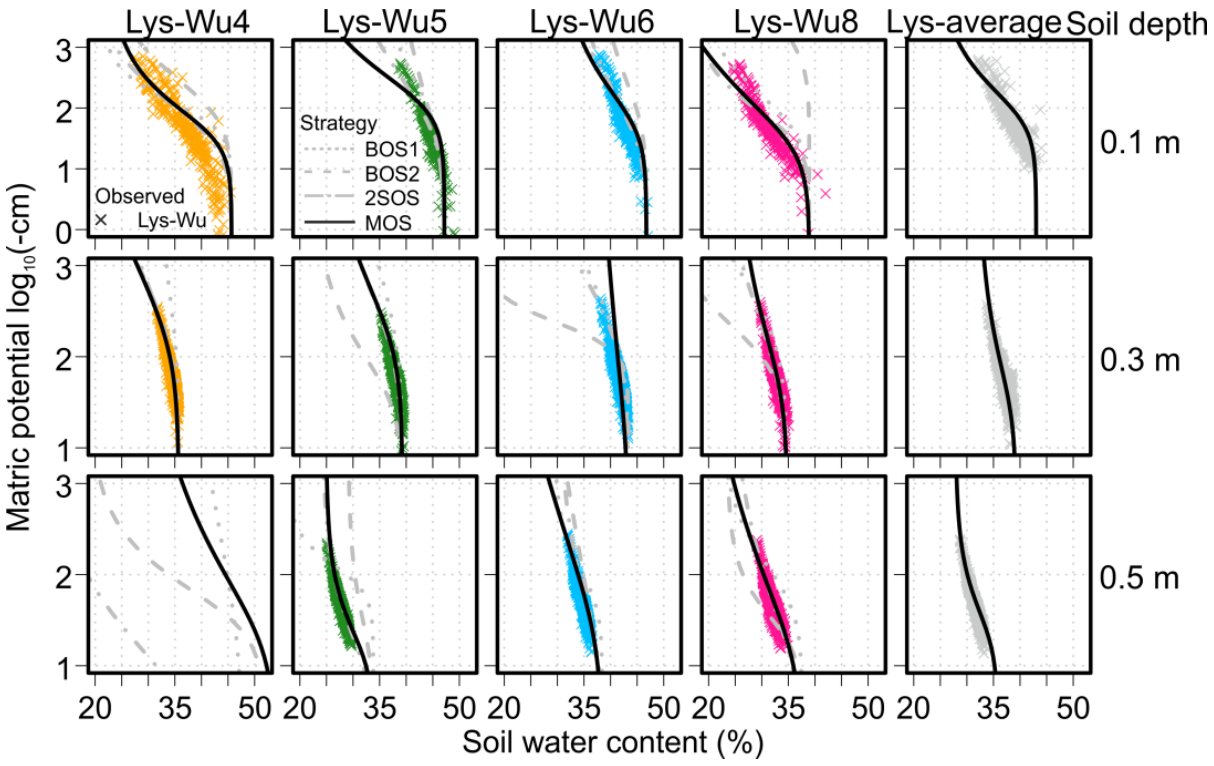

Figure V. 3: Observed field water retention data from four different lysimeters (Lys-Wu4, Lys-Wu5, Lys-Wu6, and Lys-Wu8) in three consecutive soil depths and the corresponding water retention curves from four different optimization strategies BOS1 (dotted line), BOS2 (dashed line), 2SOS (dash dotted line), and MOS (solid line). Additional average field water retention data (Lys-average) and the corresponding effective water retention curve obtained from strategy MOS are shown.

Table V. 4: Simulation results of four different inverse model strategies (BOS1, BOS2, 2SOS and MOS). Model performance values are reported aggregated for each observation type: water content (NSE-θ), matric potential (NSE-Ψ), and $\delta^{18}O$ ratios (NSE-18O). AV-NSE represents model performance for the entire vadose zone and was calculated per lysimeter from single NSE values per soil depth and observation type (equally weighted). Additionally NSE per observation type and entire vadose zone that were averaged over the four lysimeter (Lys-average) are reported.

	Lys-Wu4				Lys-Wu5				Lys-Wu6				Lys-Wu8				Lys-average			
	BOS1	BOS2	2SOS	MOS	BOS1	BOS2	2SOS	MOS	BOS1	BOS2	2SOS	MOS	BOS1	BOS2	2SOS	MOS	BOS1	BOS2	2SOS	MOS
NSE-θ	0.52	-0.68	0.54	0.52	0.65	-10.69	0.49	0.18	0.65	-2.11	0.53	0.40	0.52	-6.53	0.45	0.42	0.59	-5.00	0.50	0.38
NSE-Ψ	0.31	0.37	0.46	0.42	-2.06	0.12	0.09	-0.06	-0.66	0.43	0.24	0.26	-1.24	0.56	0.54	0.49	-0.91	0.37	0.33	0.28
NSE-18O	-0.11	-0.29	-0.97	-0.14	0.20	0.17	0.00	0.09	-0.15	0.17	-0.09	0.01	0.37	0.46	0.39	0.51	0.08	0.13	-0.17	0.12
AV-NSE	0.18	-0.11	-0.10	0.22	-0.50	-2.81	0.16	0.06	-0.11	-0.36	0.20	0.21	-0.30	-1.83	0.48	0.47	-0.18	-1.28	0.19	0.24

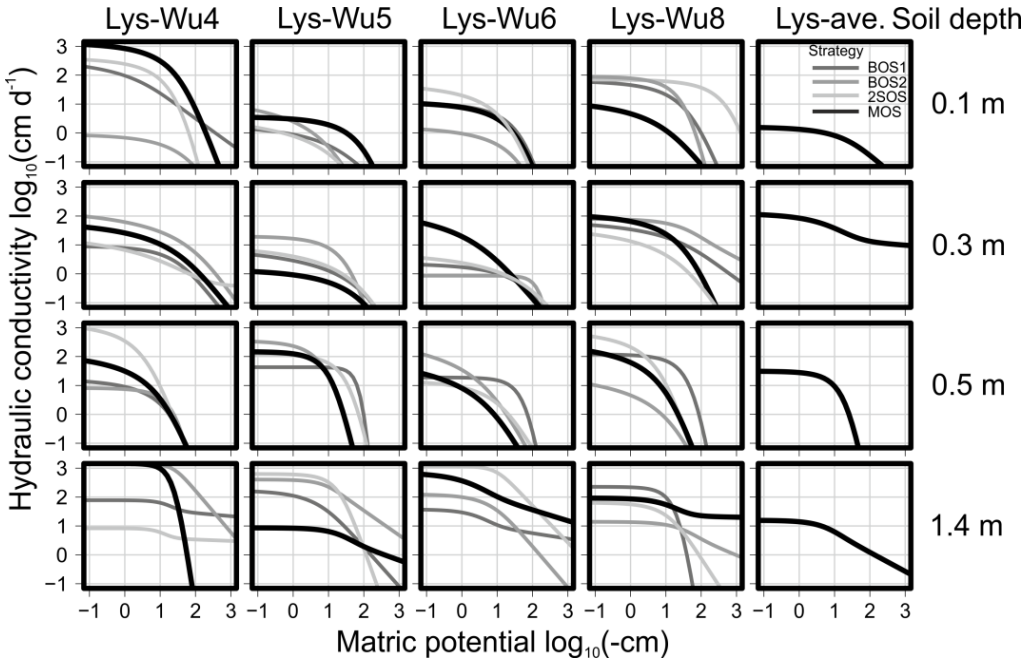

Figure V. 4: Simulated hydraulic conductivity curves at 0.1, 0.3, 0.5, and 1.4 m soil depth for lysimeter Lys-Wu4, Lys-Wu5, Lys-Wu6, and Lys-Wu8 from four different optimization strategies: BOS1, BOS2, 2SOS, and MOS. Effective simulated hydraulic conductivity curves obtain by strategy MOS are shown in Lys-average (Lys-ave.).

V.3.2.2 Model performance BOS2

For BOS2, which used matric potential and $\delta^{18}O$ ratios in the OF, measured and simulated matric potential and $\delta^{18}O$ ratios agreed well. NSE-Ψ and NSE-18O values varied between 0.12 and 0.56 and -0.29 and 0.46, respectively. Not including water content measurements in the OF led to large deviations between simulated and observed water contents at several depths (see Figure V.A 2) and consequently to small (very negative) NSE- θ values ($-10.69 <$ NSE-$\theta < -0.68$; Table V. 4). This might be related to the disequilibrium between measured *in situ* water contents and matric potentials due to different reaction times of the measuring instrument. According to the average NSE values, not including soil water content data in the OF led to a worse misfit of observations than not including matric potential measurements (average NSE Lys-average BOS2: -1.28). The optimal parameter-sets of BOS2 for each lysimeter are listed in Table V.A 2 (Appendix) and were for the most depths clearly different from values determined by BOS1 runs. The respective water retention functions yielded less reasonable fits to the observed field water retention data in comparison to results from BOS1 runs (see e.g. Lys-Wu5 in 0.5 m from Figure V. 3). Also the parameters of the unsaturated hydraulic conductivity function differed considerably between both strategies.

The $\delta^{18}O$ ratios were expected to contain some information about the prevailing water contents in the lysimeters since the advective tracer movement is determined by the water flux, which was given as a boundary condition and the water content in the soil profile. Interestingly, the $\delta^{18}O$ ratios could still be described adequately even when the water contents were off. Since water fluxes that drive the transport of the tracer are only significant when the soil is wet, the simulated tracer $\delta^{18}O$ ratios are apparently not influenced by the simulated water conditions during drier soil conditions. However, it must be noted that the small dependency of the tracer transport on the water contents during drier periods is also due to the high P amounts so that the soil is quickly rewetted and transport reactivated after a dry spell, and the timing of the transport is not affected strongly by the antecedent water content. Therefore, time series of $\delta^{18}O$ ratios may be more sensitive to simulated water contents at time periods when water fluxes are insignificant for tracer transport.

V.3.2.3 Model performance 2SOS

The simulation results from the stepwise strategy 2SOS, which used separate optimization runs to identify soil hydraulic properties based on time series of water content and matric potential and to identify the dispersivity from $\delta^{18}O$ ratios, are summarized in Table V. 4.

NSE-θ and NSE-Ψ values were relative similar to results for water content from BOS1 and for matric potential from BOS2, respectively. Thus water retention functions derived by strategy 2SOS agreed well with observed water retention data (see Figure V. 3). These findings are in line with previous studies, which showed that a combined use of information during the calibration procedure of water content and matric potential (Abbaspour et al. 2000; Zhang et al. 2003; Wöhling and Vrugt 2011; Caldwell et al. 2013; Groh et al. 2013) were beneficial for estimation of soil hydraulic parameters. The estimated parameters of the hydraulic conductivity function with strategy 2SOS differed considerable from BOS1 and BOS2.

Observed topsoil water retention data suggest at least for Lys-Wu5, Lys-Wu6 and Lys-Wu8 a bimodal pore size distribution. The use of uni-modal water retention function for the simulation led to an underestimation of soil water content in the top soil for matric potentials below approximately -110 cm. However, the Lys-average NSE-18O value was below zero (-0.17) and thus was clearly lower than obtained by strategy BOS1 (0.08) or BOS2 (0.13). Simulation results from 2SOS showed a considerable trade-off in fitting both water flow and solute transport parameters with a stepwise strategy. Hence, this suggests that time series of $\delta^{18}O$ ratios contain not only information content for optimizing solute transport, but also water flow parameters.

V.3.2.4 Model performance MOS

The temporal evolution of stable isotope and scatter plots between simulated and observed time series of water content and matric potential by strategy MOS, which included the three observation types in the OF, are depicted in Figure V.A 2, Figure V.A 3, and Figure V.A 4 (see Appendix). MOS achieved lower NSE-θ, but clearly higher NSE-Ψ than BOS1 (Table V. 4). Vice versa MOS simulations reached notable higher NSE-θ than BOS2, but lower NSE-Ψ values. NSE-180 values obtained by MOS were nearly identical to values obtained by BOS1 and BOS2. Comparing simulation results from strategy MOS with 2SOS showed that both strategies achieved rather similar values for NSE-Ψ, but lower NSE-θ. Water retention functions derived with MOS matched also reasonably well to the observed water retention. However, MOS obtained higher NSE-18O values than 2SOS (AV-NSE Lys-average MOS: 0.12; 2SOS: -0.17). This suggests, that the improved fit of $\delta^{18}O$ ratios when $\delta^{18}O$ ratios, water content, and matric potential measurements were used simultaneously in the optimization strategy, resulted in only a small trade-off in the description of the water contents and matric

potentials. Identified parameter-sets between MOS and 2SOS differed mainly in parameters of the unsaturated hydraulic function and dispersivities (see Appendix Table V.A 2 and Figure V. 4). This suggests, that $\delta^{18}O$ ratios contain additional information content for optimizing water flow parameters K_S, n and τ. Hence, the balanced solution MOS achieved in comparison to all other strategies the highest average NSE value (Lys-average: 0.24; see Table V. 4).

A recent simulation study by Sprenger et al. (2015) demonstrated the usefulness of combining soil water content measurements with $\delta^{18}O$ ratio profiles (destructive) to identify layer-wise water flow and solute transport parameters by inverse modelling. Our study supports these findings and demonstrates that a simultaneous instead of a stepwise use of hydrological and hydro-chemical data during the parameter optimization procedure increased the model realism and the parameter identifiability. In addition, we showed that expanding the dataset and including matric potentials adds important information that is required to estimate soil hydraulic parameters. Our investigation results implies for the setup of field hydrological tracer experiments to measure water content, matric potential, and water stable isotopes over time and in several depths to identify more precise estimates of soil hydraulic properties and dispersivities for layered soils. However, field experiments are often limited by e.g. budget or time. In this case it might be important to know which state variable should be monitored. Previous investigations showed that measuring only one state variable (e.g. $\delta^{18}O$ ratios) does not contain sufficient information to parametrize the vadose zone model. Thus, in case of such limiting conditions in the field, we recommend measuring at least water content and tracer data as soil water retention characteristic was much better defined by this strategy (BOS1) than using BOS2.

V.3.3 Effective parameters and boundary conditions

V.3.3.1 Effective parameters

The soil hydraulic parameters and the longitudinal dispersivity obtained from MOS varied, some considerably, between the four lysimeters and reflect the spatial heterogeneity of soil properties at the test site (see Figure V. 6). This heterogeneity was also apparent from the *in situ* soil texture analysis (Table V. 1) of two nearby located soil profiles and the spatial variability of locally observed state variables water content, matric potential, and $\delta^{18}O$ ratios within the lysimeters. The optimal parameters according to the average NSE criterion for the MOS optimization and the range of parameter values that resulted in similar average NSE

criteria (average NSE < optimal average NSE + 0.01), which is a relative measure for the parameter uncertainty (statistical inference about the parameter uncertainty was not performed and would require for instance a Bayesian framework), are depicted in Figure V. 5. The range of derived K_S values was in line with previous studies at the catchment (Borchardt 2012; Fang et al. 2016; Wiekenkamp et al. 2016b). Relatively high θ_r (up to 0.29) and low K_S values (between 3.6 and 15 cm d^{-1}, except for Lys-Wu4) were obtained for the top soil layers which had the highest clay content of the soil profile (32 % to 42 %). The high θ_r values are in line with results from Puhlmann and von Wilpert (2012) for forest soils with similar texture. Also concretions of iron were visible in the top soil layers, indicating high saturation degrees and low hydraulic conductivity in upper soil layer.

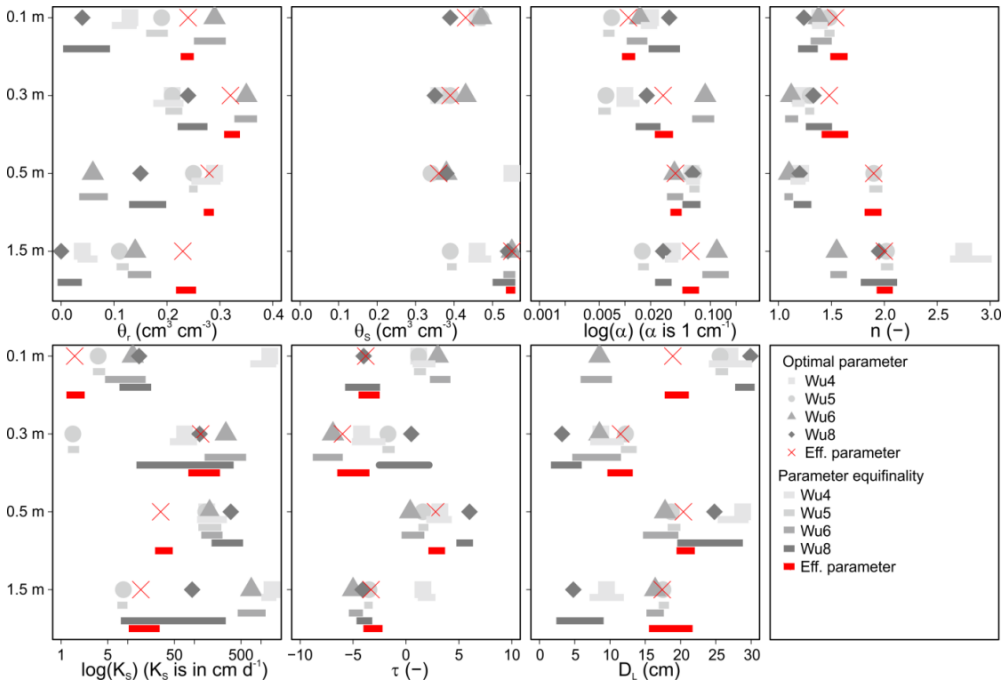

Figure V. 5: Best parameter values per depth and for each single lysimeter (Lys-Wu4, Lys-Wu5, Lys-Wu6, and Lys-Wu8) and average lysimeter (Eff. parameters) obtain from the MOS strategy. Vertical lines represent the parameter uncertainty associated with the parameter equifinality.

The parameter uncertainty ranges were for most soil hydraulic parameters and depths relatively small and smaller than the range of optimal parameter values in the different lysimeters. This low range indicates that most parameters were sensitive and identifiable. Only for Lys-Wu8 larger uncertainty ranges were obtained for θ_r, K_S, and τ. The pore connectivity parameter τ varied strongly between lysimeters and differed considerably from

the often used standard value $\tau = 0.5$ (Mualem 1976). Although negative τ are physically not feasible, because it implies a decrease of tortuosity when the soil dries out. Nevertheless, various studies showed negative τ for soils (e.g. Schaap and Leij 2000; Werisch et al. 2014; Cai et al. 2017) so that τ should be rather used as shape factor without any physical meaning (Peters et al. 2011). No consistent increase of solute dispersivity with depth was observed and dispersivity lengths ranging between 3 cm and 30 cm were in the upper range of the dispersivity lengths that were observed in soil column and field experiments under unsaturated flow conditions (Vanderborght and Vereecken 2007). The parameter uncertainty range for D_L was especially for Lys-Wu6 and Lys-Wu8 larger.

The parameter uncertainty and the variability of parameters obtained in different lysimeters, give rise to two questions. The first is whether our simulations results can predict the spatial variability in state variables that were observed between the different lysimeters. A positive answer to this question implies that the observed spatial variability can be represented by the variability of the optimized soil properties and the variability of the boundary fluxes. A negative answer indicates that other processes or variations in fluxes at a smaller spatial resolution than what is represented by the model and its boundary conditions play an important role for the generation of the observed variability.

Figure V. 6 plots the coefficient of variation (CV) versus the spatial mean of the variables at a given soil depth for both the measured and simulated variables. The CV of the water contents increase with decreasing water content, which is in line with a previous study at the catchment scale in Wüstebach (Korres et al. 2015). Water content at lower depths showed only a slight increase of spatial variability with lower water content, but was with CV of 10 % still high. For matric potential we observed a parabolic shape, with increasing spatial variability during both wetter and drier soil conditions. The lowest spatial variability was around -100 cm in the topsoil and ranged between pF -40 and -70 cm, and -24 to -80 cm in 0.3 and 0.5 m soil depth, respectively. The spatial variability of the simulated matric potentials at 1.4 m increased in the range from -10 to -1 cm (close to saturation) to ~700 % which was not observed for the measured values. However, the spatial variability in both water content and matric potential was generally well reproduced by the model simulations indicating that the spatial variability of these state variables could be reproduced using the variability of the estimated soil properties and the boundary conditions. The spatial variability of optimized parameters might be the reason for the larger observed variability of daily bottom boundary water fluxes between the lysimeters (see Figure V.A 1).

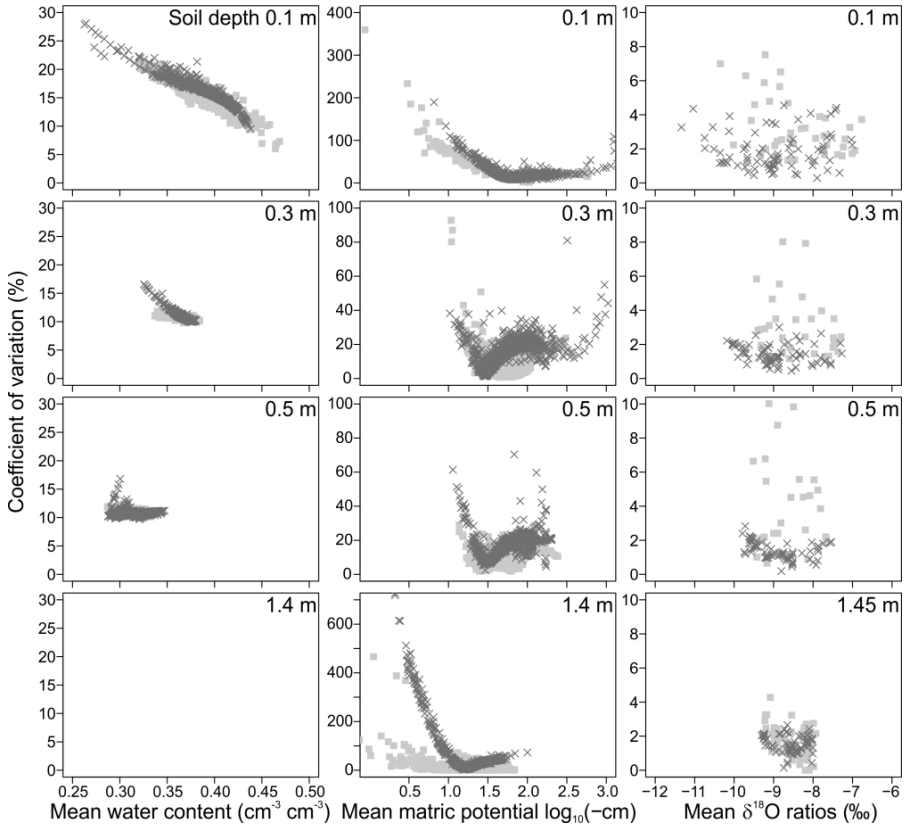

Figure V. 6: Coefficient of variation versus mean variable type of water content, matric potential and $\delta^{18}O$ ratios from field observations (light gray) and model simulations (MOS, dark gray) at different depths obtained from four lysimeters.

In contrast to the water content and matric potential, the spatial variability of the $\delta^{18}O$ ratios was largely underestimated by the simulations at 0.1, 0.3 and 0.5 m depths. This suggests that model simulations did not account for fast transport paths of tracer within macropores or local variations in water fluxes within the lysimeter. Several investigations showed that not only the model calibration but also the selection of model itself and model structure is of high importance as it affects the quality of the simulations significantly (Butts et al. 2004; Crosbie et al. 2011; Gosling et al. 2011; Moeck et al. 2016). Therefore the use of a different model structure that accounts for such fast transport paths (e.g. dual permeability; Gerke and van Genuchten 1993) and a bi-modal soil water retention characteristic (Romano and Nasta 2016) for the topsoil might have further improved simulations. However, a more complex model structure like the bi-modal water retention function would further increase the number of model parameters in the calibration process. A higher temporal tracer sampling frequency would be needed, to detect fast transport paths of water and tracer within macrospores and more sampling locations per depth to observe the spatial variability of tracer transport within

the lysimeter and to obtain a representative average of the concentrations at a certain depth in the lysimeters (Koestel et al. 2009; Garré et al. 2010).

A second question is whether the effective properties that are used to predict average water contents, matric potentials, and $\delta^{18}O$ ratios at a given depth at the site differ systematically from the parameters that were obtained for individual lysimeters. Hence, an additional model calibration run was conducted which optimized the soil hydraulic properties and longitudinal dispersivity using averaged state variables of water content, matric potential and $\delta^{18}O$ ratios and average boundary fluxes derived from four lysimeters. The model calibration reached with respect to NSE-θ, NSE-Ψ, and NSE-18O values of 0.46, 0.33, and 0.02 (Table V. 5) and thus achieved comparable results to average model performance in each individual lysimeter (Table V. 4). Effective parameters are summarized in Table V.A 2 (Appendix) and shown in Figure V. 3, 4, and 5. We did not observe a systematic difference between the effective parameters and the set of parameters that were obtained for the individual lysimeters. A cross validation of the calibrated vadose zone model with single lysimeter observations showed that the effective parameter-set was able to predict the state variables obtained from the corresponding lysimeter with only minor reduction of model performance in terms of matric potential and $\delta^{18}O$ ratios, but for water content NSE values were all below zero. Using a fixed θ_S in the cross validation from average water retention data caused a partially large offset between simulated and locally observed water content. Still, correlation analysis showed that the dynamic of simulated and observed water content agreed reasonably well (R^2 range >0.45 and <0.70).

Table V. 5: Model performance values from the effective parametrization ("Lysimeter"), the cross validation to predict with the effective parameter-set observations from the corresponding single lysimeter (Lys-Wu4, Lys-Wu5, Lys-Wu6, and Lys-Wu8), and the results from simulations using a less accurate measured precipitation (Rain-gauge) at the top and free drainage at the bottom.

	NSE-θ	NSE-Ψ	NSE-18O	AV-NSE
Lys-Wu4	-6.30	0.14	0.17	-1.14
Lys-Wu5	-4.65	0.13	0.17	-1.16
Lys-Wu6	-13.84	0.44	-0.14	-3.67
Lys-Wu8	-10.71	0.39	0.50	-3.29
Lysimeter	0.46	0.33	0.02	0.30
Rain-gauge	0.37	-45.96	0.29	-16.5

V.3.3.2 Lower precipitation accuracy

A less accurately defined atmospheric boundary condition (i.e. P) and bottom boundary (free drainage) and effective parameters obtained by MOS (see Lys-average Figure V. 3, Figure V. 4) were used to simulate water content, matric potential and $\delta^{18}O$ ratios at different measurements locations. The NSE values for the simulation (Rain-gauge) can be taken from Table V. 5. NSE values for water content decreased only a little from 0.46 to 0.39, but for matric potential NSE-Ψ showed a strong decrease from 0.33 to -45.57. The low NSE-Ψ was mainly related to matric potential simulation in 1.4 m soil depth. High n and a negative τ value in layer 5 (Figure V. 4) led in combination with the free-drainage lower boundary to low simulated matric potentials at the lysimeter bottom. This illustrates clearly that a zero-gradient bottom boundary condition cannot be used to simulate observed water fluxes in 1.45 m soil depth. For $\delta^{18}O$ an improvement of NSE-18O from 0.02 to 0.29 was achieved. However results from the simulation run "Lysimeter" captured the time series of simulated $\delta^{18}O$ ratios better than simulations from "Rain-gauge" (see Figure V. 7).

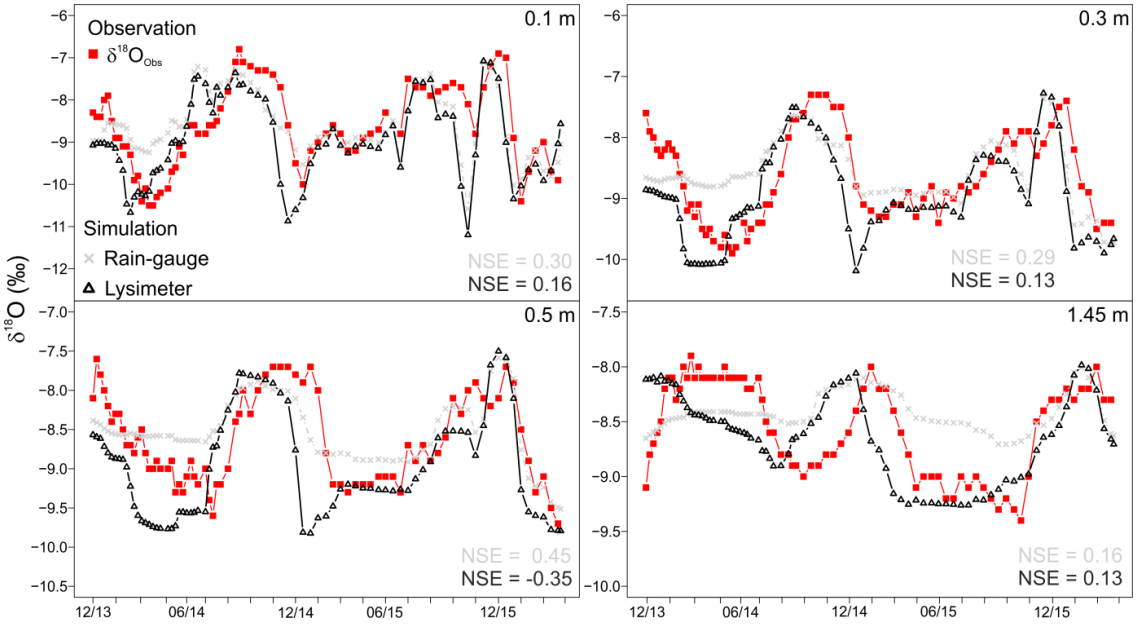

Figure V. 7: Observed and simulated $\delta^{18}O$ ratios at four soil depths from to simulation runs with upper and lower boundary conditions (i.e. Lysimeter; Rain-gauge).

Particularly $\delta^{18}O$ ratios in spring and summer did not agree well with observations, when using less accurate boundary conditions. Thus, the less pronounced shape of $\delta^{18}O$ ratios in the spring and summer led to a reduced sum of absolute squared differences between the predicted and observed isotopic signal and consequently to larger NSE-18O values.

Moreover, using a free-drainage boundary the cumulative drainage was reduced significantly by 761 mm during the calibration time. This result clearly demonstrates that using less accurately defined boundary conditions at the top (for example P) and bottom (free-drainage) clearly decreased the ability of the calibrated vadose zone model to simulate water content, matric potential and drainage.

V.3.3.3 Validation of dispersivities

The best parameter-set obtained for individual lysimeters from the MOS strategy was used to simulate the parallel conducted Br^- tracer experiment in a forward run with HYDRUS-1D for three lysimeters (Lys-Wu4, Lys-Wu6, and Lys-Wu8). Figure V. 8 plots the Br^- breakthrough curves (BTC) in four different depths for three lysimeters. Model simulation runs with the lysimeter specific best parameter-set from MOS showed a much faster simulated Br^- breakthrough than the observed breakthrough; particularly at larger depths (see gray dotted lines Figure V. 8). Hence, simulation results achieved low NSE values, with exception of layer 2 (0.1 m).

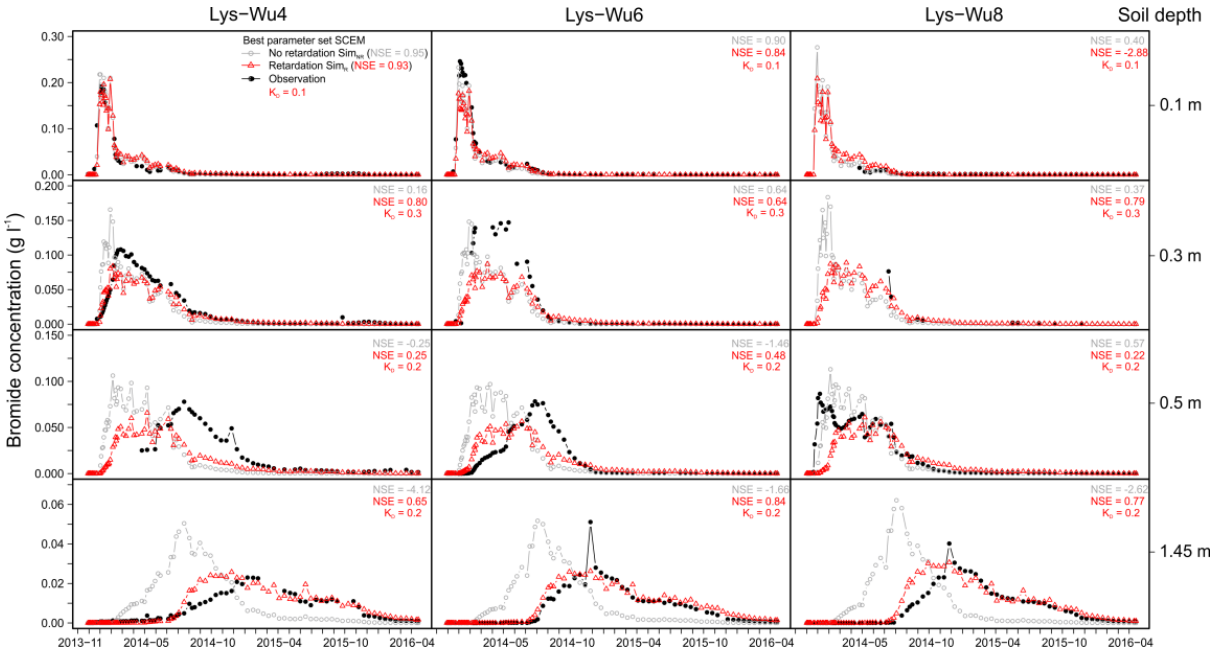

Figure V. 8: Observed (black dotted lines) and simulated bromide tracer breakthrough curves in four different soil depths and for three distinct lysimeters (Lys-Wu4, Lys-Wu6, Lys-Wu8). Solute transport simulations were conducted with the best parameter from the corresponding MOS strategy with (red dotted lines) and without (grey dotted lines) solute retardation. KD is the adsorption isotherm coefficient (cm^{-3} g^{-1}).

Br^- has been used often to study the movement of water through the vadose zone due to its presumed conservative properties in most soils (Kasteel et al. 2007; Stumpp et al. 2009; Skaggs et al. 2012). However, a non-conservative behavior (retardation factor (R) ≠ 1) of Br^- has been reported in few studies, where the faster (R < 1) or slower movement (R > 1) of Br^- than water were attributed to, respectively, anion exclusion (Gerritse and Adeney 1992; Russow et al. 1996) or anion adsorption (Boggs and Adams 1992; Seaman et al. 1995). The latter attributed retardation of Br^- in acid soils to adsorption on variable charged minerals (Al and Fe oxides or kaolinite).

The low soil pH values (range 4.2 – 4.8) and a high availability of oxides (range Fe_{ox}: 2204 to 16320 mg kg^{-1}; Mn_{ox}: 245 to 6675 mg kg^{-1}; Al_{ox}: 1412 to 6980 mg kg^{-1}), suggest that anion adsorption caused the delay of Br^-. We also observed a time lag between the simulated and observed $\delta^{18}O$ time (for example Lys-Wu4 in 0.5 m, Figure V.A 4). However, these time lags are much smaller and cannot explain the time lag between observed and simulated Br^- BTCs. When considering adsorption, the simulated Br^- BTC agreed (with exception of Lys-Wu4 0.1 m) much better with observations; particularly at the lysimeter bottom (retardation factor are reported in Figure V. 8). Our results of an overall slower movement of Br^- than water in acid soils (pH < 4.8; 0.1 M CaCl) agreed well with previous results from laboratory experiments (Goldberg and Kabengi 2010). Hence, the use of soil water $\delta^{18}O$ data in our experiment allowed us to identify the non-conservative behavior of Br^- at Wüstebach soils. The mere use of Br^- as "conservative" tracer under such geochemical conditions would have resulted in clearly different dispersivities and unsaturated hydraulic conductivities than obtained by water stable isotope data ($\delta^{18}O$). Apart from the conservative properties of $\delta^{18}O$, no extra application of tracer is required since it is an environmental tracer, and root water uptake occurs without fractionation (passive). Consequently, water stable isotopes allow monitoring transport behavior in the unsaturated zone over a much longer time period, in comparison to frequently used tracer pulses in hydrology. Additionally, we demonstrated that an experimental set-up with two tracers enables to validate the identified dispersivity parameters based on an independent tracer time series.

V.4 Conclusion

Joint observations of water contents and solute concentrations (Br^-) or isotopic ratios ($\delta^{18}O$; $\delta^{2}H$) have been used in inverse modelling strategies to estimate the soil hydraulic parameters and dispersivities. Here, we presented an inverse modeling study and investigated the

possibility to estimate soil hydraulic and dispersivity parameters from observations of water contents, $\delta^{18}O$ ratios that were extend with matric potential measurements in four undisturbed monolithic lysimeters. We evaluated different optimization strategies that considered different combinations of observed variables and sequential versus simultaneous optimizations. If either water content or matric potential were not included in the optimization, the variable that was not considered could not be reproduced well by the calibration model. This implies that the simulated relation between matric potential and water content, i.e. the water retention curve, did not reproduce the measured relation between the two variables and the obtained parameters of the retention function were not representative for the soil. When both water content and matric potential were used in the optimization, the simulated and measured water retention curve matched well. A sequential approach in which the transport parameter was fitted using $\delta^{18}O$ observations and using soil hydraulic parameters that were fitted based on water content and matric potential observations led to a less good simulation of $\delta^{18}O$ ratios than in case soil hydraulic and the transport parameters were fitted simultaneously. Including $\delta^{18}O$ in the simultaneous optimization led only to a slightly worse simulation of the water content and matric potential compared to the sequential optimization. This small trade-off indicated that $\delta^{18}O$ observations contained next to information about transport properties, also information about soil hydraulic properties. Hence, field experiments designed to inverse estimated water flow and solute transport parameters should consider the following points::

(1) combine water content and matric potential measurements to correctly identify the parameters of the soil water retention curve
(2) use water content, matric potential and tracer data (e.g. $\delta^{18}O$ ratios) simultaneously in the OF during the inverse model calibration to identify soil hydraulic properties and dispersivities of a layered soil

The water fluxes that were derived at the upper and lower boundary did not vary a lot between different lysimeter and thus suggests that a lysimeter may be considered to be representative for a larger area. However, due to soil heterogeneity local measurements of state variables vary in space. Considerable variation (particularly in local water content) was observed between different lysimeters. When local measurements in individual lysimeters are used to parameterize soil properties with the MOS strategy, the obtained water flow and solute transport parameters for a certain layer vary from lysimeter to lysimeter. Still, averaged state variables could be well described using effective parameters and simulations with these

effective parameters reproduced observations of certain states variables in the individual lysimeters fairly well and thus confirmed our assumption that lysimeters are representative for a larger area. The upper and lower boundary condition derived from lysimeter observations deviated considerably from boundary conditions obtained from other measurement types. Thus, using lysimeter observations to define accurately the boundary conditions of the model domain were highly beneficial and present an important asset of lysimeters. Methods that improve the accuracy of flux measurements in the field, especially P, are therefore central for improving inverse modeling studies. Given the cost of flux measurements in comparison with measurements of water content and matric potential, which can be carried out with relatively cheap sensors, saving on these local sensors does not seem economical.

To further confirm our soil profile parameterization, forward simulation runs with the best parameter-set using all three state variables (MOS) were evaluated for a parallel conducted bromide (Br^-) tracer experiment. Field observation of Br^- breakthrough curves showed a clear delay of tracer compared to model simulations. When accounting for anion adsorption on amorphous oxides (Al, Fe) and clay minerals in the acid forest soil (pH < 4.8), the transport of Br^- could be described successfully and hence validated the identified dispersivity parameters independently. Thus, the use of the environmental tracer $\delta^{18}O$ data was beneficial to track water movement through the soil continuously over a relative long time period (2.5 years) and to confirm the non-conservative behavior of Br^-.

VI General Conclusion and Outlook

VI.1 Conclusion

The overall aim of the investigation was to identify and quantify processes and factors that influence the transfer of water and matter across the boundaries of soil-plant-atmosphere systems to improve our understanding of the water cycle and solute transport dynamics in the vadose zone. To achieve this, synthetic and real datasets of novel lysimeter devices with a tension controlled bottom boundary system were used in this work. Such modern lysimeter systems allow the observation of water and matter fluxes in the soil monolith under natural field conditions. A synthetic dataset was used in Chapter II to investigate the impact of changes in surrounding soil texture properties and water table depths on the estimation of water fluxes at the bottom of the critical zone using transferred lysimeters with a tension controlled bottom boundary. The results was discuss especially in the context of the climate change experiment SOILCan (Pütz et al. 2016). The Chapter III and IV focused on the quantification and estimation of non-rainfall water and nighttime ET and their overall contribution to the water balance of grasslands. Outcomes from the latter two investigations were used in Chapter V as model boundary condition in a final simulation study, to develop an inverse model procedure which optimizes the estimation of soil hydraulic and solute transport parameters including water stable isotopes and lysimeter data. The following sections summarize the main hypothesis, discuss the overall aims and outcomes of this thesis in a broader context and indicate possible future research topics in the field of land surface hydrology.

i) **Changes in surrounding soil texture properties and water table depths have a significant impact on the estimation of water fluxes in transferred lysimeters with a tension controlled bottom boundary.**

Tension controlled lysimeter systems are used in the project TERENO SOILCan (Pütz et al. 2016) to study the effect of climate change on soil hydrology. Lysimeters with similar soil texture were transferred to other locations to simulate the soil water balance under different climate regimes. With the transfer of lysimeter in the simulation setup, not only the atmospheric but also the surrounding subsurface conditions changed and influenced the measured matric potentials that are used to control the bottom boundary of the transferred lysimeters.

This indicates, that the use of non-appropriate soil texture properties and water table depths which do not correspond to the conditions where the lysimeter originated from,

potentially led to large differences in soil water fluxes and seasonal water flux dynamics across the lysimeter bottom.

Thus, changes in surrounding subsurface conditions had a significant influence on the measured matric potentials that were used to control the bottom boundary of transferred lysimeter. The use of non-representative matric potentials to control the bottom boundary of transferred lysimeter had an important impact on the water fluxes in the system. This impact may override the effect of changing climate conditions in the considered terrestrial ecosystem of experimental climate change studies.

ii) **Dew and hoar frost formation contributes substantially to the water budgets of a low mountain range and alpine grassland. The seasonal amount of non-rainfall events for two different grassland ecosystems could be estimated well based on standard meteorological variables.**

Weighable precision lysimeter data over two consecutive hydrological years were used to determine dew and hoar frost formation for a low mountain range and alpine grassland. Our investigation showed that non-rainfall water from dew and hoar frost contributed with up to 6 % of the total yearly P substantially to the water budgets of grasslands. Our investigation revealed that dew was an important source of water for the grassland ecosystem during periods of drought. Hoar frost formation might take over an important ecological function during colder periods of the year as it thermally protects crops and reduce possible injuries from low temperatures. However, further plant specific measurements are of need to confirm the ecological relevance of non-rainfall water. Standard meteorological variables and the Penman-Monteith equation could be used to predict the seasonal amount of non-rainfall water from dew and hoar frost formation.

Thus, dew and hoar frost might take over a relevant ecological function in the ecosystem, contributed substantially to the water budgets of a low mountain range and alpine grassland and could be estimate from the Penman-Monteith equation.

iii) Nighttime evapotranspiration contributes substantially to the total evapotranspiration, is driven by environmental variables and changes under heat wave conditions.

Lysimeter observations from two distinct low mountain range grasslands were used to quantify the water losses from the land surface into the atmosphere during nighttime. On a yearly basis, nighttime water losses ranged between 3 – 10 % of daytime losses.

Wind was the most significant driver for nighttime ET. Rates of ET during night increased considerable in periods subjected to heat waves. Water losses during night could be predicted based on meteorological variables with the Penman-Monteith equation, when we assume that the nighttime surface resistance parameter, which is normally used to represent the effect of stomatal closure at night, equals the value for daytime calculation. However, the Penmann-Monteith model could not predict the increase of nighttime ET during heat waves.

Thus, our investigation showed that nighttime ET contributes substantially to the total ET of two low mountain range grasslands.

iv) Simultaneous multiple observation types are required in the objective function during the inverse model calibration to optimize the stimation of soil hydraulic and dispersivity parameters of a layered soil under realistic boundary conditions.

Several studies have used in the past joint observations of the state variables water content and tracer data to estimate soil hydraulic parameters and dispersivities by inverse modeling. Our investigation showed that both soil water content and matric potential data are necessary in objective function to determine the soil water characteristic. In addition, the use of stable water isotopes ($\delta^{18}O$ ratios) in soil water contained not only information content to inversely estimate solute transport but also soil hydraulic parameters. Moreover, using $\delta^{18}O$ ratios the non-conservative behavior of bromide tracer under prevailing geochemical soil conditions could be verified. Additionally our experimental set-up with two tracers ($\delta^{18}O$, bromide) allowed calibrating and validating the identified dispersivity parameters independently.

Thus, our inverse modeling study demonstrates that simultaneous information of soil water content, matric potential and tracer data are prerequisite in objective function during the model calibration to improve the estimation of water flow and solute transport parameter of layered soils.

VI.2 Synthesis

Investigations from Chapter II based on synthetic data have shown the importance to account for the interdependency of soil and land surface water fluxes dynamics. Measuring ET fluxes with lysimeter which not account for such interactions, will lead to a biased estimate of unsaturated zone evaporation and transpiration processes (Yin et al. 2015; Liu et al. 2016; Balugani et al. 2017; Satchithanantham et al. 2017). However, lysimeter with a tension-

controlled bottom boundary account for such interdependencies and feedbacks of water fluxes.

Anderson et al. (2017) presented that ET can be estimated based on a wide variety of techniques including lysimetery, micrometeorology (e.g. eddy-covariance; scintillometer), satellite remote sensing, water balance, or a combined approach. There is increasing evidence from recent investigations that ET processes also occurs during night (Caird et al. 2007a; Agam et al. 2012; Forster 2014). However, the various methods, excluding lysimtery, provide only limited or no information on nighttime water loss. Depending on the climate, vegetation and soil conditions, water loss at nighttime can reach up to 55 % of the daytime ET (Schoppach et al. 2014). Knowledge on such water fluxes are important for plant productivity, irrigation management, water footprints, transfer and redistribution of solutes, atmospheric processes (energy transfer), breeding crops, water balance, and carbon budgets.

Non-rainfall atmospheric water (e.g. dew) plays an important role on ET processes, because non-rainfall water alleviates moisture stress of plants (Uclés et al. 2013) and reduce or suppress transpiration losses by dew evaporation in the morning (Sudmeyer et al. 1994; Gerlein-Safdi et al. 2017). Ben-Asher et al. (2010) showed that plants from a semi-arid region highly benefit from a high CO_2 gradient towards the canopy, which was induced from nighttime respiration, and low transpiration water loss during dew affected morning hours. The quantity of non-rainfall water depends not only on meteorological conditions, but also on the land surface vegetation cover (Xiao et al. 2009; Xiao et al. 2013) and can be estimate by high precision lysimeter (Meissner et al. 2007). Ninari and Berliner (2002) showed that micro-lysimeter with limited soil depth might fail to correctly measure dewfall, since the temperature regime in the lysimeter are different than outside the device. This suggests an additional benefit of using modern lysimeter system, because the bottom boundary control ensure not only that water fluxes but also the temperature profile in the lysimeter is comparable to the surrounding natural soil (Podlasly and Schwärzel 2013; Pütz et al. 2016).

The use of such precise information on water fluxes constrains realistically the boundaries of inverse model simulations to estimate parameter that describe the water and solute transport behavior of the vadose zone. The experimental set-up from the last study (Chapter V) with two tracers ($\delta^{18}O$, bromide) allowed calibrating and validating the identified solute transport parameters independently. In addition using water stables isotopes the non-conservative behavior of bromide tracer under the prevailing geochemical soil conditions could be confirmed. Not using all necessary information on state variables in the parameter

optimization procedure reduced largely the parameter identification. The use of less accurate defined boundaries (i.e. P, free drainage) decreases the ability to simulate water and solute transport processes in the vadose zone.

This all demonstrates the strong interdependency of water and matter fluxes between different pools in the ground (water table; soil), the vegetation and the atmosphere. Although recent model developments have improved our ability to integrate physical, biological and chemical processes at different scales (Sato et al. 2015; Gebler et al. 2017; Klosterhalfen et al. 2017), new understandings of earth system dynamics are based on integrated observations (Baatz et al. 2017). To conclude, modern lysimeter observations account for feedbacks across the complete hydrological cycle (soil, plant, atmosphere) and thus indeed provide a more holistic consideration of water and solute movements across the boundaries of the vadose zone.

VI.3 Outlook

This study highlights the relevance of non-rainfall water, nighttime ET, bottom boundary and geochemical conditions on the water cycle and solute transport dynamics. The knowledge on the seasonal development and quantity of non-rainfall events and nighttime ET is novel for low mountain range grassland ecosystems. A next logical step would be to investigate the source of nighttime ET and the synergy of such land surface-atmosphere interactions, to clarify i) the impact of non-rainfall events and nighttime transpiration on the change of crop water use efficiency, ii) the effect of non-rainfall events on the diurnal course of photosynthesis and transpiration rates, iii) the effect on the movement of solutes in the vadose zone, iv) the impact of circadian regulation on the ecosystem nighttime transpiration, v) the influence of droughts on nighttime water fluxes, and vi) the influence of climate change on the course and quantity of such water fluxes. Furthermore, the development of models to predict within a high temporal resolution (< hourly) both water fluxes for different land surface ecosystems e.g. based on standard meteorological, soil and vegetation measurements, would be a major development in land surface hydrology research, to simulate and quantify realistic water budgets, carbon balances and energy fluxes from plot to landscape level.

Future research on dew harvesting could benefit from lysimeter measurements. Observations on the formation of dew on natural surface could be useful; to improve material properties of commercial dew condenser and help to maximize dew yield. Harvested water from non-rainfall events could be used for both, human consumption and agriculture. Using a larger quantity of non-rainfall water from fog collector (daily 3.9 L/m²; Hiatt et al. 2012), passive

(daily 0.6 L/m²; Muselli et al. 2009) or active dew collectors (50 L/day; Khalil et al. 2016) for irrigation could be a helpful and sustainable tool to reduce the depletion of groundwater resources and might minimize the emissions of CO_2 to the atmosphere from groundwater used for irrigation (Wood and Hyndman 2017) in many water scarce regions.

Climate change will alter all components of the terrestrial hydrology, because it involves an increased variability in climatic drivers and enhanced intensity and frequency of extreme events (e.g. droughts, floods). These changes will affect the fate of agrochemicals and organic pollutants, and the conditions for crop growth and soil productivity. Changing climatic drivers will potentially alter the structure, the organic carbon content, hydrophobicity, erodibility, and nutrient availability of soils. However, the impact of climate change regarding the alteration and variability of hydraulic properties and solute transport of soils has only rarely been assessed quantitatively under realistic field conditions. We initiated within this PhD a tracer experiment on in total 78 lysimeters, using stable water isotopes and/ or bromide, to investigate the effect of climate change on solute transport behavior of soils. The ongoing output of this tracer experiment will help to clarify the important question, how solute transport processes in soils are influenced by climate change.

In general the long-term TERENO SOILCan project provide such a valuable and unique datasets to evaluate the potential impact of climate change on arable- and grassland soils from different pedo- and climatological regions of Germany (Pütz et al. 2016). The outputs will help to develop and improve predictions that account for interactions between future climate conditions and soil processes at larger scale.

VII References

Abbasi, F., J. Simunek, J. Feyen, M.T. van Genuchten and P.J. Shouse. 2003. Simultaneous Inverse Estimation of Soil Hydraulic and Solute Transport Parameters from Transient Field Experiments: Homogeneous Soil. *Transactions of the ASAE* 46, no. 4.

Abbaspour, K., R. Kasteel and R. Schulin. 2000. Inverse parameter estimation in a layered unsaturated field soil. *Soil Science* 165: 109-118.

Abdou, H.M. and M. Flury. 2004. Simulation of water flow and solute transport in free-drainage lysimeters and field soils with heterogeneous structures. *European Journal of Soil Science* 55: 229-241.

Ad-hoc-Arbeitsgruppe-Boden. 2005. Bodenkundliche Kartieranleitung, Bundesanstalt für Geowissenschaften und Rohstoffe in Zusammenarbeit mit den Staatlichen Geologischen Diensten, Hannover.

Aeschbach-Hertig, W. and T. Gleeson. 2012. Regional strategies for the accelerating global problem of groundwater depletion. *Nature Geosci* 5: 853-861.

Agam, N. and P.R. Berliner. 2006. Dew formation and water vapor adsorption in semi-arid environments - A review. *Journal of Arid Environments* 65: 572-590.

Agam, N., S.R. Evett, J.A. Tolk, W.P. Kustas, P.D. Colaizzi, J.G. Alfieri, et al. 2012. Evaporative loss from irrigated interrows in a highly advective semi-arid agricultural area. *Advances in Water Resources* 50: 20-30.

Allen, R.G., L.S. Pereira, D. Raes and M. Smith. (1998). Crop evapotranspiration - Guidelines for computing crop water requirements FAO, Rome.

Allen, R.G., W.O. Pruitt, J.L. Wright, T.A. Howell, F. Ventura, R. Snyder, et al. 2006. A recommendation on standardized surface resistance for hourly calculation of reference ETo by the FAO56 Penman-Monteith method. *Agricultural Water Management* 81: 1-22.

Anderson, R., X. Zhang and T.H. Skaggs. 2017. Measurement and partitioning of evapotranspiration (ET) for application to vadose zone studies. *Vadose Zone Journal*.

Anderson, T.R., C.L. Goodale, P.M. Groffman and M.T. Walter. 2014. Assessing denitrification from seasonally saturated soils in an agricultural landscape: A farm-scale mass-balance approach. *Agriculture, Ecosystems & Environment* 189: 60-69.

ASCE-EWRI. (2005). The ASCE Standardized Reference Evapotranspiration Equation. Technical Committe report to the Environmental and Water Resources Institute of the American Society of Civil Engineers from theTask Committee on Standardization of Reference Evapotranspiration, p. 173, ASCE-EWRI, 1801 Alexander Bell Drive, Reston, VA 20191-4400.

Baatz, R., P.L. Sullivan, L. Li, S. Weintraub, H.W. Loescher, M. Mirtl, et al. 2017. Integration of terrestrial observational networks: opportunity for advancing Earth system dynamics modelling. *Earth Syst. Dynam. Discuss.* 2017: 1-30.

Baier, W. 1966. Studies on dew formation under semi-arid conditions. *Agricultural Meteorology* 3: 103-112.

Balugani, E., M.W. Lubczynski, L. Reyes-Acosta, C. van der Tol, A.P. Francés and K. Metselaar. 2017. Groundwater and unsaturated zone evaporation and transpiration in a semi-arid open woodland. *Journal of Hydrology* 547: 54-66.

Bear, J. 1972. Dynamics of fluids in porous media, American Elsevier Pub. Co, New York.

Ben-Asher, J., P. Alpert and A. Ben-Zvi. 2010. Dew is a major factor affecting vegetation water use efficiency rather than a source of water in the eastern Mediterranean area. *Water Resources Research* 46: n/a-n/a.

Beven, K. 2006. A manifesto for the equifinality thesis. *Journal of Hydrology* 320: 18-36.

Beysens, D. 1995. The formation of dew. *Atmospheric Research* 39: 215-237.

Beysens, D. 2016. Estimating dew yield worldwide from a few meteo data. *Atmospheric Research* 167: 146-155.

Bivand, R. and N. Lewin-Koch. (2016). maptools: Tools for Reading and Handling Spatial Objects. R package version 0.8-39. https://CRAN.R-project.org/package=maptools.

Blok, D., M.M.P.D. Heijmans, G. Schaepman-Strub, J. van Ruijven, F.J.W. Parmentier, T.C. Maximov, et al. 2011. The Cooling Capacity of Mosses: Controls on Water and Energy Fluxes in a Siberian Tundra Site. *Ecosystems* 14: 1055-1065.

Boesten, J.J.T.I. 2007. Simulation of Pesticide Leaching in the Field and in Zero-Tension Lysimeters. *Vadose Zone Journal* 6: 793-804.

Bogena, H., R. Kunkel, T. Pütz, H. Vereecken, E. Krüger, S. Zacharias, et al. 2012. TERENO - Ein langfristiges Beobachtungsnetzwerk für die terrestrische Umweltforschung. (In German, with English abstract.) *Hydrologie und Wasserwirtschaft* 53: 138-143.

Bogena, H., R. Bol, N. Borchard, N. Brüggemann, B. Diekkrüger, C. Drüe, et al. 2015. A terrestrial observatory approach to the integrated investigation of the effects of deforestation on water, energy, and matter fluxes. *Science China Earth Sciences* 58: 61-75.

Bogena, H., E. Borg, A. Brauer, P. Dietrich, I. Hajnsek, I. Heinrich, et al. 2016. TERENO: German network of terrestrial environmental observatories. *Journal of large-scale research facilities* 2: 1-8.

Boggs, J.M. and E.E. Adams. 1992. Field study of dispersion in a heterogeneous aquifer: 4. Investigation of adsorption and sampling bias. *Water Resources Research* 28: 3325-3336.

Borchardt, H. (2012). Einfluss periglazialer Deckschichten auf Abflusssteuerung am Beispiel des anthropogen überprägten Wüstebaches (Nationalpark Eifel). PhD Diss, RWTH Aachen, Aachen, Germany.

Brauer, C.C., A. Overeem, H. Leijnse and R. Uijlenhoet. 2016. The effect of differences between rainfall measurement techniques on groundwater and discharge simulations in a lowland catchment. *Hydrological Processes* 30: 3885-3900.

Breuer, L., K. Eckhardt and H.-G. Frede. 2003. Plant parameter values for models in temperate climates. *Ecological Modelling* 169: 237-293.

Briones, M.J.I., P. Ineson and J. Poskitt. 1998. Climate change and Cognettia sphagnetorum: effects on carbon dynamics in organic soils. *Functional Ecology* 12: 528-535.

Brown, R., A.J. Mills and C. Jack. 2008. Non-rainfall moisture inputs in the Knersvlakte: Methodology and preliminary findings. *Water SA* 34: 275-278.

Bucci, S.J., G. Goldstein, F.C. Meinzer, A.C. Franco, P. Campanello and F.G. Scholz. 2005. Mechanisms contributing to seasonal homeostasis of minimum leaf water potential and predawn disequilibrium between soil and plant water potential in Neotropical savanna trees. *Trees* 19: 296-304.

Butts, M.B., J.T. Payne, M. Kristensen and H. Madsen. 2004. An evaluation of the impact of model structure on hydrological modelling uncertainty for streamflow simulation. *Journal of Hydrology* 298: 242-266.

Buytaert, W., V. Iñiguez, R. Celleri, B. De Bièvre, G. Wyseure and J. Deckers. 2006. Environmental Role of Wetlands in Headwaters. Krecek, J. and Haigh, M. (eds), pp. 271-281, Springer Netherlands, Dordrecht.

Cai, G., J. Vanderborght, A. Klotzsche, J. van der Kruk, J. Neumann, N. Hermes, et al. 2016. Construction of Minirhizotron Facilities for Investigating Root Zone Processes. *Vadose Zone Journal* 15.

Cai, G., J. Vanderborght, V. Couvreur, C.M. Mboh and H. Vereecken. 2017. Parameterization of Root Water Uptake Models Considering Dynamic Root Distributions and Water Uptake Compensation. *Vadose Zone Journal*.

Caird, M.A., J.H. Richards and L.A. Donovan. 2007a. Nighttime Stomatal Conductance and Transpiration in C3 and C4 Plants. *Plant Physiology* 143: 4-10.

Caird, M.A., J.H. Richards and T.C. Hsiao. 2007b. Significant transpirational water loss occurs throughout the night in field-grown tomato. *Functional Plant Biology* 34: 172-177.

Caldwell, T.G., T. Wöhling, M.H. Young, D.P. Boyle and E.V. McDonald. 2013. Characterizing Disturbed Desert Soils Using Multiobjective Parameter Optimization. *Vadose Zone Journal* 12.

Carsel, R.F. and R.S. Parrish. 1988. Developing joint probability distributions of soil water retention characteristics. *Water Resources Research* 24: 755-769.

Chaves, M.M., J.M. Costa, O. Zarrouk, C. Pinheiro, C.M. Lopes and J.S. Pereira. 2016. Controlling stomatal aperture in semi-arid regions - The dilemma of saving water or being cool? *Plant Science* 251: 54-64.

Chen, X. and Q. Hu. 2004. Groundwater influences on soil moisture and surface evaporation. *Journal of Hydrology* 297: 285-300.

Claverie, E., F. Meunier, M. Javaux and W. Sadok. 2017. Increased contribution of wheat nocturnal transpiration to daily water use under drought. *Physiologia Plantarum*: n/a-n/a.

Clus, O., I. Lekouch, M. Muselli, I. Milimouk-Melnytchouk and D. Beysens. 2013. Dew, fog and rain water collectors in a village of S-Morocco (Idouasskssou). *Desalination and Water Treatment* 51: 4235-4238.

Coupel-Ledru, A., E. Lebon, A. Christophe, A. Gallo, P. Gago, F. Pantin, et al. 2016. Reduced nighttime transpiration is a relevant breeding target for high water-use efficiency in grapevine. *Proceedings of the National Academy of Sciences* 113: 8963-8968.

Cowan, I.R. and G.D. Farquhar. 1977. Stomatal function in relation to leaf metabolism and environment: Stomatal function in the regulation of gas exchange. In, Symposia of the Society for Experimental Biology. 471-505.

Crosbie, R.S., W.R. Dawes, S.P. Charles, F.S. Mpelasoka, S. Aryal, O. Barron, et al. 2011. Differences in future recharge estimates due to GCMs, downscaling methods and hydrological models. *Geophysical Research Letters* 38: n/a-n/a.

Csintalan, Z., Z. Takács, M.C.F. Proctor, Z. Nagy and Z. Tuba. 2000. Early morning photosynthesis of the moss Tortula ruralis following summer dew fall in a Hungarian temperate dry sandy grassland. *Plant Ecology* 151: 51-54.

Dawson, T.E., S.S.O. Burgess, K.P. Tu, R.S. Oliveira, L.S. Santiago, J.B. Fisher, et al. 2007. Nighttime transpiration in woody plants from contrasting ecosystems. *Tree Physiology* 27: 561-575.

De Boeck, H.J., S. Bassin, M. Verlinden, M. Zeiter and E. Hiltbrunner. 2016. Simulated heat waves affected alpine grassland only in combination with drought. *New Phytologist* 209: 531-541.

Dodd, A.N., N. Salathia, A. Hall, E. Kévei, R. Tóth, F. Nagy, et al. 2005. Plant Circadian Clocks Increase Photosynthesis, Growth, Survival, and Competitive Advantage. *Science* 309: 630-633.

Doronila, A.I. and M.A. Forster. 2015. Performance Measurement Via Sap Flow Monitoring of Three Eucalyptus Species for Mine Site and Dryland Salinity Phytoremediation. *INTERNATIONAL JOURNAL OF PHYTOREMEDIATION* 17: 101-108.

Eller, F., K. Jensen and C. Reisdorff. 2017. Nighttime stomatal conductance differs with nutrient availability in two temperate floodplain tree species. *Tree Physiology* 37: 428-440.

Evenari, M., L. Shanan and N. Tadmor. 1971. The Negev: The Challenge of a Desert, Harvard University Press, Cambridge, Massachusetts.

Ewers, B.E. 2013. Understanding stomatal conductance responses to long-term environmental changes: a Bayesian framework that combines patterns and processes. *Tree Physiology* 33: 119-122.

Fang, Z., H. Bogena, S. Kollet, J. Koch and H. Vereecken. 2015. Spatio-temporal validation of long-term 3D hydrological simulations of a forested catchment using empirical orthogonal functions and wavelet coherence analysis. *Journal of Hydrology* 529, Part 3: 1754-1767.

Fang, Z., H. Bogena, S. Kollet and H. Vereecken. 2016. Scale dependent parameterization of soil hydraulic conductivity in 3D simulation of hydrological processes in a forested headwater catchment. *Journal of Hydrology* 536: 365-375.

Fank, J. and G. Unold. 2007. High-precision weighable field Lysimeter – a tool to measure water and solute balance parameters. *International Water and Irrigation* 27: 28-32.

Fank, J. 2013. Wasserbilanzauswertung aus Präzisionslysimeterdaten. (In German, with English abstract.) In, Gumpensteiner Lysimetertagung, Lehr- und Forschungszentrum für Landwirtschaft Raumberg-Gumpenstein. 85-92.

FAO. (1990). Food and Agriculture Organization of the United Nations Expert consultation on revision of FAO methodologies for crop water requirements, ANNEX V, FAO Penman-Monteith Formula, Rome Italy.

Feddes, R.A., P.J. Kowalik and H. Zaradny. 1978. Simulation of Field Water Use and Crop Yield, John Wiley & Sons, New York.

Ferguson, I.M. and R.M. Maxwell. 2010. Role of groundwater in watershed response and land surface feedbacks under climate change. *Water Resources Research* 46: W00F02.

Fischer, E.M. and C. Schar. 2010. Consistent geographical patterns of changes in high-impact European heatwaves. *Nature Geosci* 3: 398-403.

Fisher, J.B., D.D. Baldocchi, L. Misson, T. Dawson and A.H. Goldstein. 2007. What the towers don't see at night: nocturnal sap flow in trees and shrubs at two AmeriFlux sites in California. *Tree Physiology* 27: 597–610.

Flury, M., M.V. Yates and W.A. Jury. 1999. Numerical Analysis of the Effect of the Lower Boundary Condition on Solute Transport in Lysimeters. *Soil Science Society of America Journal* 63: 1493-1499.

Foolad, F., T.E. Franz, T. Wang, J. Gibson, A. Kilic, R.G. Allen, et al. 2017. Feasibility analysis of using inverse modeling for estimating field-scale evapotranspiration in maize and soybean fields from soil water content monitoring networks. *Hydrol. Earth Syst. Sci.* 21: 1263-1277.

Forster, M.A. 2014. How significant is nocturnal sap flow? *Tree Physiology* 34: 757-765.

Garratt, J.R. and M. Segal. 1988. On the contribution of atmospheric moisture to dew formation. *Boundary-Layer Meteorology* 45: 209-236.

Garré, S., J. Koestel, T. Günther, M. Javaux, J. Vanderborght and H. Vereecken. 2010. Comparison of Heterogeneous Transport Processes Observed with Electrical Resistivity Tomography in Two Soils. *Vadose Zone Journal* 9: 336-349.

Garré, S., M. Javaux, J. Vanderborght, L. Pagès and H. Vereecken. 2011. Three-Dimensional Electrical Resistivity Tomography to Monitor Root Zone Water Dynamics. *Vadose Zone Journal* 10: 412-424.

Gauslaa, Y. 2014. Rain, dew, and humid air as drivers of morphology, function and spatial distribution in epiphytic lichens. *The Lichenologist* 46: 1-16.

Gebler, S., H.J. Hendricks Franssen, T. Pütz, H. Post, M. Schmidt and H. Vereecken. 2015. Actual evapotranspiration and precipitation measured by lysimeters: a comparison with eddy covariance and tipping bucket. *Hydrol. Earth Syst. Sci.* 19: 2145-2161.

Gebler, S., H.J. Hendricks Franssen, S.J. Kollet, W. Qu and H. Vereecken. 2017. High resolution modelling of soil moisture patterns with TerrSysMP: A comparison with sensor network data. *Journal of Hydrology* 547: 309-331.

Gerke, H.H. and M.T. van Genuchten. 1993. A dual-porosity model for simulating the preferential movement of water and solutes in structured porous media. *Water Resources Research* 29: 305-319.

Gerlein-Safdi, C., P.P.G. Gauthier and K.K. Caylor. 2017. The impact of dew-induced transpiration suppression on the water and isotope balances of *Colocasia esculenta* leaves. *bioRxiv*.

Gerritse, R.G. and J.A. Adeney. 1992. Tracers in recharge - Effects of partitioning in soils. *Journal of Hydrology* 131: 255-268.

Goetz, J.D. and J.S. Price. 2016. Ecohydrological controls on water distribution and productivity of moss communities in western boreal peatlands, Canada. *Ecohydrology* 9: 138-152.

Goldberg, S. and J.N. Kabengi. 2010. Bromide Adsorption by Reference Minerals and Soils. *Vadose Zone Journal* 9: 780-786.

Gosling, S.N., R.G. Taylor, N.W. Arnell and M.C. Todd. 2011. A comparative analysis of projected impacts of climate change on river runoff from global and catchment-scale hydrological models. *Hydrol. Earth Syst. Sci.* 15: 279-294.

Graf, A., W. Kuttler and J. Werner. 2004. Dewfall measurements on Lanzarote, Canary Islands. *Meteorologische Zeitschrift* 13: 405-412.

Graf, A., H.R. Bogena, C. Drüe, H. Hardelauf, T. Pütz, G. Heinemann, et al. 2014. Spatiotemporal relations between water budget components and soil water content in a forested tributary catchment. *Water Resources Research* 50: 4837-4857.

Gribovszki, Z., J. Szilágyi and P. Kalicz. 2010. Diurnal fluctuations in shallow groundwater levels and streamflow rates and their interpretation – A review. *Journal of Hydrology* 385: 371-383.

Groh, J., H. Puhlmann and K. von Wilpert. 2013. Calibration of a soil-water balance model with a combined objective function for the optimization of the water retention curve. (In German, with English abstract.) *Hydrologie und Wasserbewirtschaftung* 57: 152-163.

Groh, J., J. Vanderborght, T. Pütz and H. Vereecken. 2015. Estimation of evapotranspiration and crop coefficient of an intensively managed grassland ecosystem with lysimeter measurements. (In English with German abstract.). In, 16. Gumpensteiner Lysimetertagung, Raumberg-Gumpenstein. 107 - 112.

Groh, J., J. Vanderborght, T. Pütz and H. Vereecken. 2016. How to Control the Lysimeter Bottom Boundary to Investigate the Effect of Climate Change on Soil Processes? *Vadose Zone Journal* 15.

Groh, J., T. Pütz, J. Vanderborght and H. Vereecken. 2018a. Quantification of nighttime evapotranspiration for two distinct grassland ecosystems. *Geophysical Research Letters* (submitted).

Groh, J., V. Slawitsch, M. Herndl, H. Vereecken and T. Pütz. 2018b. Determining dew and hoar frost formation for a low mountain range and alpine grassland site by weighable lysimeter. *(submitted)*.

Groh, J., C. Stumpp, A. Lücke, T. Pütz, J. Vanderborght and H. Vereecken. 2018c. Inverse estimation of soil hydraulic and transport parameters of layered soils from water stable isotope and lysimeter data. *Vadose Zone Journal*.

Guadarrama-Cetina, J., A. Mongruel, M.-G. Medici, E. Baquero, A.R. Parker, I. Milimouk-Melnytchuk, et al. 2014. Dew condensation on desert beetle skin. *The European Physical Journal E* 37: 109.

Guo, X., T. Zha, X. Jia, B. Wu, W. Feng, J. Xie, et al. 2016. Dynamics of Dew in a Cold Desert-Shrub Ecosystem and Its Abiotic Controls. *Atmosphere* 7: 32.

Hagenau, J., R. Meissner and H. Borg. 2015. Effect of exposure on the water balance of two identical lysimeters. *Journal of Hydrology* 520: 69-74.

Hanisch, S., C. Lohrey and A. Buerkert. 2015. Dewfall and its ecological significance in semi-arid coastal south-western Madagascar. *Journal of Arid Environments* 121: 24-31.

Hannes, M., U. Wollschläger, F. Schrader, W. Durner, S. Gebler, T. Pütz, et al. 2015. A comprehensive filtering scheme for high-resolution estimation of the water balance components from high-precision lysimeters. *Hydrol. Earth Syst. Sci.* 19: 3405-3418.

Hanson, D.T., S.S. Stutz and J.S. Boyer. 2016. Why small fluxes matter: the case and approaches for improving measurements of photosynthesis and (photo)respiration. *Journal of Experimental Botany* 67: 3027-3039.

Heimovaara, T.J., J.A. Huisman, J.A. Vrugt and W. Bouten. 2004. Obtaining the Spatial Distribution of Water Content along a TDR Probe Using the SCEM-UA Bayesian Inverse Modeling Scheme. *Vadose Zone Journal* 3: 1128-1145.

Herbrich, M. and H.H. Gerke. 2016. Autocorrelation analysis of high resolution weighing lysimeter time series as a basis for determination of precipitation. *Journal of Plant Nutrition and Soil Science* 179: 784-798.

Herbrich, M., H.H. Gerke, O. Bens and M. Sommer. 2017. Water balance and leaching of dissolved organic and inorganic carbon of eroded Luvisols using high precision weighing lysimeters. *Soil and Tillage Research* 165: 144-160.

Herndl, M., E. Pötsch, A. Bohner and M. Kandolf. 2011. Lysimeter als Bestandteil eines technischen Versuchskonzeptes zur Simulation der Erderwärmung im Grünland. In, 14. Gumpensteiner Lysimetertagung "Lysimeter in der Klimafolgenforschung und Wasserwirtschaft". LFZ Raumberg-Gumpenstein, Raumberg-Gumpenstein, Austria. 119-126.

Herndl, M., Pötsch, E. M., Bohner, A., and M. Kandolf. 2011. Lysimeter als Bestandteil eines technischen Versuchskonzeptes zur Simulation der Erderwärmung im Grünland. (In German, with English abstract.) In, 14. Gumpensteiner Lysimetertagung. 119-126.

Hertel, C. and G. von Unold. 2014. Novel Measurement and Assessment Tools for Monitoring and Management of Land and Water Resources in Agricultural Landscapes of Central Asia. Mueller, L., Saparov, A. and Lischeid, G. (eds), pp. 175-184, Springer International Publishing, Cham.

Heusinger, J. and S. Weber. 2015. Comparative microclimate and dewfall measurements at an urban green roof versus bitumen roof. *Building and Environment* 92: 713-723.

Hiatt, C., D. Fernandez and C. Potter. 2012. Measurements of Fog Water Deposition on the California Central Coast. *Atmospheric and Climate Sciences* Vol.02No.04: 7.

Hirschi, M., D. Michel, I. Lehner and S.I. Seneviratne. 2017. A site-level comparison of lysimeter and eddy covariance flux measurements of evapotranspiration. *Hydrol. Earth Syst. Sci.* 21: 1809-1825.

Hoffman, G.J. and M.T. Van Genuchten. 1983. Limitations to Efficient Water Use in Crop Production. Taylor, H.M., Jordan, W.R. and Sinclair, T.R. (eds), pp. 73-85, American Society of Agronomy, Crop Science Society of America, Soil Science Society of America, Madison, WI.

Hoffmann, M., R. Schwartengräber, G. Wessolek and A. Peters. 2016. Comparison of simple rain gauge measurements with precision lysimeter data. *Atmospheric Research* 174–175: 120-123.

Hopmans, J.W., D.R. Nielsen and K.L. Bristow. 2013. Environmental Mechanics: Water, Mass and Energy Transfer in the Biosphere: The Philip Volume, pp. 247-258, American Geophysical Union.

Horton, R.E. 1933. The Rôle of infiltration in the hydrologic cycle. *Eos, Transactions American Geophysical Union* 14: 446-460.

Howard, A.R. and L.A. Donovan. 2007. Helianthus Nighttime Conductance and Transpiration Respond to Soil Water But Not Nutrient Availability. *Plant Physiology* 143: 145-155.

Huang, M., J.N. Hilderman and L. Barbour. 2015. Transport of stable isotopes of water and sulphate within reclaimed oil sands saline–sodic mine overburden. *Journal of Hydrology* 529, Part 3: 1550-1561.

Hughes, R.N. and P. Brimblecombe. 1994. Dew and guttation: formation and environmental significance. *Agricultural and Forest Meteorology* 67: 173-190.

Iiyama, I. 2016. Differences between field-monitored and laboratory-measured soil moisture characteristics. *Soil Science & Plant Nutrition* 62: 416-422.

Ineson, P., K. Taylor, A.F. Harrison, J. Poskitt, D.G. Benham, E. Tipping, et al. 1998. Effects of climate change on nitrogen dynamics in upland soils. 1. A transplant approach. *Global Change Biology* 4: 143-152.

Ionita, M., L.M. Tallaksen, D.G. Kingston, J.H. Stagge, G. Laaha, H.A.J. Van Lanen, et al. 2016. The European 2015 drought from a climatological perspective. *Hydrol. Earth Syst. Sci. Discuss.* 2016: 1-32.

Irmak, S., T.A. Howell, R.G. Allen, J.O. Payero and D.L. Martin. 2005. Standardized ASCE Penman-Monteith: Impact of sum-of-hourly vs. 24-hour timestep computations at reference weather station sites. *Transactions of the ASAE* 48.

Irmak, S. 2011. Dynamics of Nocturnal, Daytime, and Sum-of-Hourly Evapotranspiration and Other Surface Energy Fluxes over Nonstressed Maize Canopy. *Journal of Irrigation and Drainage Engineering* 137: 475-490.

Jacobs, A.F.G., W.A.J. van Pul and A. van Dijken. 1990. Similarity moisture dew profiles within a corn canopy. *Journal of Applied Meteorology* 29: 1300-1306.

Jacobs, A.F.G., J.H. van Boxel and J. Nieveen. 1996. Nighttime exchange processes near the soil surface of a maize canopy. *Agricultural and Forest Meteorology* 82: 155-169.

Jacobs, A.F.G., B.G. Heusinkveld and S.M. Berkowicz. 1999. Dew deposition and drying in a desert system: a simple simulation model. *Journal of Arid Environments* 42: 211-222.

Jacobs, A.F.G., B.G. Heusinkveld and S.M. Berkowicz. 2000. Dew measurements along a longitudinal sand dune transect, Negev Desert, Israel. *International Journal of Biometeorology* 43: 184-190.

Jacobs, A.F.G., B.G. Heusinkveld, R.J. Wichink Kruit and S.M. Berkowicz. 2006. Contribution of dew to the water budget of a grassland area in the Netherlands. *Water Resources Research* 42: n/a-n/a.

Jacobs, A.F.G., B.G. Heusinkveld and S.M. Berkowicz. 2008. Passive dew collection in a grassland area, The Netherlands. *Atmospheric Research* 87: 377-385.

Jacques, D., J. Šimůnek, A. Timmerman and J. Feyen. 2002. Calibration of Richards' and convection–dispersion equations to field-scale water flow and solute transport under rainfall conditions. *Journal of Hydrology* 259: 15-31.

Jarvis, N. (1994). The MACRO Model (version 3.1). Technical description and sample simulations. Reports and Dissertations - Swedish University of Agricultural Sciences. Department of Soil Sciences (Sweden). no. 19.

Jin, X.M., Y.K. Zhang, Y. Tang, G.C. Hu and R.H. Guo. 2014. Quantifying bare soil evaporation and its relationship with groundwater depth. *International Journal of Remote Sensing* 35: 7567-7582.

Kabela, E.D., B.K. Hornbuckle, M.H. Cosh, M.C. Anderson and M.L. Gleason. 2009. Dew frequency, duration, amount, and distribution in corn and soybean during SMEX05. *Agricultural and Forest Meteorology* 149: 11-24.

Kalthoff, N., M. Fiebig-Wittmaack, C. Meißner, M. Kohler, M. Uriarte, I. Bischoff-Gauß, et al. 2006. The energy balance, evapotranspiration and nocturnal dew deposition of an arid valley in the Andes. *Journal of Arid Environments* 65: 420-443.

Karimov, A.K., J. Šimůnek, M.A. Hanjra, M. Avliyakulov and I. Forkutsa. 2014. Effects of the shallow water table on water use of winter wheat and ecosystem health: Implications for unlocking the potential of groundwater in the Fergana Valley (Central Asia). *Agricultural Water Management* 131: 57-69.

Karpul, R.H. and A.G. West. 2016. Wind drives nocturnal, but not diurnal, transpiration in Leucospermum conocarpodendron trees: implications for stilling on the Cape Peninsula. *Tree Physiology* 36: 954-966.

Kaseke, K.F., L. Wang and M.K. Seely. 2017. Nonrainfall water origins and formation mechanisms. *Science Advances* 3.

Kasteel, R., T. Pütz and H. Vereecken. 2007. An experimental and numerical study on flow and transport in a field soil using zero-tension lysimeters and suction plates. *European Journal of Soil Science* 58: 632-645.

Khalil, B., J. Adamowski, A. Shabbir, C. Jang, M. Rojas, K. Reilly, et al. 2016. A review: dew water collection from radiative passive collectors to recent developments of active collectors. *Sustainable Water Resources Management* 2: 71-86.

Kidron, G.J. 2000. Analysis of dew precipitation in three habitats within a small arid drainage basin, Negev Highlands, Israel. *Atmospheric Research* 55: 257-270.

Kidron, G.J., I. Herrnstadt and E. Barzilay. 2002. The role of dew as a moisture source for sand microbiotic crusts in the Negev Desert, Israel. *Journal of Arid Environments* 52: 517-533.

Klammler, G. and J. Fank. 2014. Determining water and nitrogen balances for beneficial management practices using lysimeters at Wagna test site (Austria). *Science of The Total Environment* 499: 448-462.

Klosterhalfen, A., M. Herbst, L. Weihermüller, A. Graf, M. Schmidt, A. Stadler, et al. 2017. Multi-site calibration and validation of a net ecosystem carbon exchange model for croplands. *Ecological Modelling* 363: 137-156.

Knauer, N., J. Groh, H. Vereecken and T. Pütz. 2017. Veränderungen des Stickstoff-Haushaltes eines Waldwiesen-Standortes durch den Klimawandel. (In German.) In, 17. Gumpensteiner Lysimetertagung, Raumberg-Gumpenstein. 93 - 102.

Koestel, J., J. Vanderborght, M. Javaux, A. Kemna, A. Binley and H. Vereecken. 2009. Noninvasive 3-D Transport Characterization in a Sandy Soil Using ERT: 2. Transport Process. *Vadose Zone Journal* 8: 723-734.

Kollet, S.J. and R.M. Maxwell. 2008. Capturing the influence of groundwater dynamics on land surface processes using an integrated, distributed watershed model. *Water Resources Research* 44: W02402.

Konarska, J., J. Uddling, B. Holmer, M. Lutz, F. Lindberg, H. Pleijel, et al. 2016. Transpiration of urban trees and its cooling effect in a high latitude city. *International Journal of Biometeorology* 60: 159-172.

Korres, W., T.G. Reichenau, P. Fiener, C.N. Koyama, H.R. Bogena, T. Cornelissen, et al. 2015. Spatio-temporal soil moisture patterns – A meta-analysis using plot to catchment scale data. *Journal of Hydrology* 520: 326-341.

Kung, K.-J.S. 1990. Influence of Plant Uptake on the Performance of Bromide Tracer. *Soil Science Society of America Journal* 54: 975-979.

Küpper, W., J. Groh, L. Fürst, P. Meulendick, H. Vereecken and T. Pütz. 2017. TERENO-SOILCan-Management eines deutschlandweiten Lysimeternetzwerkes. (In German.) In, 17. Gumpensteiner Lysimetertagung, Raumberg-Gumpenstein. 175-180.

Laaha, G., T. Gauster, L.M. Tallaksen, J.P. Vidal, K. Stahl, C. Prudhomme, et al. 2016. The European 2015 drought from a hydrological perspective. *Hydrol. Earth Syst. Sci. Discuss.* 2016: 1-30.

Lai, J. and L. Ren. 2016. Estimation of effective hydraulic parameters in heterogeneous soils at field scale. *Geoderma* 264, Part A: 28-41.

Le Bourgeois, O., C. Bouvier, P. Brunet and P.A. Ayral. 2016. Inverse modeling of soil water content to estimate the hydraulic properties of a shallow soil and the associated weathered bedrock. *Journal of Hydrology* 541, Part A: 116-126.

Ledford, H. 2017. Overlooked water loss in plants could throw off climate models. *Nature* 546: 583–584.

Leterme, B., D. Mallants and D. Jacques. 2012. Sensitivity of groundwater recharge using climatic analogues and HYDRUS-1D. *Hydrology Earth System Sciences* 16: 2485-2497.

Li, H., L. Luo, E.F. Wood and J. Schaake. 2009. The role of initial conditions and forcing uncertainties in seasonal hydrologic forecasting. *Journal of Geophysical Research: Atmospheres* 114: n/a-n/a.

Li, X., S.X. Chang and K.F. Salifu. 2013. Soil texture and layering effects on water and salt dynamics in the presence of a water table: a review. *Environmental Reviews* 22: 41-50.

Liu, X., Y. Li, X. Chen, G. Zhou, J. Cheng, D. Zhang, et al. 2015. Partitioning evapotranspiration in an intact forested watershed in southern China. *Ecohydrology* 8: 1037-1047.

Liu, Z., H. Chen, Z. Huo, F. Wang and C.C. Shock. 2016. Analysis of the contribution of groundwater to evapotranspiration in an arid irrigation district with shallow water table. *Agricultural Water Management* 171: 131-141.

Lombardozzi, D.L., M.J.B. Zeppel, R.A. Fisher and A. Tawfik. 2017. Representing nighttime and minimum conductance in CLM4.5: global hydrology and carbon sensitivity analysis using observational constraints. *Geosci. Model Dev.* 10: 321-331.

Luo, W.H. and J. Goudriaan. 2000. Dew Formation on rice under varying durations of nocturnal radiative loss. *Agricultural and Forest Meteorology* 104: 303-313.

Luo, Y. and M. Sophocleous. 2010. Seasonal groundwater contribution to crop-water use assessed with lysimeter observations and model simulations. *Journal of Hydrology* 389: 325-335.

Madeira, A.C., K.S. Kim, T. S.E. and M.L. Gleason. 2001. A simple cloud-based energy balance model to estimate dew. *Agricultural and Forest Meteorology* 111: 55-63.

Magarian, D.M., M.P. Russelle, J.F.S. Lamb and J.M. Blumenthal. 1998. Bromide as a Tracer for Nitrate-N Uptake in Alfalfa Herbage. *Agronomy Journal* 90: 651-657.

Malek, E. 1992. Night-time evapotranspiration vs. daytime and 24h evapotranspiration. *Journal of Hydrology* 138: 119-129.

Malek, E., G. McCurdy and B. Giles. 1999. Dew contribution to the annual water balances in semi-arid desert valleys. *Journal of Arid Environments* 42: 71-80.

Malik, F.T., R.M. Clement, D.T. Gethin, D. Beysens, R.E. Cohen, W. Krawszik, et al. 2015. Dew harvesting efficiency of four species of cacti. *Bioinspiration & Biomimetics* 10: 036005.

Mannschatz, T. and P. Dietrich. 2017. Sensitivity Analysis in Earth Observation Modelling. Srivastava, P.K. (ed), pp. 25-52, Elsevier.

Marek, W.G., R.S. Evett, H.P. Gowda, A.T. Howell, S.K. Copeland and R.L. Baumhardt. 2014. Post-Processing Techniques for Reducing Errors in Weighing Lysimeter Evapotranspiration (ET) Datasets. *Transactions of the ASABE* 57: 499.

Maxwell, R.M. and S.J. Kollet. 2008. Interdependence of groundwater dynamics and land-energy feedbacks under climate change. *Nature Geoscience* 1: 665-669.

McCarter, C.P.R. and J.S. Price. 2014. Ecohydrology of Sphagnum moss hummocks: mechanisms of capitula water supply and simulated effects of evaporation. *Ecohydrology* 7: 33-44.

Medrano, H., M. Tomás, S. Martorell, J. Flexas, E. Hernández, J. Rosselló, et al. 2015. From leaf to whole-plant water use efficiency (WUE) in complex canopies: Limitations of leaf WUE as a selection target. *The Crop Journal* 3: 220-228.

Meeus, J. 1991. Astronomical algorithms, Willmann-Bell, Richmond, Virginia, USA

Meissner, R., H. Rupp and M. Schubert. 2000. Novel lysimeter techniques - a basis for the improved investigation of water, gas, and solute transport in soils. *Journal of Plant Nutrition and Soil Science* 163: 603-608.

Meissner, R., J. Seeger, H. Rupp, M. Seyfarth and H. Borg. 2007. Measurement of dew, fog, and rime with a high-precision gravitation lysimeter. *Journal of Plant Nutrition and Soil Science* 170: 335-344.

Meissner, R., H. Rupp, J. Seeger and G. Gee. 2009. Accuracy of water flux measuring with a passive-wick water sampler in comparison to a high-precision gravitation lysimeter. (In English with German abstract.). In, 13. Gumpensteiner Lysimetertagung, Raumberg-Gumpenstein. 21-26.

Meissner, R., M.N.V. Prasad, G. Du Laing and J. Rinklebe. 2010. Lysimeter application for measuring the water and solute fluxes with high precision. *Current Science* 99: 601.

Mertens, J., H. Madsen, M. Kristensen, D. Jacques and J. Feyen. 2005. Sensitivity of soil parameters in unsaturated zone modelling and the relation between effective, laboratory and in situ estimates. *Hydrological Processes* 19: 1611-1633.

Meunier, D. and D. Beysens. 2016. Dew, fog, drizzle and rain water in Baku (Azerbaijan). *Atmospheric Research* 178-179: 65-72.

Mishra, S. and J.C. Parker. 1989. Parameter estimation for coupled unsaturated flow and transport. *Water Resources Research* 25: 385-396.

Moeck, C., P. Brunner and D. Hunkeler. 2016. The influence of model structure on groundwater recharge rates in climate-change impact studies. *Hydrogeology Journal* 24: 1171-1184.

Monteith, J.L. 1957. Dew. *Quarterly Journal of the Royal Meteorological Society* 83: 322-341.

Monteith, J.L. and M.H. Unsworth. 1990. Principles of environmental physics, Arnold, London, UK.

Monteith, J.L. and M.H. Unsworth. 2013. Principles of Environmental Physics (Fourth Edition), pp. 217-247, Academic Press, Boston.

Mosley, M.P. 1979. Streamflow generation in a forested watershed, New Zealand. *Water Resources Research* 15: 795-806.

Mualem, Y. 1976. A new model for predicting the hydraulic conductivity of unsaturated porous media. *Water Resources Research* 12: 513-522.

Munné-Bosch, S. and L. Alegre. 1999. Role of Dew on the Recovery of Water-Stressed Melissa officinalis L. Plants. *Journal of Plant Physiology* 154: 759-766.

Muselli, M., D. Beysens, M. Mileta and I. Milimouk. 2009. Dew and rain water collection in the Dalmatian Coast, Croatia. *Atmospheric Research* 92: 455-463.

Neumann, J. 1956. Estimating the amount of dewfall. *Archive for Meteorology, Geophysics and Bioclimatology* 9: 197-203.

Ninari, N. and P.R. Berliner. 2002. The role of dew in the water and heat balance of bare loess soil in the Negev Desert: quantifying the actual dew deposition on the soil surface. *Atmospheric Research* 64: 323-334.

Nolz, R., G. Kammerer and P. Cepuder. 2013. Interpretation of lysimeter weighing data affected by wind. *Journal of Plant Nutrition and Soil Science* 176: 200-208.

Novick, K.A., R. Oren, P.C. Stoy, M.B.S. Siqueira and G.G. Katul. 2009. Nocturnal evapotranspiration in eddy-covariance records from three co-located ecosystems in the Southeastern U.S.: Implications for annual fluxes. *Agricultural and Forest Meteorology* 149: 1491-1504.

O'Keefe, K. (2016). Patterns and ecological consequences of water uptake, redistribution, and loss in tallgrass prairie (Doctoral dissertation). Retrieved from K-REx. (http://hdl.handle.net/2097/34514). Division of Biology College of Arts and Sciences Kansas State University, Manhattan, Kansas.

Oliva, F., E. Vegas, S. Civit, T. Garrido, J. Fraile and A. Munné. 2016. Experiences from Ground, Coastal and Transitional Water Quality Monitoring: The EU Water Framework Directive Implementation in the Catalan River Basin District (Part II). Munné, A., Ginebreda, A. and Prat, N. (eds), pp. 25-62, Springer International Publishing, Cham.

Pangle, L.A., J.W. Gregg and J.J. McDonnell. 2014. Rainfall seasonality and an ecohydrological feedback offset the potential impact of climate warming on evapotranspiration and groundwater recharge. *Water Resources Research* 50: 1308-1321.

Paniconi, C. and M. Putti. 2015. Physically based modeling in catchment hydrology at 50: Survey and outlook. *Water Resources Research* 51: 7090-7129.

Pattey, E., I.B. Strachan, R.L. Desjardins and J. Massheder. 2002. Measuring nighttime CO2 flux over terrestrial ecosystems using eddy covariance and nocturnal boundary layer methods. *Agricultural and Forest Meteorology* 113: 145-158.

Pereira, A.B., N.A. Villa Nova, L.F. Pires, L.R. Angelocci and G.C. Beruski. 2014. Estimation method of grass net radiation on the determination of potential evapotranspiration. *Meteorological Applications* 21: 369-375.

Pessarakli, M. 2014. Handbook of Plant and Crop Physiology, Third Edition, Ed.: Third Edition. Hoboken : CRC Press. 2014.

Peters-Lidard, C.D., D.M. Mocko, M. Garcia, J.A. Santanello, M.A. Tischler, M.S. Moran, et al. 2008. Role of precipitation uncertainty in the estimation of hydrologic soil properties using remotely sensed soil moisture in a semiarid environment. *Water Resources Research* 44: n/a-n/a.

Peters, A. and W. Durner. 2006. Improved estimation of soil water retention characteristics from hydrostatic column experiments. *Water Resources Research* 42: n/a-n/a.

Peters, A. and W. Durner. 2008. Simplified evaporation method for determining soil hydraulic properties. *Journal of Hydrology* 356: 147-162.

Peters, A., W. Durner and G. Wessolek. 2011. Consistent parameter constraints for soil hydraulic functions. *Advances in Water Resources* 34: 1352-1365.

Peters, A., T. Nehls, H. Schonsky and G. Wessolek. 2014. Separating precipitation and evapotranspiration from noise - a new filter routine for high resolution lysimeter data. *Hydrol. Earth Syst. Sci. Discuss.* 18: 1189 - 1198.

Peters, A., S.C. Iden and W. Durner. 2015. Revisiting the simplified evaporation method: Identification of hydraulic functions considering vapor, film and corner flow. *Journal of Hydrology* 527: 531-542.

Peters, A., T. Nehls and G. Wessolek. 2016. Technical note: Improving the AWAT filter with interpolation schemes for advanced processing of high resolution data. *Hydrol. Earth Syst. Sci.* 20: 2309-2315.

Peters, A., J. Groh, F. Schrader, W. Durner, H. Vereecken and T. Pütz. 2017. Towards an unbiased filter routine to determine precipitation and evapotranspiration from high precision lysimeter measurements. *Journal of Hydrology* 549: 731-740.

Phillips, N.G., J.D. Lewis, B.A. Logan and D.T. Tissue. 2010. Inter- and intra-specific variation in nocturnal water transport in Eucalyptus. *Tree Physiology* 30: 586-596.

Piggin, I. and P. Schwerdtfeger. 1973. Variations in the albedo of wheat and barley crops. *Archiv für Meteorologie, Geophysik und Bioklimatologie, Serie B*.

Podlasly, C. and K. Schwärzel. 2013. Development of a Continuous Closed Pipe System for Controlling Soil Temperature at the Lower Boundary of Weighing Field Lysimeters. *Soil Sci. Soc. Am. J.* 77: 2157-2163.

Price, J. and R. Clark. 2014. On the Measurement of Dewfall and Fog-Droplet Deposition. *Boundary-Layer Meteorology* 152: 367-393.

Price, J.S. and P.N. Whittington. 2010. Water flow in Sphagnum hummocks: Mesocosm measurements and modelling. *Journal of Hydrology* 381: 333-340.

Pronger, J., D.I. Campbell, M.J. Clearwater, S. Rutledge, A.M. Wall and L.A. Schipper. 2016. Low spatial and inter-annual variability of evaporation from a year-round intensively grazed temperate pasture system. *Agriculture, Ecosystems & Environment* 232: 46-58.

Puhlmann, H. and K. von Wilpert. 2012. Pedotransfer functions for water retention and unsaturated hydraulic conductivity of forest soils. *Journal of Plant Nutrition and Soil Science* 175: 221-235.

Pütz, T., K. Kiese, U. Wollschläger, E. Priesack, E. Borg, H. Gerke, et al. 2013. TERENO-SOILCan - Ein Lysimeternetzwerk zur Untersuchung des Klimawandels . (In German, with English abstract.) In, 15. Gumpensteiner Lysimetertagung, Raumberg-Gumpenstein. 57-62.

Pütz, T., R. Kiese, U. Wollschläger, J. Groh, H. Rupp, S. Zacharias, et al. 2016. TERENO-SOILCan: a lysimeter-network in Germany observing soil processes and plant diversity influenced by climate change. *Environmental Earth Sciences* 75: 1-14.

Qu, W., H.R. Bogena, J.A. Huisman, G. Martinez, Y.A. Pachepsky and H. Vereecken. 2014. Effects of Soil Hydraulic Properties on the Spatial Variability of Soil Water Content: Evidence from Sensor Network Data and Inverse Modeling. *gsvadzone* 13: -.

R-Core-Team. (2016). R: A language and environment for statistical computing, R Foundation for Statistical Computing, Vienna, Austria.

Raat, K.J., J.A. Vrugt, W. Bouten and A. Tietema. 2004. Towards reduced uncertainty in catchment nitrogen modelling: quantifying the effect of field observation uncertainty on model calibration. *Hydrol. Earth Syst. Sci.* 8: 751-763.

Resco de Dios, V., J. Roy, J.P. Ferrio, J.G. Alday, D. Landais, A. Milcu, et al. 2015. Processes driving nocturnal transpiration and implications for estimating land evapotranspiration. *Scientific Reports* 5: 10975.

Richards, K. 2005. Urban and rural dewfall, surface moisture, and associated canopy-level air temperature and humidity measurements for vancouver, canada. *Boundary-Layer Meteorology* 114: 143-163.

Richter, D. (1995). Results of methodological studies on the correction of the systematic measurement error of the Hellmann-type precipitation gauge. (In German.). Wetterdienstes, I.B.d.D. (ed), p. 93, Offenbach am Main, Germany.

Ries, F., J. Lange, S. Schmidt, H. Puhlmann and M. Sauter. 2015. Recharge estimation and soil moisture dynamics in a Mediterranean, semi-arid karst region. *Hydrol. Earth Syst. Sci.* 19: 1439-1456.

Rogiers, S.Y., D.H. Greer, R.J. Hutton and J.J. Landsberg. 2009. Does night-time transpiration contribute to anisohydric behaviour in a Vitis vinifera cultivar? *Journal of Experimental Botany* 60: 3751-3763.

Romano, N. and P. Nasta. 2016. How effective is bimodal soil hydraulic characterization? Functional evaluations for predictions of soil water balance. *European Journal of Soil Science* 67: 523-535.

Rosenbaum, U., H.R. Bogena, M. Herbst, J.A. Huisman, T.J. Peterson, A. Weuthen, et al. 2012. Seasonal and event dynamics of spatial soil moisture patterns at the small catchment scale. *Water Resources Research* 48: n/a-n/a.

Rühle, F.A., N. Zentner and C. Stumpp. 2015. Changes in water table level influence solute transport in uniform porous media. *Hydrological Processes* 29: 875-888.

Russow, R., H. Segschneider and H. Förstel. 1996. Vergleich der Wasser- und Anionenbewegung in agrarisch genutzten Sandlöss- und Löss-Schwarzerde-Böden an Hand von Multitracer-Untersuchungen. (In German.). *Arch. Acker-Pfl. Boden* 40: 453-471.

Saab, O.J.G.A., F. Griesang, K.A. Alves, L.R. Higashibara and W. Genta. 2017. Pesticides deposition in vineyards on different conditions of leaf wetness. *Engenharia Agrícola* 37: 286-291.

Satchithanantham, S., H.F. Wilson and A.J. Glenn. 2017. Contrasting patterns of groundwater evapotranspiration in grass and tree dominated riparian zones of a temperate agricultural catchment. *Journal of Hydrology* 549: 654-666.

Sato, H., A. Ito, A. Ito, T. Ise and E. Kato. 2015. Current status and future of land surface models. *Soil Science and Plant Nutrition* 61: 34-47.

Scanlon, B.R., D.G. Levitt, R.C. Reedy, K.E. Keese and M.J. Sully. 2005. Ecological controls on water-cycle response to climate variability in deserts. *Proceedings of the National Academy of Sciences* 102: 6033-6038.

Schaap, M.G. and F.J. Leij. 2000. Improved prediction of unsaturated hydraulic conductivity with the Mualem-van Genuchten model. *Soil Sciecne Society of America Journal* 64: 843-851.

Schaap, M.G., F.J. Leij and M.T. van Genuchten. 2001. rosetta: a computer program for estimating soil hydraulic parameters with hierarchical pedotransfer functions. *Journal of Hydrology* 251: 163-176.

Scharnagl, B., J.A. Vrugt, H. Vereecken and M. Herbst. 2011. Inverse modelling of in situ soil water dynamics: investigating the effect of different prior distributions of the soil hydraulic parameters. *Hydrol. Earth Syst. Sci.* 15: 3043-3059.

Schelle, H., S.C. Iden, J. Fank and W. Durner. 2012. Inverse Estimation of Soil Hydraulic and Root Distribution Parameters from Lysimeter Data. *Vadose Zone Journal* 11.

Schelle, H., W. Durner, S.C. Iden and J. Fank. 2013a. Simultaneous Estimation of Soil Hydraulic and Root Distribution Parameters from Lysimeter Data by Inverse Modeling. *Procedia Environmental Sciences* 19: 564-573.

Schelle, H., W. Durner, S. Schlüter, H.-J. Vogel and J. Vanderborght. 2013b. Virtual Soils: Moisture Measurements and Their Interpretation by Inverse Modeling. *Vadose Zone Journal* 12.

Schlüter, S., H.-J. Vogel, O. Ippisch and J. Vanderborght. 2013. Combined Impact of Soil Heterogeneity and Vegetation Type on the Annual Water Balance at the Field Scale. *Vadose Zone Journal* 12.

Schnabel, R.R., W.L. Stout and J.A. Shaffer. 1995. Uptake of a Hydrologic Tracer (Bromide) by Ryegrass from Well and Poorly-Drained Soils. *Journal of Environmental Quality* 24: 888-892.

Schoppach, R., E. Claverie and W. Sadok. 2014. Genotype-dependent influence of night-time vapour pressure deficit on night-time transpiration and daytime gas exchange in wheat. *Functional Plant Biology* 41: 963-971.

Schrader, F., W. Durner, J. Fank, S. Gebler, T. Pütz, M. Hannes, et al. 2013. Estimating Precipitation and Actual Evapotranspiration from Precision Lysimeter Measurements. *Procedia Environmental Sciences* 19: 543-552.

Schubert, R., W. Hilbig and S. Klotz. 2001. Bestimmungsbuch der Pflanzengesellschaften Deutschlands. (In German.), Spektrum Akademischer Verlag Heidelberg.

Schwabe, W.W. 1952. Effects of Photoperiodic Treatment on Stomatal Movement. *Nature* 169: 1053-1054.

Schwaerzel, K. and H.P. Bohl. 2003. An easily installable groundwater lysimeter to determine waterbalance components and hydraulic properties of peat soils. *Hydrology and Earth System Science* 7: 23-32.

Seaman, J.C., P.M. Bertsch and W.P. Miller. 1995. Ionic tracer movement through highly weathered sediments. *Journal of Contaminant Hydrology* 20: 127-143.

Seki, K., P. Ackerer and F. Lehmann. 2015. Sequential estimation of hydraulic parameters in layered soil using limited data. *Geoderma* 247–248: 117-128.

Shah, T., J. Bruke, K. Vullholth, M. Angelica, E. Custodio, F. Daibes, et al. 2007. Water for food, water for life: a Comprehensive Assessment of Water Management in Agriculture. David, M. (ed), pp. 395-423, Earthscan; Colombo, Sri Lanka: International Water Management Institute (IWMI), London, UK.

Sharma, M.L. 1976. Contribution of dew in the hydrologic balance of a semi-arid grassland. *Agricultural Meteorology* 17: 321-331.

Šimůnek, J. and D.L. Suarez. 1993. Modeling of carbon dioxide transport and production in soil: 1. Model development. *Water Resources Research* 29: 487-497.

Šimůnek, J., M. Šejna, H. Saito, M. Sakai and M.T. van Genuchten. (2013). The Hydrus-1D Software Package for Simulating the Movement of Water, Heat, and Multiple Solutes in Variably Saturated Media. Version 4.16, HYDRUS Software Series 3, p. 340, Department of Environmental Sciences, University of California Riverside, Riverside, California, USA.

Šimůnek, J., M.T. van Genuchten and M. Šejna. 2016. Recent Developments and Applications of the HYDRUS Computer Software Packages. *Vadose Zone Journal*.

Singh, G., G. Kaur, K. Williard, J. Schoonover and J. Kang. 2017. Monitoring of Water and Solute Transport in the Vadose Zone: A Review. *Vadose Zone Journal*.

Singh, S. 2014. Advances in Agronomy. Donald, L.S. (ed), pp. 97-135, Academic Press.

Skaggs, K.E. and S. Irmak. 2011. Characterization of Nighttime Evapotranspiration and Other Surface Energy Fluxes and Interactions with Microclimatic Variables in Subsurface Drip and Center-Pivot Irrigated Soybean Fields. *Transactions of the ASABE* 54: 941-952.

Skaggs, T.H., D.L. Suarez, S. Goldberg and P.J. Shouse. 2012. Replicated lysimeter measurements of tracer transport in clayey soils: Effects of irrigation water salinity. *Agricultural Water Management* 110: 84-93.

Snyder, R.L., J.P. de Melo-Abreu and S. Matulich. 2005. Frost Protection: fundamentals, practice and economics volume 1, FAO, Rome.

Soylu, M.E., E. Istanbulluoglu, J.D. Lenters and T. Wang. 2011. Quantifying the impact of groundwater depth on evapotranspiration in a semi-arid grassland region. *Hydrology and Earth System Science* 15: 787-806.

Soylu, M.E., C.J. Kucharik and S.P. Loheide II. 2014. Influence of groundwater on plant water use and productivity: Development of an integrated ecosystem – Variably

saturated soil water flow model. *Agricultural and Forest Meteorology* 189–190: 198-210.

Sprenger, M., T.H.M. Volkmann, T. Blume and M. Weiler. 2015. Estimating flow and transport parameters in the unsaturated zone with pore water stable isotopes. *Hydrol. Earth Syst. Sci.* 19: 2617-2635.

Sprenger, M., M. Erhardt, M. Riedel and M. Weiler. 2016a. Historical tracking of nitrate in contrasting vineyards using water isotopes and nitrate depth profiles. *Agriculture, Ecosystems & Environment* 222: 185-192.

Sprenger, M., S. Seeger, T. Blume and M. Weiler. 2016b. Travel times in the vadose zone: Variability in space and time. *Water Resources Research*: n/a-n/a.

Stenitzer, E. and J. Fank. 2007. "Tension-free" Lysimeters versus "Controlled tension" Lysimeters – A Simulation Study. In, Proceedings of the Conference"Diffuse Inputs into Groundwater – Monitoring, Modelling, Management", Graz. 149-152.

Stockinger, M.P., A. Lücke, J.J. McDonnell, B. Diekkrüger, H. Vereecken and H.R. Bogena. 2015. Interception effects on stable isotope driven streamwater transit time estimates. *Geophysical Research Letters* 42: 5299-5308.

Stockinger, M.P., H.R. Bogena, A. Lücke, B. Diekkrüger, T. Cornelissen and H. Vereecken. 2016. Tracer sampling frequency influences estimates of young water fraction and streamwater transit time distribution. *Journal of Hydrology* 541: 952-964.

Stofberg, S.F., J. van Engelen, J.-P.M. Witte and S.E. van der Zee. 2016. Effects of root mat buoyancy and heterogeneity on floating fen hydrology. *Ecohydrology*: n/a-n/a.

Stumpp, C., G. Nützmann, S. Maciejewski and P. Maloszewski. 2009. A comparative modeling study of a dual tracer experiment in a large lysimeter under atmospheric conditions. *Journal of Hydrology* 375: 566-577.

Stumpp, C., W. Stichler, M. Kandolf and J. Šimůnek. 2012. Effects of Land Cover and Fertilization Method on Water Flow and Solute Transport in Five Lysimeters: A Long-Term Study Using Stable Water Isotopes. *Vadose Zone Journal* 11.

Sudmeyer, R.A., R.A. Nulsen and W.D. Scott. 1994. Measured dewfall and potential condensation on grazed pasture in the Collie River basin, southwestern Australia. *Journal of Hydrology* 154: 255-269.

Suzuki, K., J. Kubota, H. Yabuki, T. Ohata and V. Vuglinsky. 2007. Moss beneath a leafless larch canopy: influence on water and energy balances in the southern mountainous taiga of eastern Siberia. In, 16th International Northern Research Basins Symposium and Workshop Petrozavodsk, Russia.

Tataw, J.T., R. Hall, E. Ziss, T. Schwarz, C. von Hohberg und Buchwald, H. Formayer, et al. 2014. Soil types will alter the response of arable agroecosystems to future rainfall patterns. *Annals of Applied Biology* 164: 35-45.

Taylor, R.G., B. Scanlon, P. Doll, M. Rodell, R. van Beek, Y. Wada, et al. 2013a. Ground water and climate change. *Nature Clim. Change* 3: 322-329.

Taylor, R.G., M.C. Todd, L. Kongola, L. Maurice, E. Nahozya, H. Sanga, et al. 2013b. Evidence of the dependence of groundwater resources on extreme rainfall in East Africa. *Nature Climate Change* 3: 374-378.

Thornton, P.K., P.J. Ericksen, M. Herrero and A.J. Challinor. 2014. Climate variability and vulnerability to climate change: a review. *Global Change Biology* 20: 3313-3328.

Thorsen, S.M., A.-G. Roer and M.v. Oijen. 2010. Modelling the dynamics of snow cover, soil frost and surface ice in Norwegian grasslands. *Polar Research* 29: 110-126.

Tomaszkiewicz, M., M. Abou Najm, D. Beysens, I. Alameddine and M. El-Fadel. 2015. Dew as a sustainable non-conventional water resource: a critical review. *Environmental Reviews* 23: 425-442.

Tomaszkiewicz, M., M. Abou Najm, D. Beysens, I. Alameddine, E. Bou Zeid and M. El-Fadel. 2016. Projected climate change impacts upon dew yield in the Mediterranean basin. *Science of The Total Environment* 566: 1339-1348.

Tomaszkiewicz, M., M. Abou Najm, R. Zurayk and M. El-Fadel. 2017. Dew as an adaptation measure to meet water demand in agriculture and reforestation. *Agricultural and Forest Meteorology* 232: 411-421.

Uclés, O., L. Villagarcía, Y. Cantón and F. Domingo. 2013. Microlysimeter station for long term non-rainfall water input and evaporation studies. *Agricultural and Forest Meteorology* 182-183: 13-20.

Unold, G. and J. Fank. 2008. Modular Design of Field Lysimeters for Specific Application Needs. *Water, Air, & Soil Pollution: Focus* 8: 233-242.

van Genuchten, M.T. 1980. A Closed-form Equation for Predicting the Hydraulic Conductivity of Unsaturated Soils. *Soil Science Society of America Journal* 44: 892-898.

Van Genuchten, M.T., F.J. Leij and S.R. Yates. (1991). The RETC Code for Quantifying the Hydraulic Functions of Unsaturated Soils, Version 1.0, U.S. Salinity Laboratory, USDA, ARS, Riverside, California.

van Walsum, P.E.V. and I. Supit. 2012. Influence of ecohydrologic feedbacks from simulated crop growth on integrated regional hydrologic simulations under climate scenarios. *Hydrology and Earth System Science* 16: 1577-1593.

Vanderborght, J. and H. Vereecken. 2007. Review of Dispersivities for Transport Modeling in Soils. *Vadose Zone Journal* 6: 29-52.

Vereecken, H. and M. Dust. 1998. The Lysimeter Concept. Führ, R., Hance, R.J., Plimmer, J.R. and Nelson, J.O. (eds), pp. 189-202, American Chemical Society, Washington DC.

Vereecken, H., J.A. Huisman, H. Bogena, J. Vanderborght, J.A. Vrugt and J.W. Hopmans. 2008. On the value of soil moisture measurements in vadose zone hydrology: A review. *Water Resources Research* 44: n/a-n/a.

Vrugt, J.A., H.V. Gupta, W. Bouten and S. Sorooshian. 2003. A Shuffled Complex Evolution Metropolis algorithm for optimization and uncertainty assessment of hydrologic model parameters. *Water Resources Research* 39: n/a-n/a.

Vrugt, J.A., P.H. Stauffer, T. Wöhling, B.A. Robinson and V.V. Vesselinov. 2008a. Inverse Modeling of Subsurface Flow and Transport Properties: A Review with New Developments. *Vadose Zone Journal* 7: 843-864.

Vrugt, J.A., C.J.F. ter Braak, M.P. Clark, J.M. Hyman and B.A. Robinson. 2008b. Treatment of input uncertainty in hydrologic modeling: Doing hydrology backward with Markov chain Monte Carlo simulation. *Water Resources Research* 44: n/a-n/a.

Vuollekoski, H., M. Vogt, V.A. Sinclair, J. Duplissy, H. Järvinen, E.M. Kyrö, et al. 2015. Estimates of global dew collection potential on artificial surfaces. *Hydrol. Earth Syst. Sci.* 19: 601-613.

Wang, H., P. Zhao, D. Hölscher, Q. Wang, P. Lu, X.A. Cai, et al. 2012. Nighttime sap flow of Acacia mangium and its implications for nighttime transpiration and stem water storage. *Journal of Plant Ecology* 5: 294-304.

Wang, K. and R.E. Dickinson. 2012. A review of global terrestrial evapotranspiration: Observation, modeling, climatology, and climatic variability. *Reviews of Geophysics* 50.

Wang, L., K.F. Kaseke and M.K. Seely. 2017. Effects of non-rainfall water inputs on ecosystem functions. *Wiley Interdisciplinary Reviews: Water* 4: e1179-n/a.

Wang, M.-H. and Y.-S. Ho. 2011. Research articles and publication trends in environmental sciences from 1998 to 2009. *Archives of Environmental Science* 5: 1-10.

Werisch, S., J. Grundmann, H. Al-Dhuhli, E. Algharibi and F. Lennartz. 2014. Multiobjective parameter estimation of hydraulic properties for a sandy soil in Oman. *Environmental Earth Sciences* 72: 4935-4956.

Wesseling, J.G., J.A. Elbers, P. Kabat and B.J. van den Broek. (1991). SWATRE: instructions for input, Internal Note, Winand Staring Centre, Wageningen, Netherlands.

Western, A.W., R.B. Grayson, G. Blöschl, G.R. Willgoose and T.A. McMahon. 1999. Observed spatial organization of soil moisture and its relation to terrain indices. *Water Resources Research* 35: 797-810.

Wiekenkamp, I., J.A. Huisman, H.R. Bogena, A. Graf, H.S. Lin, C. Drüe, et al. 2016a. Changes in measured spatiotemporal patterns of hydrological response after partial deforestation in a headwater catchment. *Journal of Hydrology* 542: 648-661.

Wiekenkamp, I., J.A. Huisman, H.R. Bogena, H.S. Lin and H. Vereecken. 2016b. Spatial and temporal occurrence of preferential flow in a forested headwater catchment. *Journal of Hydrology* 534: 139-149.

WMO-TT-DEWCE. (2015). Draft version of the Guidelines on the Definition and Monitoring of Extreme Weather and Climate Events; Draft Version – first review by TT-DEWCE December 2015.

Wöhling, T., J.A. Vrugt and G.F. Barkle. 2008. Comparison of Three Multiobjective Optimization Algorithms for Inverse Modeling of Vadose Zone Hydraulic Properties. *Soil Science Society of America Journal* 72: 305-319.

Wöhling, T. and J.A. Vrugt. 2011. Multiresponse multilayer vadose zone model calibration using Markov chain Monte Carlo simulation and field water retention data. *Water Resources Research* 47: n/a-n/a.

Wood, W.W. and D.W. Hyndman. 2017. Groundwater Depletion: A Significant Unreported Source of Atmospheric Carbon Dioxide. *Earth's Future*: n/a-n/a.

Xiao, H., R. Meissner, J. Seeger, H. Rupp and H. Borg. 2009. Effect of vegetation type and growth stage on dewfall, determined with high precision weighing lysimeters at a site in northern Germany. *Journal of Hydrology* 377: 43-49.

Xiao, H., R. Meissner, J. Seeger, H. Rupp, H. Borg and Y. Zhang. 2013. Analysis of the effect of meteorological factors on dewfall. *Science of The Total Environment* 452–453: 384-393.

Xu, S., A.C. Leri, S.C.B. Myneni and P.R. Jaffé. 2004. Uptake of Bromide by Two Wetland Plants (Typha latifolia L. and Phragmites australis (Cav.) Trin. ex Steud). *Environmental Science & Technology* 38: 5642-5648.

Yang, J., S. Wan, W. Deng and G. Zhang. 2007. Water fluxes at a fluctuating water table and groundwater contributions to wheat water use in the lower Yellow River flood plain, China. *Hydrological Processes* 21: 717-724.

Yin, L., Y. Zhou, J. Huang, J. Wenninger, E. Zhang, G. Hou, et al. 2015. Interaction between groundwater and trees in an arid site: Potential impacts of climate variation and groundwater abstraction on trees. *Journal of Hydrology* 528: 435-448.

Zacharias, S., H. Bogena, L. Samaniego, M. Mauder, R. Fuß, T. Pütz, et al. 2011. A Network of Terrestrial Environmental Observatories in Germany. *Vadose Zone Journal* 10: 955-973.

Zeppel, M.J.B., J.D. Lewis, N.G. Phillips and D.T. Tissue. 2014. Consequences of nocturnal water loss: a synthesis of regulating factors and implications for capacitance, embolism and use in models. *Tree Physiology* 34: 1047-1055.

Zhang, Z.F., A.L. Ward and G.W. Gee. 2003. Estimating Soil Hydraulic Parameters of a Field Drainage Experiment Using Inverse Techniques. *Vadose Zone Journal* 2: 201-211.

VIII Appendix

VIII.1 Figures

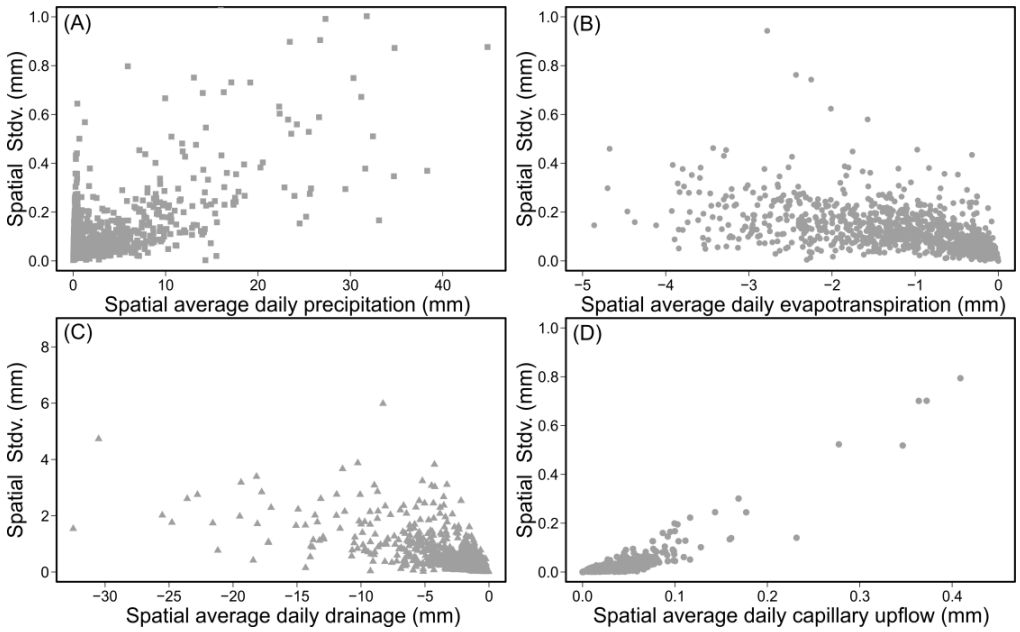

Figure V.A 1: Spatial variability of average daily precipitation (A), evapotranspiration (B), drainage (C), and capillary rise (D) obtained from four lysimeters (Lys-Wu4, Lys-Wu5, Lys-Wu6, and Lys-Wu8).

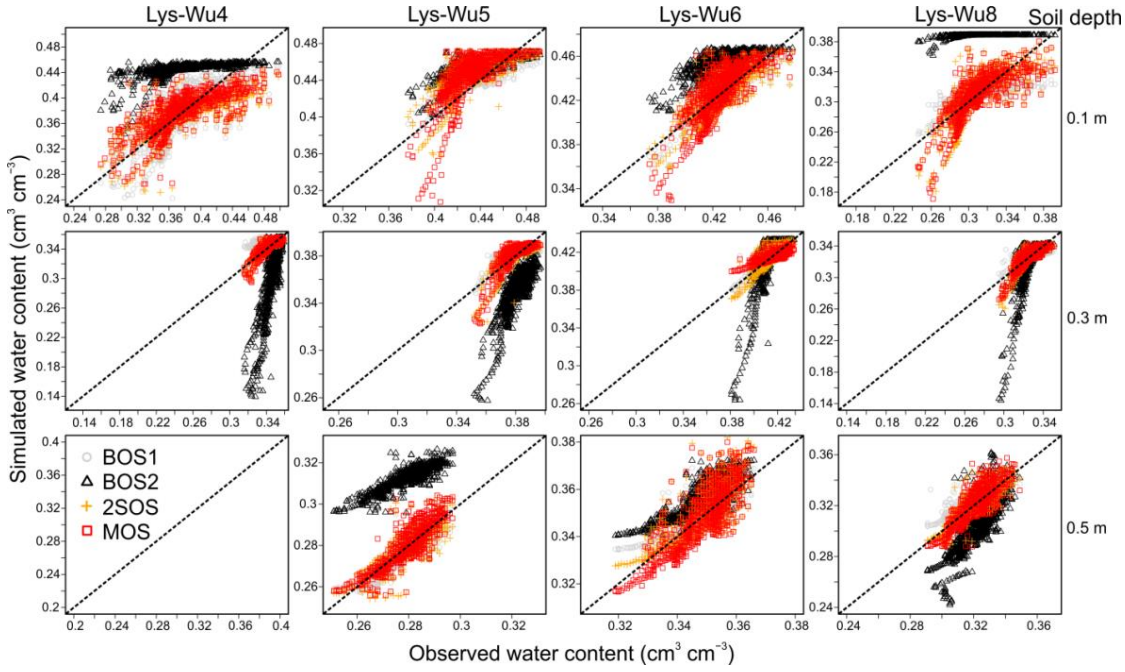

Figure V.A 2: Observed and simulated water content at three soil depths of each lysimeter (Lys-Wu4, Lys-Wu5, Lys-Wu6, and Lys-Wu8) and four different model optimization strategies (BOS1, BOS2, 2SOS, MOS).

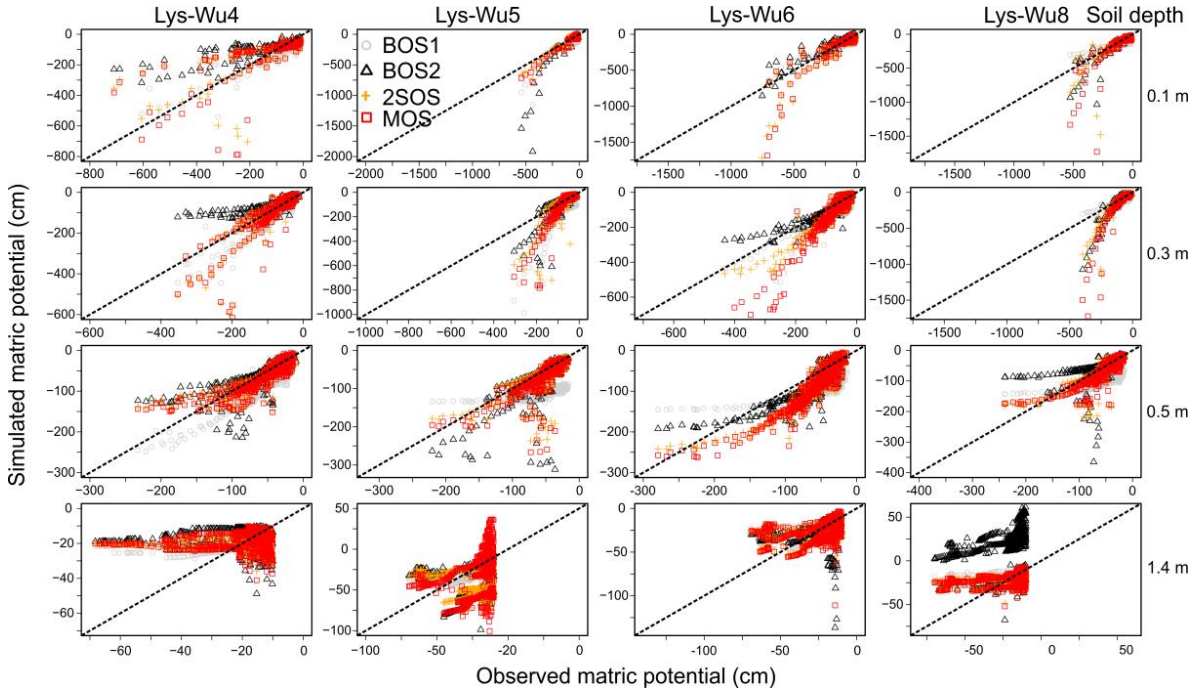

Figure V.A 3: Observed and simulated matric potential at four soil depths of each lysimeter (Lys-Wu4, Lys-Wu5, Lys-Wu6, and Lys-Wu8) and four different model optimization strategies (BOS1, BOS2, 2SOS, MOS).

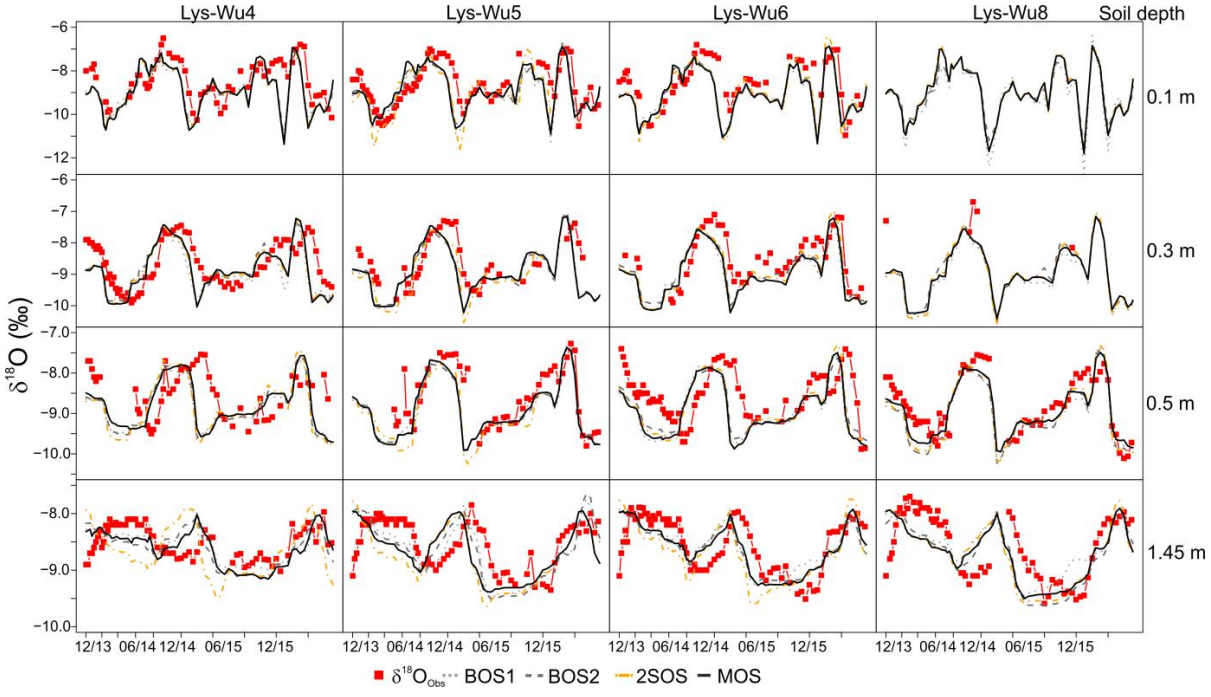

Figure V.A 4: Observed and simulated $\delta^{18}O$ ratios at four soil depths of each lysimeter (Lys-Wu4, Lys-Wu5, Lys-Wu6, and Lys-Wu8) and four different model optimization strategies (BOS1, BOS2, 2SOS, MOS).

VIII.2 Tables

Table IV.A 1: Results of a stepwise linear regression analysis to identify which environmental variables drive the average evapotranspiration rates during different day times (dawn, day, dusk, nocturnal) on a monthly basis for the entire dataset. Environmental variables are the following: air temperature (T_{air}), net radiation (R_n), vapor pressure deficit (VPD), air pressure (P_a), relative humidity (RH), wind speed (W_s), soil heat flux (G), and soil water content 0.1 m (θ). Linear correlation analysis between average monthly ET and PET rates at different daytime periods (ET~PET).

Station	Daytime period	Non- growing and growing season				
		Environmental factors	ET		ET~PET	
			R^2	P	R^2	P
Rollesbroich	Dawn	P_a ‘*’;W_s ‘.’;R_n ‘**’	0.33	‘.’	0.03	
	Day	R_n ‘***’;VPD ‘***’	0.96	‘***’	0.96	‘***’
	Dusk	P_a ‘**’;T_{air} ‘**’;RH‘**’;	0.32	‘***’	-0.02	‘ ’
	Nocturnal	P_a ‘***’;W_s ‘*’;R_n ‘*’	0.32	‘***’	0.12	‘.’
Wüstebach	Dawn	T_{air} ‘*’;θ‘.’	0.09	‘ ’	0.07	‘ ’
	Day	R_n ‘***’;VPD‘***’,RH‘***’	0.96	‘***’	0.94	‘***’
	Dusk	W_s ‘**’	0.25	‘***’	0.16	‘**’
	Nocturnal	W_s ‘**’	0.11	‘*’	0.09	‘.’
P-signif. Codes: 0 ‘***’ 0.001 ‘**’ 0.01 ‘*’ 0.05 ‘.’ 0.1 ‘ ’ 1						

Table V.A 1: Simulation results of four different inverse model approaches (BOS1, BOS2, 2SOS, MOS). Model performance values are reported for each single observation type and depth. Observation types are: water content (θ), matric potential (Ψ), and $\delta^{18}O$ ratios (18O). Observations were available in 0.1 m, 0.3 m, 0.5 m, 1.4 m, and 1.45 m.

	Lys-Wu4				Lys-Wu5				Lys-Wu6				Lys-Wu8			
	BOS1	BOS2	2SOS	MOS	BOS1	BOS2	2SOS	MOS	BOS1	BOS2	2SOS	MOS	BOS1	BOS2	2SOS	MOS
$NSE_{\theta,0.1}$	0.42	-1.84	0.41	0.36	0.74	0.28	0.40	-0.48	0.64	-2.51	0.58	0.27	0.53	-10.32	0.26	0.31
$NSE_{\theta,0.3}$	0.63	0.49	0.66	0.67	0.50	-18.43	0.41	0.36	0.68	-3.67	0.59	0.58	0.51	-5.84	0.49	0.56
$NSE_{\theta,0.5}$	‡	‡	‡	‡	0.70	-13.92	0.64	0.66	0.64	-0.16	0.41	0.34	0.51	-0.341	0.60	0.40
$NSE_{\Psi,0.1}$	0.40	0.58	0.52	0.46	-0.48	0.56	0.44	0.59	0.22	0.69	0.65	0.68	-0.79	0.53	0.58	0.62
$NSE_{\Psi,0.3}$	0.26	0.70	0.73	0.63	-2.92	0.65	0.51	0.56	-1.10	0.59	0.30	0.36	-1.61	0.69	0.74	0.67
$NSE_{\Psi,0.5}$	0.64	0.57	0.72	0.61	-5.07	0.49	0.50	0.52	-2.14	0.45	-0.02	0.12	-2.77	0.62	0.71	0.62
$NSE_{\Psi,1.4}$	-0.05	-0.40	-0.12	-0.02	0.23	-1.20	-1.10	-1.92	0.39	-0.03	0.01	-0.11	0.20	0.38	0.11	0.06
$NSE_{18O,0.1}$	-0.20	-0.07	-0.09	-0.15	0.42	0.25	0.28	0.13	0.22	0.10	0.16	0.15	‡	‡	‡	‡
$NSE_{18O,0.3}$	0.24	0.18	-0.05	0.21	0.01	0.06	0.26	-0.01	0.42	0.30	0.19	0.19	‡	‡	‡	‡
$NSE_{18O,0.5}$	-0.56	-0.57	-1.32	-0.57	0.33	0.38	0.36	-1.02	-0.33	-0.82	-0.67	-0.81	0.53	0.55	0.62	0.72
$NSE_{18O,1.45}$	0.07	-0.42	-2.42	-0.03	-0.09	-0.34	-0.89	0.31	0.36	0.46	-0.06	0.45	0.22	0.38	0.16	0.30

‡ no observation data

Table V.A 2: Estimated best parameter-sets for water flow and solute transport per lysimeter and four different optimization strategies (BOS1, BOS2, 2SOS, MOS). Average fluxes and state variable observation were used to identify „effective soil hydraulic and solute dispersivity parameter“(Eff. Parameters) with the MOS strategy.

Layer	Parameter		Lys-Wu4				Lys-Wu5				Lys-Wu6				Lys-Wu8				MOS Eff. parameter
			BOS1	BOS2	2SOS	MOS	BOS1	BOS2	2SOS	MOS	BOS1	BOS2	2SOS	MOS	BOS1	BOS2	2SOS	MOS	
2	θ_r	$cm^3\ cm^{-3}$	0.17	0.19	0.15	0.13	0.31	0.32	0.10	0.19	0.31	0.36	0.30	0.29	0.15	0.28	0.16	0.04	0.24
	θ_s	$cm^3\ cm^{-3}$	0.46	0.46	0.46	0.46	0.47	0.47	0.47	0.47	0.47	0.47	0.47	0.47	0.39	0.39	0.39	0.39	0.43
	α	cm^{-1}	0.051	0.008	0.023	0.020	0.014	0.053	0.021	0.007	0.012	0.012	0.029	0.015	0.015	0.001	0.020	0.033	0.011
	n	-	1.22	1.43	1.40	1.39	1.28	1.12	1.13	1.48	1.44	1.31	1.27	1.38	1.44	1.58	1.69	1.24	1.54
	K_S	$cm\ d^{-1}$	390	1	402	1351	2	26	5	4	12	2	52	12	64	71	90	15	2
	τ	-	-7.0	-2.1	5.9	1.2	-4.9	1.5	1.8	1.2	3.6	3.7	3.5	3.0	0.2	1.2	2.55	-4.0	-3.8
	D_L	cm	12.8	5.2	14.1	27.0	9.2	18.4	19.5	25.6	13.2	13.5	3.2	8.5	3.0	15.1	29.9	29.9	18.9
3	θ_r	$cm^3\ cm^{-3}$	0.30	0.00	0.00	0.21	0.18	0.22	0.15	0.21	0.26	0.14	0.08	0.35	0.00	0.08	0.13	0.24	0.32
	θ_s	$cm^3\ cm^{-3}$	0.36	0.36	0.36	0.36	0.39	0.39	0.39	0.39	0.43	0.43	0.43	0.43	0.35	0.35	0.35	0.35	0.39
	α	cm^{-1}	0.013	0.004	0.007	0.010	0.005	0.019	0.007	0.006	0.005	0.005	0.005	0.087	0.004	0.008	0.015	0.018	0.028
	n	-	1.60	1.15	1.12	1.20	1.14	1.61	1.19	1.30	1.37	2.99	1.45	1.12	1.21	1.68	1.18	1.33	1.480
	K_S	$cm\ d^{-1}$	9	202	34	72	10	20	11	2	2	1	6	296	73	80	48	120	124
	τ	-	-2.7	-3.3	-19.2	-4.2	0.6	1.6	-0.9	-1.7	1.2	0.7	-3.9	-6.9	-7.4	-4.0	-2.9	0.5	-6.0
	D_L	cm	11.2	29.9	15.1	8.7	21.1	23.2	6.4	12.2	15.2	4.2	9.8	8.5	18.8	10.8	4.0	3.2	11.5
4	θ_r	$cm^3\ cm^{-3}$	0.30	0.19	0.09	0.29	0.18	0.29	0.24	0.25	0.29	0.15	0.30	0.06	0.22	0.23	0.22	0.15	0.28
	θ_s	$cm^3\ cm^{-3}$	0.54	0.39	0.41	0.55	0.34	0.34	0.34	0.34	0.38	0.38	0.38	0.38	0.38	0.38	0.38	0.38	0.36
	α	cm^{-1}	0.025	0.023	0.17	0.060	0.009	0.052	0.079	0.064	0.013	0.092	0.042	0.038	0.013	0.039	0.083	0.062	0.039
	n	-	1.344	1.82	1.37	1.21	2.94	1.77	1.66	1.90	2.11	1.07	1.45	1.10	1.77	2.13	1.28	1.20	1.90
	K_S	$cm\ d^{-1}$	18	8	1469	153	43	120	354	148	19	1391	15	169	120	38	880	351	31
	τ	-	5.8	3.9	1.7	3.2	5.8	3.0	2.2	1.6	2.7	3.0	-1.8	0.4	5.2	3.7	6.0	6.0	2.8
	D_L	cm	29.8	19.4	30.0	28.8	19.9	16.5	29.9	18.7	16.0	29.9	18.2	17.8	17.5	10.9	13.5	24.8	20.4
5	θ_r	$cm^3\ cm^{-3}$	0.05	0.15	0.10	0.04	0.25	0.21	0.04	0.11	0.14	0.14	0.06	0.14	0.08	0.07	0.00	0.00	0.23
	θ_s	$cm^3\ cm^{-3}$	0.55	0.49	0.55	0.46	0.53	0.53	0.41	0.39	0.54	0.49	0.35	0.55	0.55	0.42	0.52	0.54	0.55
	α	cm^{-1}	0.033	0.026	0.053	0.036	0.062	0.044	0.039	0.016	0.113	0.057	0.057	0.119	0.037	0.011	0.046	0.028	0.059
	n	-	2.77	2.99	2.99	2.75	1.57	2.22	2.19	2.02	1.95	1.76	2.72	1.55	2.22	1.94	1.88	1.95	2.00
	K_S	$cm\ d^{-1}$	78	1472	8	14623	172.2	404	631	9	38	125	1174	713	227	14	64	93	16
	τ	-	-3.1	-2.3	-3.0	1.6	-3.1	-2.9	-0.78	-3.5	-3.9	-2.8	-2.4	-5.0	3.0	-3.6	-2.1	-4.1	-3.3
	D_L	cm	6.8	20.4	9.8	9.5	3.1	2.3	6.9	17.5	14.6	24.2	0.4	16.4	9.9	8.5	8.2	4.8	17.4

IX Danksagung

An dieser Stelle möchte ich mich ganz herzlich bei Thomas Pütz und Jan Vanderborght für ihre gute Betreuung, Geduld, konstruktive Kritik, sowie zahlreichen und langen Diskussionen bedanken, die diese Arbeit vorangebracht haben.

Harry Vereecken danke ich für die halbjährlichen Gespräche, seine Unterstützung und Ratschläge. Bernd Diekkrüger danke ich für die Übernahme des Korreferats. Ein Dank gilt auch all den Kollegen aus dem SOILCan-Projekt, die mich bei der Planung und Durchführung des Tracerversuches unterstützt haben. Bei Christine bedanke ich mich für ihre Unterstützung und Diskussionen während meines Besuchs in München. Meinen österreichischen Kollegen Veronika und Markus danke ich ganz herzlich für die gute Zusammenarbeit und Interesse am Thema Tau.

Für die Unterstützung im Feld und Labor möchte ich mich ganz herzlich bei den tollen Kollegen Andrea Ecker, Ferdinand Engels, Leander Fürst, Rainer Harms, Martina Krause, Werner Küpper, Philipp Meulendick und Stephanie Storck aus dem TERENO-SOILCan Team bedanken. Ein Dank gilt auch Holger Wissel und Andreas Lücke für die Analyse und der Hilfe bei den zahlreichen Isotopendaten. Ein riesen extra Dankeschön gebührt Werner Küpper (Wernitsch), der immer 200 % für die Lysimeter gegeben hat, für die zahlreichen interessanten Diskussionen und offenen Fragestellungen zum Thema Lysimeter und natürlich für die super gemeinsame Zeit im Büro (danke auch fürs Stollberger Platt). Ein großer Dank geht auch an Sebastian Gebler, Nina Gottselig, Francois Jonard, Max Koch, Anna Missong, Joanna Makselon, Michael Stockinger, Inge Wiekenkamp, Jan Wolff (Pomelo) und den lieben Kollegen aus der Mittagsrunde Sirgit Kummer, Christian Lichters, Thomas Muckenheim und Wolfgang Tappe.

Ein besonderes Dankeschön geht an Nils Güting für die tolle gemeinsame Zeit und super Diskussionen während der unzähligen Lunch und Coffee Breaks.

Von ganzem Herzen danke ich meinen lieben Eltern, meiner Frau und meinen Geschwister für ihre Unterstützung, Verständnis und Vertrauen, ihr seid die Besten.